Heliyon 7 (2021) e08436

Contents lists available at ScienceDirect

Heliyon

journal homepage: www.cell.com/heliyon

Review article

Natural resources for dye-sensitized solar cells

Yuly Kusumawati [a,*], Aulia S. Hutama [b], Diana V. Wellia [c], Riki Subagyo [a]

[a] Department of Chemistry, Institut Teknologi Sepuluh Nopember, Sukolilo Campus, Surabaya, 60111, Indonesia
[b] Department of Chemistry, Faculty of Mathematics and Natural Sciences, Universitas Gadjah Mada, Jalan Sekip Utara, Bulaksumur, Yogyakarta, 55281, Indonesia
[c] Department of Chemistry, Faculty of Mathematics and Natural Sciences, Universitas Andalas, Padang, 24516, Indonesia

ARTICLE INFO

Keywords:
Dye sensitized solar cells
Natural resources
Biopolymer
Natural counter electrode
Green synthesis

ABSTRACT

While the development of dye-sensitized solar cells (DSSCs) has been ongoing for more than 30 years, the currently obtained efficiency is unsatisfactory. However, the study of DSSC development has produced a fundamental understanding of cell performance and inspired other devices, such as perovskite cell solar cells. DSSCs consist of a dye-sensitized photoanode, a counter electrode, and a redox couple in the electrolyte system. Each of the components has an important role and cofunctions with each other to obtain a high power conversion efficiency. Various modifications to each DSSC component have been applied to improve their performance. Additionally, to generate improvements, the effort to reduce production costs has been crucial. The utilization of natural sources for DSSC components is a possible solution to this issue. The utilization of natural resources also aims to increase the value of the natural resource itself. In this review, the applications of various natural sources for DSSC components are described, as well as the modification efforts that have been made to enhance their performance. The discussion covers the utilization of natural dye for sensitizer dyes in liquid DSSC applications: (1) utilization of biopolymers for quasi-solid DSSC electrolytes, (2) green synthesis methods for photoanode semiconductors, and (3) development of natural carbon counter electrodes. The detailed factors that influence improvements in cell performance are also addressed.

1. Introduction

Multiple renewable energy sources must be developed to meet rapidly increasing energy demand and human population growth. Countries around the world should utilize their natural resources as renewable energy to ensure sustainability. Solar energy is an abundant resource available in many countries. It has enabled continuous growth in the development of solar cells in recent decades. Among solar technologies, dye-sensitized solar cells (DSSCs) are photovoltaic devices that have attracted much attention since the 1990s.

Figure 1 presents a model of DSSC structure and function. It consists of two electrodes. One electrode is an oxide-semiconductor mesoporous layer deposited onto fluorine-doped tin oxide (FTO) glass and sensitized by a dye, which acts as a photoanode. The other is platinized FTO glass as a cathode, also called a counter electrode. An electrolyte system is placed between these two electrodes. The most common DSSC liquid electrolyte consists of an I_3^-/I^- redox couple dissolved in an organic solvent such as acetonitrile.

Electricity in the DSSC is produced by the electron transfer process displayed in the inset section in Figure 1. When the dye – which acts as a sensitizer in DSSC – receives solar radiation, the electron from the highest occupied molecular orbital (HOMO) excites the lowest unoccupied molecular orbital (LUMO). Electrons are subsequently injected into the oxide semiconductor conduction band. After that, the electrons travel to the external circuit through the anode and cathode. Once the electrons arrive at the external circuit, they change the redox couple species state from oxidized to reduced. The electrons obtained from the reversal of the redox couple utilize dye regeneration. This cycle is repeated until electricity is gathered. General article reviews have already been published on the primary or fundamental concepts of DSSCs [1, 2, 3], the electron transfer mechanism in DSSCs [4, 5, 6, 7], and recent progress about DSSC development [8, 9, 10, 11], which will be beneficial for readers who need additional information.

The assessed performance for the DSSC is the light-to-electricity conversion efficiency or power conversion efficiency (PCE, %). The PCE is contributed by the photoanode, counter electrode, electrolyte, and dye employed in the DSSC device. The PCE is proportional to the short circuit current density (J_{sc}), open-circuit voltage (V_{oc}), and fill factor (*FF*) as follows.

* Corresponding author.
E-mail address: y_kusumawati@chem.its.ac.id (Y. Kusumawati).

https://doi.org/10.1016/j.heliyon.2021.e08436
Received 28 August 2021; Received in revised form 14 October 2021; Accepted 16 November 2021

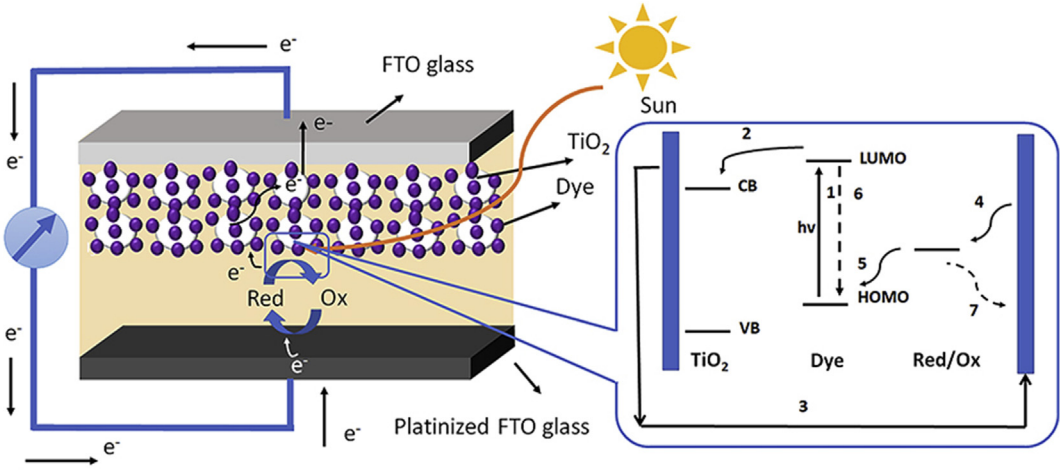

Figure 1. A model of dye-sensitized solar-cell structure and function. (Red/Ox = the coupled redox species for example I_3^-/I^-; VB = Valence band; CB = Conduction band).

$$\eta \sim J_{sc} \times V_{oc} \times FF \tag{1}$$

The short circuit current (J_{sc}) correlates with both the photoanode and counter electrode performance. The value of J_{sc} can be increased by improving the efficiency of light harvesting. The improvement can be conducted, for instance, by finding a proper sensitizer that can more strongly attach to TiO_2 surfaces or pores [12]. The counter electrode has a crucial role in catalyzing the redox couple in the electrolyte solution. The reduced species will be transported to the photoanode, reduce the oxidized dye, and continue the light absorption cycle. Therefore, a counter electrode with high electrocatalytic activity, charge transport activity, and low resistance is highly desirable to increase the J_{sc}.

The open-circuit voltage (V_{oc}) is the difference in the Fermi level of electrons in TiO_2 (E_F) and the redox potential of the electrolyte (E_{redox}) over the charge (q)

$$V_{oc} = \frac{(E_F - E_{redox})}{q} \tag{2}$$

Theoretically, V_{oc} can reach up to 1.6 V. However, due to the energy mismatches between the E_{redox} and HOMO levels of the dye and between the conduction band level (E_c) of TiO_2 and the LUMO of the dye, the maximum voltage is reduced to $\frac{(E_c - E_{redox})}{q}$ [13]. The V_{oc} can be tuned by several means. An example of this is putting additives into the electrolyte to shift the conduction band level of TiO_2 and/or proper choice of I^- salt source [14, 15, 16].

The *FF* depends on the serial resistance and shunt resistance of the devices. Serial resistance in DSSCs is the resistance of the electron transfer process in the external circuit to the counter electrode. Shunt resistance is the resistance of the back electron transfer to the photoanode. Therefore, to increase the *FF* value, the serial resistance must be minimal, while the shunt resistance must be maximal. The DSSCs first published by Grätzel in 1991 gained a cell PCE of 7.1–7.9% [17].

For the last three decades, increasing the PCE has remained a challenge in enhancing DSSC performance. Ideally, DSSC improvement requires the optimization of all device components. For example, the oxide semiconductor layer of the photoanode is expected to have a mesoporous structure to immobilize a maximum amount of dye to absorb adequate solar light [18, 19]. To have a mesoporous structure, various methods have been proposed. Surfactants are the most straightforward templating agents to control the surface area of the resulting semiconductors [20, 21, 22]. The use of sodium dodecyl sulfate in the oxide synthesis step can improve the cell performance to 6.08% compared to the 4.06% cell performance when using TiO_2 P25 [20]. The template-free semiconductor synthesis method, with controllable size and surface area, can also be carried out to synthesize the oxide photoanodes. This has been demonstrated by Hosni et al., who prepared a zinc oxide nanotubes with a diameter of 35 nm [23]. The layer of this particle is highly porous, which is beneficial for DSSC performance. Another method for photoanode improvement is to prepare an oxide semiconductor with a one-dimensional structure. It has been proven that the one-dimensional structure will be beneficial for electron transport within the oxide matrix [23, 24, 25, 26]. Zhang et al. developed a TiO_2 nanotube DSSC, and they obtained a satisfactory PCE of 9.86%. The necks formed between TiO_2 nanotube particles are responsible for charge transport [27].

Dye sensitizer optimization has been studied to improve cell performance and reduce the cell production cost. Metal-free organic dyes have become an alternative to classical organo-ruthenium complexes due to multiple advantages, such as low cost, tunable properties, and high molar extinction coefficients [28]. Dye design works usually utilize quantum chemical calculations in conjunction with the experimental works. Quantum chemical calculations are pivotal in predicting the electronic properties of dyes to provide a molecular-level explanation of the electronic process. Experimental and theoretical molecular engineering has been carried out to arrange the donor (D), π-spacer (π-conjugation section of the dye) and acceptor (A) units to obtain either D-π-A [29], D-A-π –A [30], or D-D- π-A structures [31]. Despite the endeavor, not all results were satisfactory. For example, the D- π-A thiophene dyes developed by Babu et al. only achieved a PCE of 4.24 %. On the other hand, Wang et al. succeeded in preparing a D-A-π –A-based DSSC and produced a PCE value of 9.83%. The study of the binding of dyes onto the oxide surface is also vital to ensure an efficient electron injection process [32, 33]. Additionally, it is important to tune the HOMO and LUMO levels of the dyes to obtain an efficient intramolecular charge transfer process and electron injection into the photoanode.

Studies on electrolytes focus on finding alternatives to iodine/triiodide liquid-based electrolyte solution, which presents. This has led to a replacement of the I_3^-/I^- redox couple by other redox couples, such as Co^{2+}/Co^{3+} [34, 35, 36], nitroxide radicals [37, 38], copper complexes [39, 40], thiolate/disulfide [41], and ferrocenium/ferrocene [42, 43]. In addition, to overcome electrolyte leakage, quasi-solid DSSCs, which use a polymer gel as an electrolyte medium, have been considered [44, 45, 46]. Unfortunately, quasi-solid DSSCs have not shown a better PCE value than liquid DSSCs, with PCE values ranging from 4% to 5 % [44]. A few have a PEC value of 7%, such as a PAN (polyacrylonitrile)-based DSSC combined with RbI and tetrahexylammonium iodide salt developed by Bandara et al. [47].

For the counter electrode component, research has been focused on finding a platinum substitute. It is evident that platinum-based DSSC show superior performance as catalyst for the reduction of I_3^- to I^-. However, since it is a noble metal, the production cost of platinum-based

DSSCs are expensive [48, 49]. Various materials have then been proposed to replace platinum, such as carbon-based materials, including allotrope graphene [50, 51, 52, 53] or carbon nanotubes [54, 55], conductive polymers such as PEDOT [56], metal-organic frameworks (MOF) [49, 57], and perovskites [58, 59]. Research on counter electrodes also focuses on flexible counter electrodes to extend DSSC applications [60, 61]. In general, most nonplatinum counter electrode-based DSSCs have a lower PCE than the platinum DSSCs. However, some materials outperform the platinum materials and appear to be promising for further development [48, 62]. For instance, the graphene nanoplate-based counter electrode prepared by Kakiage et al. has a PCE value of 14.7% [53].

The best performance of DSSC currently recorded is one that uses copper complex redox couple-based electrolytes developed by Zhang et al. This cell employs a sensitizer constructed by a bulky donor N-(2′,4′-bis (dodecyloxy)-[1,1′-biphenyl]-4-yl)-2′,4′-bis(dodecyloxy)-N-phenyl-[1,1′-biphenyl]-4-amine and an electron acceptor 4-(benzo[c] [1, 2, 5] thiadiazol-4-yl) benzoic acid coupled with the PEDOT (poly(3,4-ethylenedioxythiophene) counter electrode. This cell shows a PCE value of 34.5% under warm white fluorescent light at 1000 lux. Based on these results, the cell is the best cell for ambient light device applications [63].

To improve DSSC performance and decrease their cost, the utilization of natural resources has attracted much attention. Natural resources aim to achieve sustainability and reliability and support an eco-friendly environment [64, 65]. In this review, the current progress on natural resource utilization in DSSC development is presented. Although Mariotti et al. [66] recently reviewed the development of eco-friendly and cost-effective materials for DSSCs, the point of view of that work is slightly different from the current review. In the present review, the natural resources as material sources that build DSSCs will be further elaborated on. The purposes of this review are to describe the utilization of natural resources in DSSCs and their shortcomings. The discussion will point out the natural resource utilization in each DSSC component: natural dyes for sensitizers, natural polymers for quasi-solid DSSC electrolytes, and natural carbon for counter electrodes. In most DSSCs, TiO_2 and ZnO photoanode are usually taken from either commercial sources or chemically and physically controlled synthetic procedures. Here, we also present the possibility of preparing photoanodes from the oxides obtained through green synthesis with controllable structures and morphologies. Figure 2 presents the illustration of the scope of this review.

2. Natural dye for sensitizer DSSC

The sensitizer is one of the vital components in DSSCs. It aids in capturing visible to near-infrared light over a broad spectrum range with high molar extinction coefficients. It must also produce good charge separation to avoid electron recombination and efficient electron injection into oxide semiconductors [67]. Ruthenium-based dyes have shown good performance in fulfilling sensitizer requirements. Due to their rare availability and high cost, alternative dyes have been developed to replace ruthenium complex dyes [68]. Natural dyes offer good opportunities. They have been considered due to their high molar extinction coefficient and their abundant availability [68, 69]. Families of natural dyes that have been explored for sensitizers applications in DSSCs include betanin or betalain [70, 71, 72, 73, 74, 75, 76, 77, 78], chlorophyll [72, 73, 74, 75, 76, 77, 78, 79, 80], and anthocyanin [28, 88, 89, 90, 91, 92, 93, 94]. The cosensitization of two dyes is also of high interest to enhance their performance [95, 96]. In the following sections, we present details of the various families of natural dyes and explain multiple research efforts undertaken to overcome their limitations.

2.1. Betanin

Betanins are a category of pigments that belong to the betalain class. The betanin structure is presented in Figure 3. In their chemical structure, betalains contain an N-heterocyclic bearing hydroxyl functional group. Betalain compounds are divided into betacyanins, red–violet pigments, and betaxanthin, yellow pigments. Approximately 75–95% of red–violet pigments are composed of betanin. Notably, this pigment can be extracted from Caryophyllales plants [66, 97]. Betanins have inspired researchers to utilize these compounds for sensitizers in DSSCs [70, 71, 72, 73, 74, 75, 76, 77, 78].

The betanin sensitizer was first reported in 2005 by a research group from Uppsala University [80]. Unfortunately, the DSSC performance was still considered relatively poor. They conducted the research using an unsealed cell and reported a poor performance with a very low J_{SC}, even with an *FF* value in the same range of the standard ruthenium dye cell. Among the tested cells, the use of an ethanol solvent for the electrolyte showed the best result [80]. In 2011, Sandquist et al. from Washington State University reported a relatively higher PCE of the betanin-based DSSC than the previous study [71]. They made improvements by using 3-methoxypropionate (MPN) as the electrolyte solvent and employing a blocking layer. Their improvement led to a PCE of 2.7% [71]. This report showed that using MPN as an electrolyte solvent gives a better result than acetonitrile.

Table 1 summarizes the results of betanin-based DSSCs. It highlights the efforts and modifications that have been conducted thus far. Based on Table 1, we can conclude that the factors that have to be considered to develop betanin-based DSSCs are (1) the extraction process of the dyes [70, 71, 72]; (2) the immersion system for sensitizing the photoanode [71, 72, 73]; (3) the incorporation of a small amount of metal/cation to tune the electronic properties of the photoanode [73, 74, 77]; and (4) the choice of the electrolyte system [70, 72, 74, 77].

Table 1 shows that most PCEs of the betanin-based DSSCs do not exceed 3%. The best result was obtained for cells using medium-pressure liquid chromatography-extracted betanin [71]. Incorporating Ag and Au nanoparticles into the photoanode can also enhance light absorption due to the surface plasmon resonance effect [74, 77]. Moreover, Au

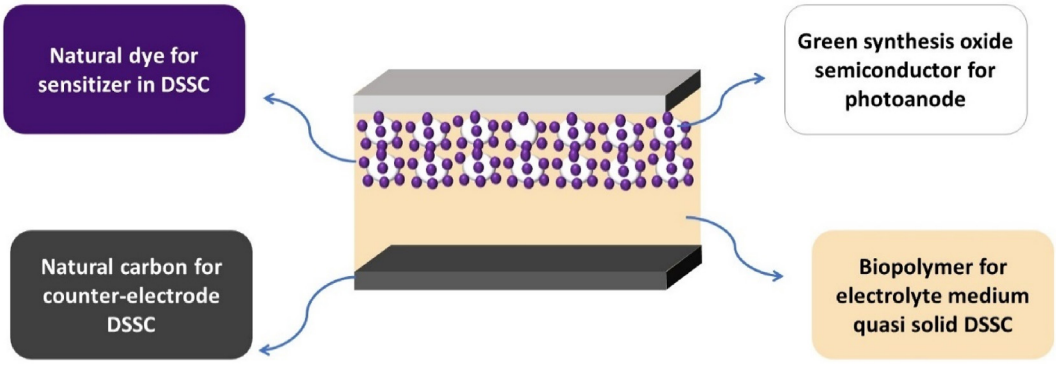

Figure 2. The illustration of natural resources for DSSC application.

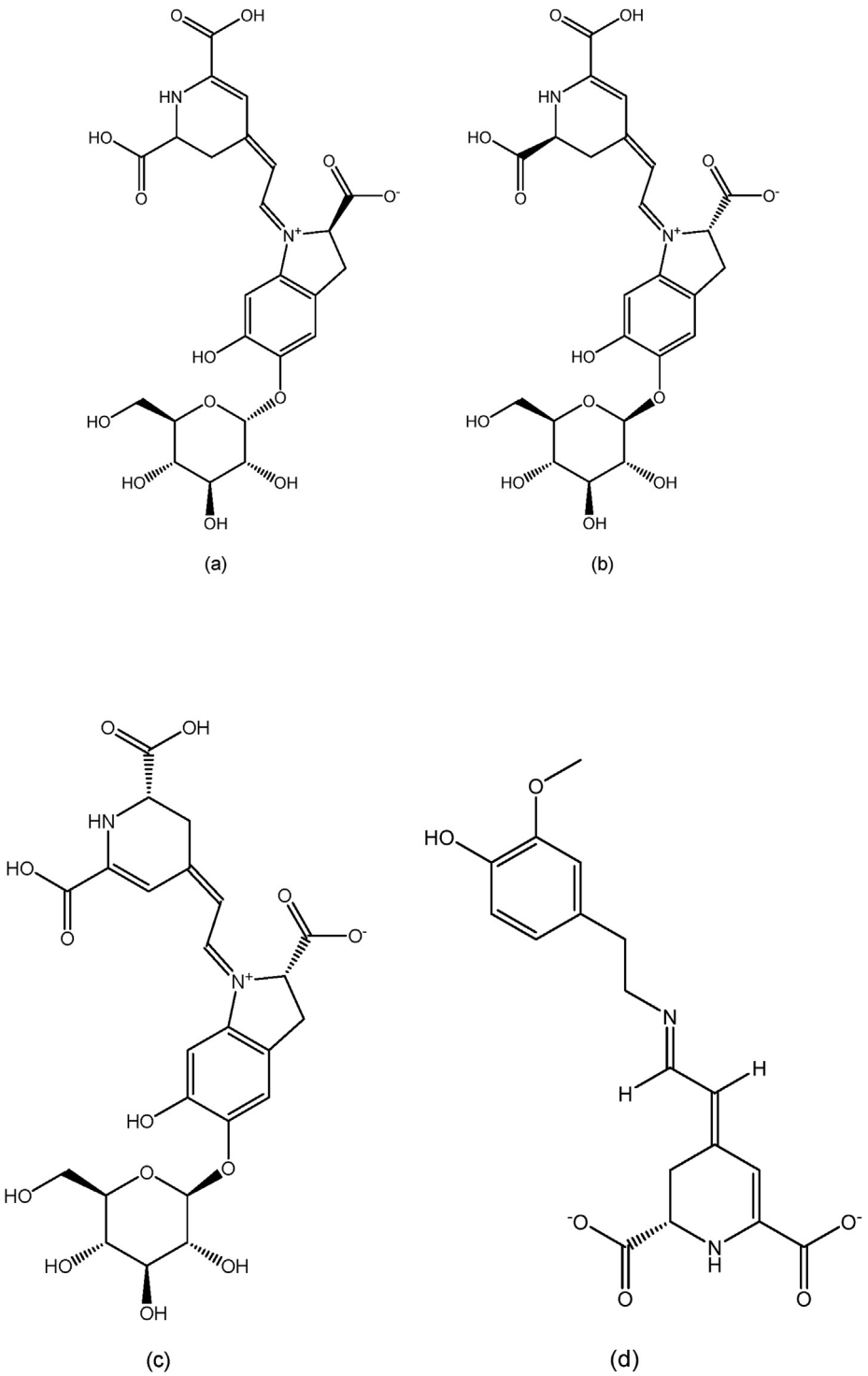

Figure 3. Structure of (a) Betalain and (b) Betanin and structure of the constituent pigment, namely (c) betacyanin and (d) betaxanthin.

incorporation provokes a Schottky barrier effect at the Au and TiO_2 interface. This effect can reduce the charge recombination from the oxide conduction band to the LUMO of dyes or electrolyte species [77]. Maintaining the acidic condition of the solvent upon the extraction process or photoanode immersion can also be considered since the structure of betanin is known to be influenced by the solution pH [73].

Multiple experimental and computational studies have also been performed to gain insights into the intramolecular electronic properties of betanin and the charge electron mechanism on the TiO_2 surface. Many findings explain betanin limitations that should help to find solutions for cell improvement. Knorr et al. reported that during the recombination process of electron injection, a radical species is formed. This radical species provokes betanin oxidation [98]. Damayanti et al. revealed that one of the three carboxyl moieties of betanin limits the betanin charge transfer to the oxide semiconductor [99]. Based on these findings, betanin modification can be carried out to develop a betanin-based DSSC. Dye aggregation is also prominent in betanin-based DSSC performance. This phenomenon can either be beneficial or detrimental to cell performance. The absorbed photon energy will be partly lost due to thermal processes and noncharge collection [100]. In contrast, Treat et al. found

Table 1. The summarized results on betanine-based DSSCs.

No	Source	Pigmen	Solvent of extraction	Technique of purification	Photoanode	Counter electrode	Redox couple	Electrolyte solvent	J_{SC} (mA/cm^2)	V_{OC} (V)	FF	η (%)	Reference
1	Red beetroot (*Beta vulgaris*)	Betanin	0.1 M HCl in ethanol	Collum chromatography (Waters MCX ion-exchange column or Sephadex G25) for purifying	P25 TiO_2	Pt	I_2, LiI	acetonitrile (ACN)	0.52	0.27	0.47	0.07	[70]
								3-methoxypropinitrile (MPN)	0.89	0.26	0.47	0.11	
								3-methoxypropinitrile (MPN) with HCl and 4-tert-Butylpyridine (TBP)	2.42	0.44	0.63	0.67	
2	Red beetroot (*Beta vulgaris*)	Betanin	Potassium phosphate buffer	Develop the reverse-phase medium pressure liquid chromatography for purifying the extracted betanine	P25 TiO_2 without bloking layer	Pt	I_2, LiI	acetonitrile (ACN)	10.55	0.35	0.57	2.04	[71]
					P25 TiO_2 with $TiCl_4$ post treated				9.34	0.44	0.57	2.27	
					P25 TiO_2 with bloking layer				13.91	0.36	0.56	2.71	
					P25 TiO_2 without bloking layer			3-methoxypropinitrile (MPN)	7.64	0.39	0.51	1.46	
					P25 TiO_2 with $TiCl_4$ post treated				10.13	0.36	0.55	1.93	
					P25 TiO_2 with bloking layer				8.61	0.44	0.61	2.22	
3	Red beetroot (*Beta vulgaris*)	Betalain	Water-HCl	-	The TiO_2 porous film electrode was manufactured by using the sol–gel method, starting from the commercial titanium(IV) oxide, anatase, nanopowder <25 nm, from Sigma–Aldrich, and titanium isopropoxide (Sigma–Aldrich)	Pt	I_2, KI	Ethyleneglicole:acetonitrile (4:1, volume ratio)	0.38	0.36	0.69	0.12	[72]
			Water-ascorbic acid						0.39	0.35	0.62	0.11	
			Methanol-HCl						0.09	0.36	0.65	0.03	
			Water-HCl	pressure liquid chromatography (MPLC) for purifiying					2.95	0.36	0.30	0.40	
			Water-ascorbic acid						0.42	0..40	0.56	0.12	
			Methanol-HCl						0.16	0.37	0.65	0.05	
4	Paper flower (*Bougainville glabra*)	Betaxanthin betacyanine	Water-HCl pH = 5.70	-	TiO_2 film from blending P25 and Triton x-100	Pt	-	-	2.27	0.41	0.61	0.57	[73]
			Water-HCl pH = 3						3.72	0.44	0.59	0.98	
			Water-HCl pH = 1.23						1.13	0.44	0.43	0.21	
5	Beetroot (*Beta vulgaris*)	Betanin	Potassium phosphate buffer	Develop the reverse-phase medium pressure liquid chromatography for purifying the extracted betanine	TiO_2	Pt	I_2,LiI	N-methyl-2-pyrrolidone (NMP) solvent with 6% by weight polyvinylidene fluoride (PVDF)	1.47	0.49	0.63	0.58	[74]
					AgNPs coated onto TiO_2				1.65	0.51	0.64	0.68	
6	Bracks of paper flower (*Bougainville glabra*)	Betaxanthin betacyanine	Acetone-water	-	TiO_2 NPs	Pt	I_2, LiI, TBP	3-methoxypropinitrile (MPN)	-	-	0.59	0.25	[75]
7	Sicilian prickly pears (*Opuntia ficus indica*)	Betalain (the dominant pigmen is betaxantin)	Ethanol and HCl/ carboxylic acid/ tartaric acid as acids and co-adsorbers.	-	TiO_2 nanocrystalline	Pt	GuNCS, TBP	Acetonitrile:valeronitrile (85:15)	7.85	0.38	0.62	1.87	[76]
	Blackberry ( )								5.85	0.32	0.57	1.07	
8	Red Beetroot (*Beta vulgaris*)	Betanin	Water-HCl	-	ZnO/Au	Pt	I_2, KI	Water	0.05	0.25	0.33	0.48	[77]
								Asetonitrile	0.99	0.15	0,21	2.99	
								PVA	0.01	0.06	0.29	0.01	
9	Red boot (*Beta Vulgaris* L.)	Betanin	Ethanol-HCl	Sephadex DEAE A25 column and Phenomenex Strata C18 SPE Column	TiO_2	Pt	I_2, LiI	Acetonitrile	14	0.38	-	3.00	[78]

that aggregated dye induces a broadened absorbance spectrum, increasing the light-harvesting efficiency [78]. A comprehensive review of the dye aggregation phenomena and their implications for DSSC performance can be found in Ref. [101].

2.2. Chlorophyll

Chlorophylls are a family of pigments classified into chlorin family. They consist of a tetrapyrrole derivative as a chelating ligand and an Mg^{2+} ion as a central ion. Based on the ligand structure, chlorophyll is divided into chlorophyll-a, chlorophyll-b, chlorophyll-c1, chlorophyll-c2, and chlorophyll-f. The motivation to consider chlorophyll as natural DSSC sensitizers is to mimic the photosynthesis phenomenon. Based on our records, Kay et al. were the first to investigate chlorophyll-based DSSCs in 1993. They also compared the cell performance with a modified chlorophyll in which a Cu^{2+} ion replaced the Mg^{2+} ion. They reported the following cell parameters: J_{SC} of 9.4 mA cm^{-2}, V_{OC} of 0.52 V, and PCE of 2.6%. This best result was obtained with the addition of a coadsorbate using polyhydroxyl compounds such as glucose, glycerol, or sorbitol [79]. Coadsorbates were used to reduce electron recombination from the couple redox species to the photoanode surface. We also noted that even though Kay et al. were the first group to develop chlorophyll-based DSSCs, Cu-chlorophyll TiO_2 sensitization was first observed by Kamat et al. in 1986. They investigated the photoelectrochemical mechanism in a sensitized TiO_2 system using laser flash photolysis, time-resolved microwave absorption, and spectrofluorometry techniques. For these experiments, they measured the sample in dispersion form [102].

In the next decade, research on chlorophyll-based DSSCs was continued by Amao et al. They used a dye derived from chlorophyll extracted from *Spirulina*, namely, Chl-e6. The obtained results were not satisfactory since the J_{SC} was only 0.305 mA cm^{-2} and the V_{OC} was 0.426 V [80]. Wang and coworkers reported research results on chlorophyll-based DSSCs in Refs. [103, 104, 105, 106]. They developed DSSCs using a modified chlorophyll as a photosensitizer. They added a natural conjugated redox spacer to prevent the recombination of electrons with the oxidized sensitizer. Approximately 30% of the cell performance was improved after performing this modification [82, 103]. They also compared the performance of chlorophyll-based DSSCs using TiO_2 and ZnO photoanodes. They concluded that the limitation of chlorophyll-ZnO-based DSSCs was caused by far location of the molecular orbital involved in the electron excitation process from the anchoring site [105]. A complete summary of the research on chlorophyll-based DSSCs is summarized in Table 2.

Many works have already focused on applying chlorophyll dye in DSSCs due to its role in the photosynthesis process. There have also been many reports on the utilization of synthetic porphyrin-sensitized DSSCs. The first was due to Jasieniak et al. from Flinders University, Australia, in 2004. They did not obtain a satisfactory result at that time, and their best cell efficiency was only 0.69% [107]. Impressively, in 2011, Yella et al. succeeded in preparing DSSCs based on multiple synthetic porphyrin dyes with a cobalt redox couple. The efficiency of their device reached 12% [108]. This promising result suggests the need for further investigation in the utilization of porphyrin dyes as sensitizers in DSSC applications.

2.3. Anthocyanins

Research on the application of anthocyanins as natural dyes in DSSCs is relatively abundant. These dyes are present in almost all colorful fruit and flowers and offer a large panel of potentially interesting dyes for DSSC applications. By looking at their chemical structure, anthocyanins have hydroxyl moieties, and some of them possess a catechol group [109]. They can act as anchoring groups to attach the dye onto the semiconductor surface. The catechol group showed better performance as an anchoring group than the carboxylic group because the latter presents an electron-withdrawing character [110]. Table 3 summarizes the main published results on anthocyanin utilization as a sensitizer for DSSCs. This table shows that the anthocyanin performance is still lower than that of the chlorophyll derivative dyes.

2.4. Remarks on natural dyes

In the last twenty years, reports from the scientific community on using natural dyes as a sensitizer for DSSCs have given unsatisfactory results in terms of efficiency. Many works have reported efficiencies below 2% [70, 83, 89]. Some of them have succeeded in reaching a PCE of 5% [82]. The motivations to develop natural dyes for sensitizers in DSSCs are their abundant availability, environmental friendliness, cost effectiveness, and biodegradable. Unfortunately, no one reported a PCE higher than 10% for natural dyes based on our record. Most of them have relatively low PCE values of approximately 3–4%. The deficiency of natural dyes lies in their stability. They also easily agglomerate, and then the photogenerated charges are not efficiently collected [111]. Almost all of them attach poorly to the oxide semiconductor surface [69, 99].

The incorporation of natural dyes in working DSSC devices remains a challenging task. Chlorophyll derivatives display the best performance among the outlined dyes, making chlorophyll derivative dyes the most researched compared to others. The strong performance of chlorophyll inspires synthetic chlorophyll-based dyes, which are no longer natural dyes. However, the lack of research on the other dyes presents the opportunity for further investigations, as the derivatives of the other dyes have not been much explored.

3. Biopolymer for quasi-solid DSSC

3.1. Development of biopolymer used in DSSC

The first DSSC employed a liquid electrolyte that contained a redox couple. The utilization of a liquid electrolyte faces various problems, including solvent leakages, desorption of dye attached to the photoanode, and some practical issues of sealing [112, 113]. These reasons encouraged many researchers to develop quasi-solid electrolytes. They notably developed polymers, and among them, biopolymers have attracted much attention in line with sustainability issues and the utilization of natural resources.

Research on the utilization of biopolymers for DSSC applications started in 2010. The initial study was carried out by Buraidah et al., who used a chitosan biopolymer for solid electrolytes. The composition of 27.5% chitosan, 22.5% NH_4I, and 50% BMII (w%) produced a good conductivity of 3.34×10^{-5} S cm^{-1}, which at the time was comparable with other polymer cells [114]. In the following years, Buraidaeh et al. developed copolymer chitosan and poly(vinyl alcohol) (PVA) to improve polymer electrolyte conductivity [115]. Several reports emerged during the same period where agarose had been used for quasi-solid DSSCs [116]. Several biopolymers that have been widely developed for quasi-solid DSSCs in the past were agarose, carrageenan, cellulose, and chitin/chitosan [117].

A more comprehensive list of the previous research is summarized in Table 4. Figure 4 presents a map of conductivity and cell performance of various biopolymer-based DSSCs. Among natural biopolymers, agarose and cellulose show promising results. Their cell efficiency value ranges from 4.5 to 7%. Table 4 also mentions various modifications that have been carried out to improve cell performance. The presence of an ionic liquid can increase the conductivity and improve the charge transfer. Singh et al. investigated the influence of a 1-ethyl-3-methylimidazolium ionic liquid in an agarose-based electrolyte. This ionic liquid increased the short circuit current from 1 mA cm^{-2} to 3.3 mA cm^{-2}. Moreover, Huang et al. showed that the presence of a 1-methyl-3-hexylimidazolium iodide (MHII) ionic liquid in cyanoethylated hydroxypropyl cellulose (CN-HPC) reduced the charge recombination between redox couple species and the oxide semiconductor surface due to the bulky structure of

Table 2. The summarized research on chlorophyll-based DSSCs.

No	Sources	Solvent of extraction	Modification	Photoanodes	Counter electrode	Redox couple	Electrolyte Solvent	J_{SC} (mA/cm^2)	V_{OC} (V)	FF	η (%)	Reference
1	Commercial chlorophyll from Sigma	-	Replaced Mg^{2+} with Cu^{2+}	TiO_2	Pt-foil	KI, I_2	80%ethylene carbonate and 20% propylene carbonate	0.54	0.42	-	2.6	[80]
2	Commercial chlorine-e6 derived from chlrophyll extracted from *Spirullina*	-	-	TiO_2 nanocrystalline	C-OTE	KI, I_2	Ethylene glycol/ acetonitrile	0.305	0.43	0.45	0.73	[79]
3	Spinach leave (*Spinacia oleracea L.*)	Ethanol T = 50 °C	-	TiO_2 nanofluid	Plate of lower conductive glass	I^-/I_3^-	Acetonitrile	0.467	0.55	0.51	0.13	[81]
	Ipomoea (*Ipomoea carnea*)	Ethanol T = 50 °C						0.914	0.54	0.56	0.28	
		Ethanol T = 50 °C pH = 3						0.915	0.51	0.55	0.25	
		Ethanol T = 50 °C pH = 2						0.982	0.54	0.56	0.29	
		Ethanol T = 50 °C pH = 1						1.120	0.57	0.59	0.32	
4	*Spirulina geitleri*	Methanol Modification function group (hydrocarbon) by transesterification using methyl esther	Chlorine-1 (methyl)	TiO_2 NPs	Pt wire	BMII, I_2, Additive: GNCS, TPB	Acetonitrile-valeronitrile	15	0.60	0.72	6.5	[82]
			Chlorine-2 (hexyl)					15.5	0.62	0.73	7.0	
			Chlorine-3 (dodecyl)					17.4	0.64	0.72	8.0	
			Chlorine-4 (2-butyloctyl)					13.9	0.65	0.74	6.6	
			Chlorine-5 (cholesteryl)					13.6	0.64	0.70	6.1	
5	Pomegranate leaves (*Punica granatum L.*)	Ethanol	-	TiO_2 NPs	Pt-thin film on FTO	I_2, LiI Additive: TBP	Acetonitrile	2.05	0.56	0.52	0.59	[83]
6	Pandan leaves (*Pandanus amaryllifolius*)	Ethanol-tartaric acid	-	TiO_2	Pt-FTO	NaI	PVDF-HFP	1.91	0.48	0..56	0.51	[84]
7	Spinach (*Spinacia oleracea L.*)	Ethanol using ultrasonic technique	-	TiO_2	Graphite-ITO	I^-/I_3^-	Acetonitrile	0.32	0.38	0.36	1–2	[85]
		water using ultrasonic technique						0.35	0.44	0.49		
8	Marigold leaves (*Tagetes patula*)	Water	Effect dipping time of ZnS in dye solution	ZnS (0 h)	Graphite	S^{2-}/S_n^{2-}	NaOH–Na_2S	0.297	0.21	0.30	0.05	[86]
				ZnS (2 h)				0.400	0.23	0.21	0.05	
				ZnS (4 h)				0.463	0.29	0.28	0.10	
				ZnS (6 h)				0.520	0.24	0.24	0.09	
				ZnS (8 h)				0.533	0.30	0.31	0.12	
9	Bryophyte	Ethanol	-	TiO_2	Pt-FTO	TPAI(2%)-I_2(0.17%w/w)	PAN-EC-PC	0.94	0.63	0.75	0.45	[87]
						TPAI(4%)-I_2(0.34%w/w)		4.08	0.54	0.58	1.27	
						TPAI(6%)-I_2(0.51%w/w)		5.51	0.53	0.53	1.52	
						TPAI(8%)-I_2(0.68%w/w)		6.10	0.53	0.51	1.66	
						TPAI(10%)-I_2(0.85%w/w)		5.78	0.6	0.57	1.97	
						TPAI(12%)-I_2(0.97%w/w)		5.96	0.62	0.50	1.86	

Table 3. The summarized research on anthocyanin based DSSCs.

No	Sources	Solvent of extraction	Photoanode	Counter electrode	Redox couple	Solvent of electrolyte	J_{SC} (mA/cm^2)	V_{OC} (V)	FF	η (%)	Reference
1	Henna leaves (*Lawsonia inermis*)	Ethanol	TiO_2	Pt	KI, I_2	Ethylene glycol-acetonitrile	1.87	0.59	0.58	0.66	[88]
		Ethanol-water					1.35	0.59	0.65	0.52	
2	*Canna indica*	Ethanol-water	TiO_2	Pt	LiI, I_2, TBP and BMII	Acetonitrile-valeronitrile	0.82	0.54	0.59	0.29	[89]
	Salvia splendens						0.7	0.56	0.61	0.26	
	Cow berry (*Vaccinium vitis-idaea*)						0.4	0.56	0.54	0.13	
	Solanum nigrum						1.01	0.54	0.51	0.31	
3	Mulberry Fruits (*Morus nigra*)	Metanol:water:acetic-acid: 25:21:4	P25 TiO_2	Purified SWCNTs	I^-/I^{3-}	Acetonitrile	2.65	0.59	0.51	0.67	[90]
				SWCNTs			2.41	0.47	0.38	0.42	
				Purified MWCNTs			3.12	0.48	0.39	0.52	
				MWCNTs			1.71	0.51	0.44	0.39	
4	Roselle (*Hibiscus sabdariffa*)	Citric acid	TiO_2	Pt	I^-/I^{3-}	Acetonitrile	4.8	0.45	0.43	0.92	[28]
			Na–TiO_2 (6%)				5.5	0.55	0.55	1.65	
			Na(6%)-Yeast (4%)-TiO_2				6.2	0.58	0.60	2.17	
			Na(6%)-Yeast (6%)-TiO_2				6.9	0.62	0.56	2.40	
5	Mangosteen pericarp (*Garcinia mangostana L.*)	Methanol:HCl (99:1) + add benzoic acid (1:0)	TiO_2 NTs	Pt	I^-/I^{3-}	Acetonitrile	0.0069	0.26	0.39	0.23	[91]
		Methanol:HCl (99:1) + add benzoic acid (1:0.5)					0.0125	0.16	0.36	0.23	
		Methanol:HCl (99:1) + add benzoic acid (1:0.8)					0.0043	0.31	0.66	0.29	
		Methanol:HCl (99:1) + add benzoic acid (1:1)					0.0065	0.36	0.48	0.37	
6	Seduduk fruit *(Malabtrichum Melastoma L)*	Ethanol-HCl	P25 TiO_2	C	NaI,I_2	PEG	-	-	-	0.62	[92]
		Ethanol-HCl with salicylic acid								1.32	
7	*Vaccinium meridionale*	Ethanol-water bu procalation method	P25 TiO_2	Pt	KI, I_2, $KClO_4$	Acetonitrile	-	-	-	-	[93]
8	Jabuticaba fruits (*Plinia cauliflora*)	Absolute ethanol	TiO_2 (doctorblade)	C	I_2, KI	PVP	0.23	0.35	0.23	0.08	[94]
			TiO_2 (spin coating)				0.38	0.41	0.29	0.13	

MHII compared to I^- [118]. The addition of Co_3O_4, NiO, and TiO_2 nanoparticles can also improve conductivity [119]. The presence of cross-linking networks between nanoparticles and polymers facilitates ion transport within the polymer matrix. The addition of nanoparticles can also be detrimental due to the formation of nanoparticle aggregates [120].

3.2. Structural aspects of biopolymer for quasi-solid DSSC

All of the biopolymers mentioned previously, which are widely applied to polymer gel electrolytes, are polysaccharides. These biopolymers consist of the hexa-pyranose building block of D-glucose as a monomer with various glycosidic linkages, either α-1,3 or β-1,4. In chitin or chitosan, D-glucose is substituted by amine or acetyl amine groups. Table 5 presents the chemical structure information and conductivity of these biopolymers.

The hydroxyl groups in polymer chains are responsible for establishing the bond with the ionic species in the electrolyte, which subsequently contributes to the ionic conductivity [121, 122, 123]. Furthermore, the functional groups on the polymer chain play an essential role in creating the bond with the liquid as a dispersed phase in the gelation process [124]. The gel polymer electrolyte system in a DSSC consists of the polymer matrix and liquid. The polymer matrix acts as the immobilizer or dispersion medium, while the liquid functions as a dispersed phase. Liquid can also function as a solvent for ionic species or redox couples. The interaction of these three components is vital for charges to be transferred to ensure good cell performance. One of the studies on this topic was conducted by Shih et al., where the interfacial interaction of iodide as a redox couple and agarose as a polymer matrix was investigated. The XPS study confirmed the formation of polyiodide in the electrolyte, which benefited the charge transfer channels after adding TiO_2 nanoparticles into the electrolyte gel system [119].

Molecular–level studies concerning this background are necessary. Unfortunately, only a small number of previous studies that are relevant to natural polymer systems were found. Yoon et al. theoretically observed the interaction between the ionic liquid 1-propyl-3-methyl imidazolium iodide (PMII) and the synthetic polymer poly(styrene-block-ethylene oxide-block-styrene) (SEOS) to investigate the complex structure of PMII and SEOS during the interaction stages. This experiment will then be used to explain the typical bonding and charge transfer [125]. Thus, to do so, further studies in natural polymer systems are still needed.

3.3. Remarks on biopolymer quasi solid DSSCs

Biopolymer electrolytes for DSSCs have been chosen as a solution to overcome the shortcomings of liquid electrolytes, such as solvent volatilization, poor stability due to leakage or counter electrode corrosion,

Table 4. The summary of various researches reported on the biopolymer-based quasi solid DSSC.

No	Biopolymer as Gel electrolyte	Modification biopolymer	Electrolyte solvent	Redox couple	Photoanode	Counter electrode	Dye	Conductivity (mS/cm)	J_{SC} (mA/cm^2)	V_{OC} (V)	FF	η (%)	Reference
1	Agarose	Ratio agarose (%)	1-methyl-2-pyrrolidinone (NMP)	I_2,LiI	P25 TiO_2	Pt	-						[116]
		1						0.28	6.16	0.58	0.67	3.20	
		1.5						0.39	7.56	0.62	0.63	3.97	
		2						0.36	8.24	0.60	0.62	4.14	
		2.5						0.32	5.16	0.63	0.69	3.01	
		3						0.65	5.32	0.62	0.64	2.83	
		4						-	4.44	0.63	0.72	2.73	
		5						0.66	2.12	0.68	0.78	1.49	
		Ratio TiO_2 in agarose (%)											
		0						0.30	7.76	0.66	0.53	3.77	
		2.5						0.44	10.96	0.55	0.57	4.74	
		5						0.51	8.84	0.55	0.56	4.45	
		7.5						0.33	9.20	0.55	0.52	3.64	
		10						0.34	9.04	0.57	0.48	3.42	
		-	NMP	10%LiI, I_2	P25 TiO_2	Pt	N719	1.99	Not measured				[212]
				15%LiI, I_2				3.16					
				20%LiI, I_2				3.98					
				25%LiI, I_2				2.39					
				30%LiI, I_2				3.31					
				35%LiI, I_2				3.89					
				65%LiI, I_2				5.62					
				85%LiI, I_2				5.62					
		-	DMSO/PC	GuSCN, NMBI, I_2	P25 TiO_2	Pt	N719	14.2	4.65	0.73	0.58	1.97	[213]
			DMSO/4EG					4.4	3.69	0.65	0.57	1.38	
			DMSO/3EG					4.6	4.01	0.61	0.57	1.39	
			DMSO/PEG					6.2	3.21	0.58	0.57	1.06	
			DMSO (20v%)					5.0	3.69	0.58	0.54	1.15	
		0.5% agarose	PC/DMSO (8:2)	MPII	Double-layer TiO_2	Pt	N719	-	11.73	0.70	0.64	5.25	[214]
				AEII					11.71	0.72	0.65	5.45	
				APII					11.53	0.70	0.62	4.97	
				DAII					11.84	0.70	0.60	4.96	
		0wt% agarose		AEII					12.26	0.66	0.60	4.97	
		0.5wt% agarose							11.71	0.72	0.65	5.45	
		0.65wt% agarose							11.45	0.76	0.68	5.89	
		0.8wt% agarose							11.82	0.75	0.64	5.68	
		1.0wt% agarose							11.96	0.70	0.63	5.31	
		0 mT NiO-agarose	NMP	LiI, I_2	P25 TiO_2	Pt	N719	-	4.5	0.77	0.45	1.61	[215]
		14 mT NiO-agarose							4.7	0.80	0.56	2.32	
		25 mT NiO-agarose							5.9	0.74	0.64	2.95	

(*continued on next page*)

Table 4 (*continued*)

No	Biopolymer as Gel electrolyte	Modification biopolymer	Electrolyte solvent	Redox couple	Photoanode	Counter electrode	Dye	Conductivity (mS/cm)	J_{SC} (mA/cm^2)	V_{OC} (V)	FF	η (%)	Reference
		35 mT NiO-agarose							6.0	0.77	0.62	2.94	
		45 mT NiO-agarose							4.2	0.76	0.61	2.24	
		55 mT NiO-agarose							2.5	0.78	0.70	1.37	
		-	PC/DMSO	AEII, GuSCN, NMBI, I_2	a-TiO_2	Pt	N719	-	10.39	0.80	0.71	5.89	[216]
					a-TiO_2 + 30% PEG (0 min)				13.29	0.74	0.66	6.54	
					a-TiO_2 + 30% PEG (30 min)				14.18	0.74	0.69	7.18	
					a-TiO_2 + 30% PEG (60 min)				14.32	0.75	0.69	7.43	
					a-TiO_2 + 30% PEG (90 min)				14.57	0.73	0.68	7.28	
					a-TiO_2 + 30% PEG (120 min)				13.89	0.74	0.68	7.04	
					a-TiO_2 + 30% PEG (150 min)				11.36	0.68	0.65	4.98	
		TiO_2-agarose	NMP	LiI,I_2	TiO_2 NPs	Pt	N719	2.66	5.28	0.61	0.55	1.71	[120]
		Co_3O_4-agarose						4.37	7.24	0.64	0.46	2.11	
		NiO-agarose						3.33	6.20	0.63	0.52	2.02	
		-	NMP/MPN	LiI,I_2, PMI, NMBI	TiO_2 NPs	Pt	Ruthenizer 520-DN	14.09	10.7	0.82	-	4.9	[119]
		Agarose						8.31	10.7	0.78	-	-	
		TiO_2-agarose						12.12	11.8	0.80	-	5.1	
		-	DMSO	KI, I_2	TiO_2	Pt	N_3 dye	-	1.00	0.57	0.56	0.33	[217]
				KI, I_2, IL					1.90	0.75	0.77	0.47	
			DMF	KI, I_2					1.00	0.63	0.60	0.72	
				KI, I_2, IL					3.30	0.62	0.66	1.36	
2	Kappa-Carrageenan	Carboxymethyl kappa-carrageenan/ wt-carboxymethyl cellulose:NH_4I (30% wt)	Acetic acid	NH_4I, I_2	TiO_2	Pt	N719	2.41	0.42	0.50	0.64	0.13	[218]
		Carboxymethyl kappa-carrageenan/ wt-carboxymethyl cellulose:LiI (10% wt)	Acetic acid	LiI, I_2	TiO_2	Pt	N719	1.66	0.05	0.50	0.90	0.02	[219]
		Carboxymethyl kappa-carrageenan/ wt-carboxymethyl cellulose:LiI (20% wt)						2.73	0.12	0.49	0.80	0.05	
		Carboxymethyl kappa-carrageenan/ wt-carboxymethyl cellulose:LiI (30% wt)						3.89	0.40	0.49	0.57	0.11	
3	Iota Carrageenan	-	Water	NaI, I_2	TiO_2	Pt	N719	-	2.58	0.41	0.60	0.63	[220]
		Iota carrageenan +10%wt ionic liquid							3.63	0.43	0.42	0.64	
		Iota carrageenan +20%wt ionic liquid							2.71	0.45	0.54	0.65	
		Iota carrageenan +30%wt ionic liquid							3.38	0.46	0.47	0.72	
		Iota carrageenan +40%wt ionic liquid							1.74	0.43	0.54	0.40	
4	Chitosan	27.5%wt chitosan	DMF	22.5% wt NH_4I – 50%wt I_2	TiO_2	Pt	Anthocyanin	1.51	0.76	0.38	0.48	0.14	[114]

(*continued on next page*)

Table 4 (*continued*)

No	Biopolymer as Gel electrolyte	Modification biopolymer	Electrolyte solvent	Redox couple	Photoanode	Counter electrode	Dye	Conductivity (mS/cm)	J_{SC} (mA/cm^2)	V_{OC} (V)	FF	η (%)	Reference
		11%wt chitosan		9% wt NH_4I – 80%wt I_2				3.02	0.90	0.37	0.45	0.15	
		11%wt of chitosan-PEO (ratio 30:70)		9% wt NH_4I – 80%wt I_2				5.52	1.21	0.40	0.47	0.23	
		adding PEG as plasticiszer	Formic acid	KI, I_2	$Bi_2Ti_2O_7$	Pt	N719	-	2.72	0.63	0.36	0.73	[221]
					$Bi_2Ti_2O_7$: 2% Sm				3.65	0.69	0.49	1.45	
					$Bi_2Ti_2O_7$: 2% Eu				8.42	0.72	0.39	2.77	
					$Bi_2Ti_2O_7$: 2% Gd				8.36	0.72	0.55	3.88	
					$Bi_2Ti_2O_7$: 2% Dy				8.83	0.74	0.50	3.86	
					$Bi_2Ti_2O_7$: 2% Ho				5.90	0.72	0.52	2.58	
					$Bi_2Ti_2O_7$: 2% Er				6.36	0.67	0.43	2.18	
		Chitosan	Acetic acid	KI, I_2	TiO_2	Pt	N719	-	1.29	0.62	0.82	0.66	[222]
		Chitosan NPs by ultrasonication methods							2.18	0.58	0.78	0.99	
		Chitosan NPs by ionic gelatin methods							3.66	0.55	0.61	1.23	
		Hexanoyl chitosan/PVC	THF	20%NaI, I_2	TiO_2	Pt	N719	-	5.31	0.63	0.54	1.80	[223]
				30%NaI, I_2					8.62	0.58	0.59	2.93	
				40%NaI, I_2					6.32	0.67	0.62	2.59	
				30%NaI, I_2, GuSCN, TBP					17.69	0.65	0.46	5.31	
5	Cellulose	-	Acetonitrile	LiI, I_2, TBP, TBAI	TiO_2	Pt	N719	-	17.05	0.67	0.57	6.51	[224]
		Adding 3.5 wt% ethyl cellulose as gelator							14.94	0.70	0.61	6.37	
		Adding 5.8 wt% ethyl cellulose as gelator							14.91	0.68	0.59	5.98	
		Adding 8.8 wt% ethyl cellulose as gelator							14.23	0.68	0.57	5.51	
		Grafted cellulose	-	KI, I_2	TiO_2	Pt	Ru dye		12.65	0.71	0.61	5.51	[225]
		CN-HPC (cyanoethylated hydroxypropyl cellulose)	MPN	MHII, LiI, I_2, TBP	TiO_2 adding MgO	Pt	N719	-	13.67	0.74	0.69	7.02	[118]
							SD2		12.17	0.74	0.75	6.76	
				MHII, LiI, I_2, TBP			N719		14.40	0.76	0.70	7.55	
							SD2		12.65	0.78	0.75	7.40	
		3% micro-cellulose	-	LiI, I_2, MPII, EMISCN, TBP	TiO_2	Pt	N719	-	5.45	0.54	0.60	1.75	[226]
		4% micro-cellulose							5.42	0.53	0.57	1.64	
		5% micro-cellulose							7.37	0.61	0.58	2.69	
		6% micro-cellulose							7.47	0.58	0.61	2.62	
		0%-Nanoscale microfibrillated cellulose	Acetonitrile	NaI, I_2, TBP	TiO_2	Pt	N719	-	11.7	0.65	0.59	4.42	[227]
		5%-Nanoscale microfibrillated cellulose							11.9	0.68	0.58	4.71	
		10%-Nanoscale microfibrillated cellulose							12.3	0.71	0.59	5.11	
		20%-Nanoscale microfibrillated cellulose							13.2	0.73	0.60	5.84	

(*continued on next page*)

Table 4 (*continued*)

No	Biopolymer as Gel electrolyte	Modification biopolymer	Electrolyte solvent	Redox couple	Photoanode	Counter electrode	Dye	Conductivity (mS/cm)	J_{SC} (mA/cm^2)	V_{OC} (V)	FF	η (%)	Reference
		30%-Nanoscale microfibrillated cellulose							15.2	0.76	0.61	7.03	
		0%-cellulose nanocrystall	water	NaI, I_2, TBP	TiO_2	Pt	Cu based dye	-	0.3	0.63	0.48	0.08	[228]
		5%-cellulose nanocrystal							1.9	0.49	0.27	0.26	
		10%-cellulose nanocrystal							2.5	0.51	0.30	0.39	
		20%-cellulose nanocrystal							2.6	0.53	0.39	0.54	
		40%-cellulose nanocrystall							2.3	0.57	0.67	0.89	
		60%-cellulose nanocrystal							2.8	0.57	0.60	0.96	
		80%-cellulose nanocrystal							2.8	0.58	0.66	1.09	
		100%-cellulose nanocrystall							2.0	0.60	0.50	0.61	
		Hydroxylpropyl cellulose (HPC) and EC/PC as plasticizer	-	NaI	P25 TiO_2	Pt	N719	4.94	13.65	0.49	0.58	3.94	[229]
				NaI-40%wt MPII				5.85	11.69	0.58	0.62	4.23	
				NaI-60%wt MPII				5.79	12.72	0.55	0.61	4.27	
				NaI-80%wt MPII				5.93	13.20	0.58	0.63	4.80	
				NaI-100%wt MPII				6.49	14.71	0.57	0.63	5.19	
				NaI-100%wt MPII				7.37	13.73	0.61	0.69	5.79	
		Cellulose nanocrystal blend with POEGMA	Sulfuric acid	HSE-EL, MPN	TiO_2	Pt	Dyesol (Ru dye)	-	13.6	0.69	0.53	4.98	[230]

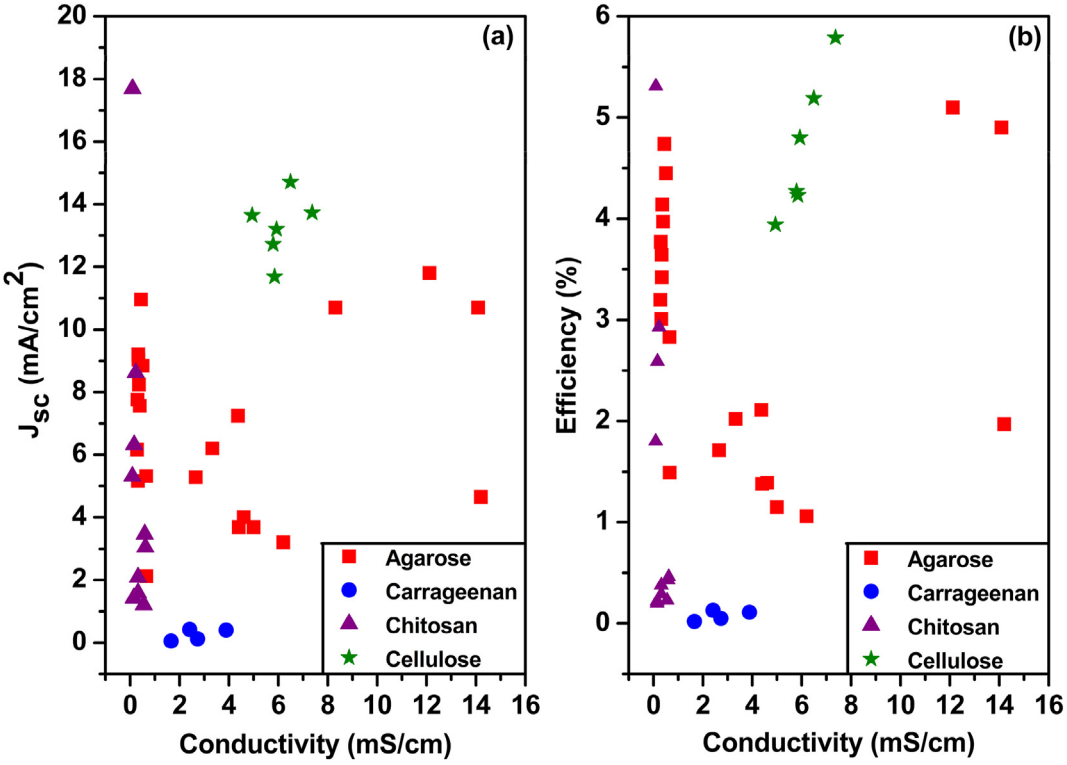

Figure 4. The map of conductivity towards the cell performance various biopolymer based DSSC.

Table 5. The most used biopolymers as electrolyte in quasi-solid DSSC.

Biopolymer	Monomer unit	Linkage	Dimer	Electrolyte	Conducti-vity value (S/cm)	Referen-ce
Agarose	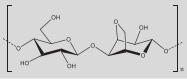	α-1,3 β-1,4	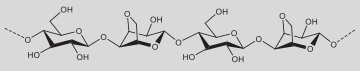	LiI/I_2 (2.5 wt%)	3.94×10^{-4}	[116]
Carrageenan	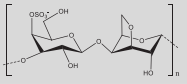	α-1,3 β-1,4	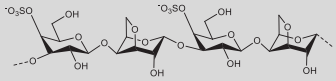	-	2.79×10^{-6}	[231]
				NH_4I/I_2	2.41×10^{-3}	[218]
	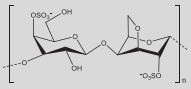		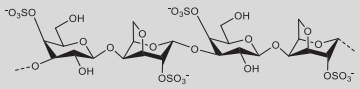	$MgTf_2$: AmNTFSI (27:10 wt%)	9.25×10^{-5}	[232]
Cellulose	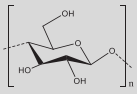	β-1,4	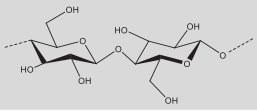	-	9.33×10^{-9}	[233]
				$(NH_4)_2CO_3$ (11 wt%)	2.28×10^{-6}	
Chitin	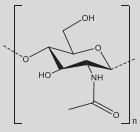	β-1,4	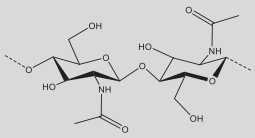	-	1.55×10^{-9}	[234]
Chitosan	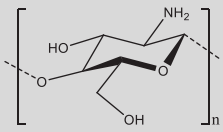	β-1,4	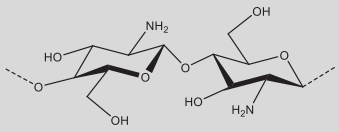	NH_4I/I_2	5.52×10^{-3}	[114]

and dye photodegradation. The improvement of biopolymers for quasi-solid DSSCs is focused on increasing ionic transport through the polymer matrix. As mentioned in the previous section, the modeling or computational studies will be a good choice to study the interaction of responsible species involved in charge transfer.

4. Natural carbon for DSSC counter electrode

The high cost and rarity of platinum as the counter electrode in DSSCs prompts one to replace the noble metal with an alternative conducting material with a relative or similar efficiency. However, platinum-based

DSSCs remain the benchmark for assessing the performance of DSSCs [48, 62]. Thus far, several materials have been employed as alternative replacements of platinum as the counter electrode. These include carbonaceous materials [62, 126], conducting polymers [127, 128], transition metal carbides, nitrides, oxides, sulfides [129], and alloys [130].

Among the proposed materials for the platinum replacement of the DSSC counter electrode, carbonaceous or carbon-based materials remain one of the most studied platinum-replacement counter electrode candidates for DSSCs [62] due to their remarkable intrinsic chemical and physical characteristics, such as a high surface area, high catalytic activity, high electrical conductivity, excellent thermal stability, and good corrosion resistance, accompanied by their beneficial economic and environmental aspects. Due to the versatility of carbon-based materials, they are employed not only as counter electrodes in DSSCs but also as electrodes in electrochemical capacitors (supercapacitors) [131], and Li-ion batteries [132].

The usage of carbon-based materials dates back to the original formulation of the DSSC by the Grätzel research group [133]. Grätzel and coworkers employed a graphite powder/carbon black composite attached to a SnO_2 (TO) substrate as a counter electrode with a standard DSSC arrangement of I_2/I_3^- electrolyte and TiO_2 (anatase) photoelectrode, achieving a power conversion efficiency (PCE) of 6.7%. The encouraging results on the PCE of the low-cost carbon-based counter electrode prompted researchers to further develop the carbon-based counter electrodes by employing new microstructures of carbon materials such as porous carbon, carbon nanotube, graphene, and carbon nanofiber [61, 134, 135, 136, 137, 138, 139, 140, 141, 142, 143, 144, 145, 146, 147, 148, 149, 150, 151, 152, 153, 154, 155, 156, 157], modifying of the existing phases such as doping or functionalizing with heteroatoms [158, 159, 160, 161] or incorporating with other materials like silica [162].

In the context of the current review, natural products such as biomass have become essential sources of carbon-based materials. Biomasses are undoubtedly rich in carbonaceous materials, yet their low retrieval cost and high availability make them promising candidates for the mass production of carbon-based materials and waste valorization. There are at least 60 different biomass sources for carbon-based electrodes employed in supercapacitors, Li-ion batteries, and fuel cells, as summarized in a recent review [163]. In environmental applications, biomass-derived carbon materials have become routinely employed as adsorbents for dyes, heavy metals, and so on [164, 165] in water and wastewater, owing to their large surface area and active adsorption sites.

This section will discuss natural product-derived counter electrodes to gain insight into the relationship between the synthetic method, structure, and performance in DSSC cells. Figure 5 and Table 6 show the available literature on counter electrodes from various biomasses, wastes, and commercial biomasses, which will be included in the discussion. Interestingly, most of, if not all, the literature comes from authors who reside in Asia, more specifically, East and Southeast Asian countries. Due to the high diversity of primary natural resources from these regions, the current review results may benefit researchers from these countries to valorize natural products as more functional materials. It is worth mentioning that the natural products discussed here are not necessarily waste but also commercially produced biomass such as humic acid and ovalbumin.

4.1. Preparation of counter electrode materials from natural products

As listed in Table 6, a wealth of natural product resources is available for counter electrodes. Describing detailed procedures of the material extraction and counter electrode fabrication for each study would be too exhaustive. Nevertheless, this subsection will present the general trend of the resulting products with each of the preparation routes of counter electrode materials.

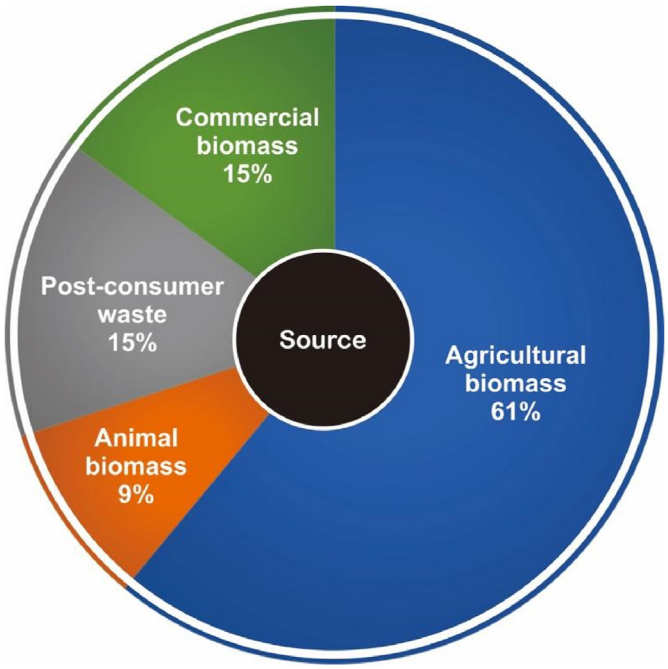

Figure 5. Typical sources for counter electrode materials from natural products based on the number of available articles.

Table 6. Various available sources for carbon electrode derived from natural products.

Type	Source	References
Agricultural biomass	Rice husk	[165, 235, 236]
	Coconut shell	[170, 237, 238]
	Pumpkin stem	[183]
	Mangosteen peel	[167]
	Pine cone flower	[239]
	Various leaves	[240, 241, 242]
	Various woods	[241, 243]
	Sunflower stalk	[173]
	Aloe peel	[174, 175, 176, 177, 178, 179, 180]
	Kelp	[244]
	Orange fiber	[185]
	Pomelo peel	[181]
Animal biomass	Fish	[166, 245]
	Human hair	[246]
Post-consumer waste	Ground coffee	[188]
	Facial tissue	[241]
	Paper	[241]
	Carton	[182]
Commercial biomass	Bagasse	[171]
	Table sugar	[184]
	Sucrose	[184]
	Humic acid	[247]
	Ovalbumin	[248]

It seems evident that natural product resources mostly contain carbon obtained from macromolecule constituents. As seen from Figure 6, the extracted materials for counter electrodes from the literature are primarily carbon-based materials, with several types ranging from porous carbon to biochar, depending on the preparation route and sources. They can be categorized based on different chemical compositions, porous sizes, and surface areas. Other extracted materials include silicon or silica-based materials, such as rice husk ash, which seem to gain less attention due to more unsatisfactory DSSC performance than carbon-based materials.

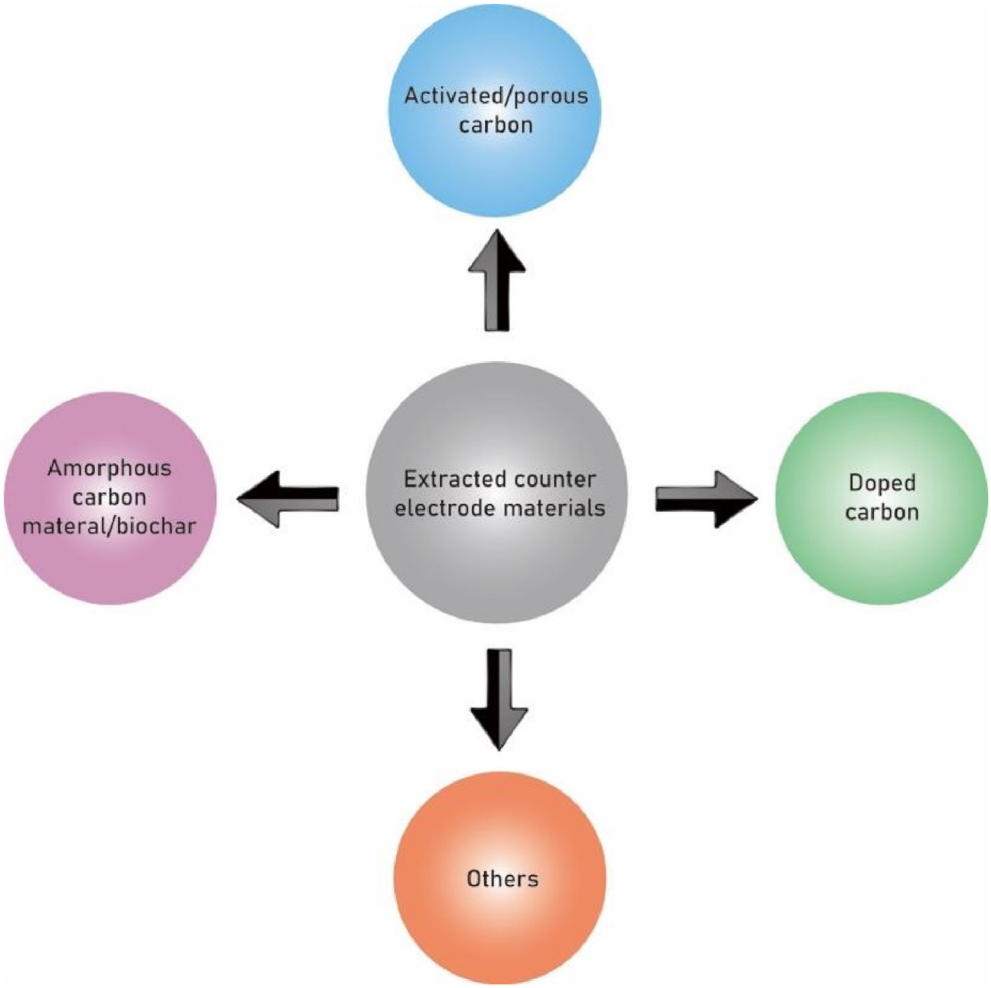

Figure 6. Typical counter electrode materials extracted from natural products and from literature.

The types of extracted carbon-based materials based on morphology are explained in greater detail in this section. These materials can be divided into two groups: inactivate carbon material and porous carbon material. However, the naming for the former is somehow quite ambiguous across the literature. Inactivate carbon material in this review refers to carbon material that is mainly prepared by carbonization techniques, such as heat treatment (pyrolysis), without any further treatment apart from washing and/or drying. By this definition, the simple "carbon material," amorphous carbon material, and biochar listed in Table 7 belong to this group. Spherical carbon materials can also be categorized into this group. The second group seems to have a more obvious definition. The carbon-based materials in this group have porous structures, as revealed mostly by SEM images, and quantitatively, the total porous size. More specifically, the materials usually have a mesoporous structure. According to the morphology, activated carbon and porous carbon belong to the second group of carbon-based materials.

Generally, the preparation of carbon-based counter electrode materials usually involves several procedures, including pretreatment, carbonization, and activation. Figure 7 summarizes the general procedure for preparing carbon-based counter electrode materials. The pretreatment step is conducted to remove impurities and water, which can be achieved by washing, drying, and mechanical treatments such as cutting, grinding, and sieving. The second procedure is carbonization, which occurs through high-temperature annealing under an inert atmosphere (pyrolysis) and hydrothermal carbonization. The former carbonization technique will yield amorphous carbon, charcoal, and biochar, while the latter gives the spherical carbon morphology.

Depending on the intended final target material, further activation and carbonization may be conducted to enhance the surface area and develop the pores, carried out by either physical or chemical activation to prepare "porous carbon". The resulting "inactivate carbon material" is usually mixed with chemical activators such as KOH and $ZnCl_2$, followed by further heating at high temperatures. The base can react with the carbon to develop pores within the carbon structure. Simultaneous physical activation and carbonization, along with chemical activation, can be carried out by microwave treatment.

One issue regarding the utilization of natural products is their inhomogeneous content, which can bring either benefits or drawback to the extraction processes of the intended counter electrode material and DSSC performance. The impurities contained in the source have to be removed using harsh chemicals if necessary. On the other hand, impurities can also benefit DSSC performance due to the introduction of defective sites into the counter electrode structure, enhancing the electrocatalytic activities. Another issue is the reproducibility of the material extracted from the natural product, where the material obtained can have a different structure, morphology, and surface area. However, there seems to be a consistent preparation route for porous carbon. While the resulting materials have a quantitatively different surface area, the characterization reveals that they belong to a similar class of porous carbon.

4.2. The performance of the natural carbon-based DSSC

Table 7 lists the photovoltaic performances of DSSC devices that used counter electrodes derived from natural products. Before further

Table 7. Photovoltaic parameters of DSSCs based on the various counter electrodes in comparison with standard Pt counter electrode.

Source	Counter electrode material	Natural product-based counter electrode				Pt counter electrode				Electrolyte solution	Photoanode/ Dye	Reference
		J_{sc} ($mA{\cdot}cm^{-2}$)	V_{oc} (V)	*FF* (%)	η (%)	J_{sc} ($mA{\cdot}cm^{-2}$)	V_{oc} (V)	*FF* (%)	η (%)			
Rice husk	Porous carbon	14.53	0.680	64	6.32	14.61	0.69	66	6.69	LiI/I_2/1-methyl-3-hexylimidazolium iodide/4-tert-butylpyridine in 3-methoxypropionitrile	TiO_2/N3	[165]
Rice husk	ACs/ Acetylene Black	15.01	0.73	60	6.57	15.20	0.74	64	7.20	LiI/I_2/1-methyl-3-propyl imidazolium iodide/4-tert-butyl pyridine/guanidinium thiocyanate in acetonitrile and valeronitrile (85:15)	TiO_2/N719	[235]
Rice husk	Nano-Si@ACs/ Acetylene Black	15.50	0.76	67	8.01	15.20	0.74	64	7.20	LiI/I_2/1-methyl-3-propyl imidazolium iodide/4-tert-butyl pyridine/guanidinium thiocyanate in acetonitrile and valeronitrile (85:15)	TiO_2/N719	[235]
Rice husk	Rice husk ash/MoS_2	10.95	0.60	32	2.10	-	-	-	-	Phtaloychitosan electrolyte polymer/DMF/ethylene carbonate/ tetrapropylammonium iodide/I_2	TiO_2/N3	[236]
Coconut shell	Amorphous activated carbon	7.60	0.77	32	0.84	-	-	-	-	LiI/I_2/4-tertbutylpyridine in acetonitrile	TiO_2/N719	[237]
Coconut shell	Graphitic carbon	10.00	0.77	36	1.24	-	-	-	-	LiI/I_2/4-tertbutylpyridine in acetonitrile	TiO_2/N719	[237]
Coconut shell	Activated charcoal	19.49	0.65	62	7.85	19.52	0.69	70	9.41	LiI/I_2/1,2-dimethyl-3-propyl imidazolium iodide/ tert-butylpyridine in acetonitrile	TiO_2/N719	[170]
Pumpkin stem	Activated carbon	3.84	0.611	0.475	2.79	4.54	0.736	49.3	4.04	KI/I_2 in ethylene glycol	TiO_2/N719	[183]
Mangosteen peel	Carbon material	5.58	0.70	0.51	1.99	5.42	0.62	52	1.75	NaI/I_2/Li_2CO_3 in acetonitrile	TiO_2/ Mangosteen peel exctract	[167]
Mangosteen peel	Carbon material	8.70	0.60	50	2.63	4.72	0.57	54	1.47	di-5-(1-methyltetrazole)/5-mercapto-1-methyltetrazole N-tetramethylammonium salt)/4-tert-butylpyridine/ $LiCO_4$ in acetonitrile	TiO_2/ Mangosteen peel exctract	[167]
Pine cone flower	honeycomb-like activated porous carbon	13.51	0.71	52	4.98	14.29	0.71	62	6.25	HPE	TiO_2/N719	[239]
Fallen leaves	Honeycomb porous carbon	14.99	0.70	53	5.52	15.96	0.70	58	6.56	HPE	TiO_2/N719	[240]
Lotus	Biochar	14.33	0.44	23	1.42	-	-	-	-	LiI/I_2/4-tert-butylpyridine in 3-methoxypropionitrile	TiO_2/N719	[242]
Lotus	Biochar	1.50	0.43	23	0.15	1.05	0.52	66	0.36	LiI/I_2/4-tert-butylpyridine in 3-methoxypropionitrile	TiO_2/Lotus leaf exctract	[242]
Weeping willow wood	Amorphous carbon	11.31	0.67	21	1.55	15.81	0.64	62	6.23	LiI/I_2/4-tert-butylpyridine in 3-methoxypropionitrile	TiO_2/N719	[241]
Phoenix wood	Amorphous carbon	12.14	0.65	24	1.91	15.81	0.64	62	6.23	LiI/I_2/4-tert-butylpyridine in 3-methoxypropionitrile	TiO_2/N719	[241]
Camphor wood	Amorphous carbon	11.31	0.64	22	1.58	15.81	0.64	62	6.23	LiI/I_2/4-tert-butylpyridine in 3-methoxypropionitrile	TiO_2/N719	[241]
Chinese fir wood	Amorphous carbon	10.79	0.65	20	1.38	15.81	0.64	62	6.23	LiI/I_2/4-tert-butylpyridine in 3-methoxypropionitrile	TiO_2/N719	[241]
Maple wood	Amorphous carbon	11.58	0.67	22	1.68	15.81	0.64	62	6.23	LiI/I_2/4-tert-butylpyridine in 3-methoxypropionitrile	TiO_2/N719	[241]
Peach wood	Amorphous carbon	11.42	0.67	19	1.48	15.81	0.64	62	6.23	LiI/I_2/4-tert-butylpyridine in 3-methoxypropionitrile	TiO_2/N719	[241]
Poplar wood	Amorphous carbon	12.15	0.62	24	1.83	15.81	0.64	62	6.23	LiI/I_2/4-tert-butylpyridine in 3-methoxypropionitrile	TiO_2/N719	[241]
Cypress wood	Amorphous carbon	10.94	0.67	17	1.23	15.81	0.64	62	6.23	LiI/I_2/4-tert-butylpyridine in 3-methoxypropionitrile	TiO_2/N719	[241]
Tea-oil camellia wood	Amorphous carbon	10.54	0.62	21	1.37	15.81	0.64	62	6.23	LiI/I_2/4-tert-butylpyridine in 3-methoxypropionitrile	TiO_2/N719	[241]

(*continued on next page*)

Table 7 (*continued*)

Source	Counter electrode material	Natural product-based counter electrode				Pt counter electrode				Electrolyte solution	Photoanode/ Dye	Reference
		J_{sc} (mA·cm^{-2})	V_{oc} (V)	*FF* (%)	η (%)	J_{sc} (mA·cm^{-2})	V_{oc} (V)	*FF* (%)	η (%)			
Orange wood	Amorphous carbon	12.19	0.67	22	1.81	15.81	0.64	62	6.23	LiI/I_2/4-tert-butylpyridine in 3-methoxypropionitrile	TiO_2/N719	[241]
Chinaberry wood	Amorphous carbon	12.58	0.64	21	1.66	15.81	0.64	62	6.23	LiI/I_2/4-tert-butylpyridine in 3-methoxypropionitrile	TiO_2/N719	[241]
Oak wood	Mesoporous carbon				7.98				7.93	LiI/I_2/1,2-dimethyl-3-propylimidazolium iodide/ 4-tert-butyl pyridine in acetonitrile	TiO_2/N719	[243]
Bamboo	Mesoporous carbon				4.53				7.93	LiI/I_2/1,2-dimethyl-3-propylimidazolium iodide/ 4-tert-butyl pyridine in acetonitrile	TiO_2/N719	[243]
Pine needles leaf	Amorphous carbon	10.14	0.62	17	1.07	15.81	0.64	62	6.23	LiI/I_2/4-tert-butylpyridine in 3-methoxypropionitrile	TiO_2/N719	[241]
Camphor leaf	Amorphous carbon	11.98	0.53	22	1.37	15.81	0.64	62	6.23	LiI/I_2/4-tert-butylpyridine in 3-methoxypropionitrile	TiO_2/N719	[241]
Palm leaf	Amorphous carbon	11.53	0.63	25	1.85	15.81	0.64	62	6.23	LiI/I_2/4-tert-butylpyridine in 3-methoxypropionitrile	TiO_2/N719	[241]
Maple leaf	Amorphous carbon	9.64	0.51	25	1.20	15.81	0.64	62	6.23	LiI/I_2/4-tert-butylpyridine in 3-methoxypropionitrile	TiO_2/N719	[241]
Poplar leaf	Amorphous carbon	10.96	0.49	25	1.33	15.81	0.64	62	6.23	LiI/I_2/4-tert-butylpyridine in 3-methoxypropionitrile	TiO_2/N719	[241]
Chinese fir leaf	Amorphous carbon	9.07	0.53	23	1.09	15.81	0.64	62	6.23	LiI/I_2/4-tert-butylpyridine in 3-methoxypropionitrile	TiO_2/N719	[241]
Red after-wood leaf	Amorphous carbon	10.07	0.62	18	1.14	15.81	0.64	62	6.23	LiI/I_2/4-tert-butylpyridine in 3-methoxypropionitrile	TiO_2/N719	[241]
Sunflower stalk	Layered activated carbon	15.20	0.67	64	6.56	15.77	0.70	65	7.19	LiI/I_2/1-butyl-3-methylimidazolium iodide/ 4-tert-butyl pyridine/ guanidinium thiocyanate in acetonitrile	TiO_2/N719	[173]
Aloe peel	Honeycomb-like porous carbon/ acetylene black	14.15	0.72	0.68	6.92	15.77	0.70	65	7.19	LiI/I_2/1-butyl-3-methylimidazolium iodide/ 4-tert-butyl pyridine/ guanidinium thiocyanate in acetonitrile	TiO_2/N719	[174]
Aloe peel	Spherical carbon	12.46	0.68	30	2.43	15.38	0.67	60	6.34	LiI/I_2/1-butyl-3-methylimidazolium iodide/ 4-tert-butyl pyridine/ guanidinium thiocyanate in acetonitrile	TiO_2/N719	[175]
Aloe peel	Spherical carbon/ $FeTa_2O_6$	15.16	0.70	65	6.85	15.38	0.67	60	6.34	LiI/I_2/1-butyl-3-methylimidazolium iodide/ 4-tert-butyl pyridine/ guanidinium thiocyanate in acetonitrile	TiO_2/N719	[175]
Aloe peel	Spherical carbon/ $CoTa_2O_6$	15.79	0.70	62	6.79	15.38	0.67	60	6.34	LiI/I_2/1-butyl-3-methylimidazolium iodide/ 4-tert-butyl pyridine/ guanidinium thiocyanate in acetonitrile	TiO_2/N719	[175]
Aloe peel	Spherical carbon/ $CuTa_{10}O_{26}$	15.19	0.68	63	6.53	15.38	0.67	60	6.34	LiI/I_2/1-butyl-3-methylimidazolium iodide/ 4-tert-butyl pyridine/ guanidinium thiocyanate in acetonitrile	TiO_2/N719	[175]
Aloe peel	Porous carbon	14.12	0.71	65	6.52	15.77	0.70	65	7.14	LiI/I_2/1-butyl-3-methylimidazolium iodide/ 4-tert-butyl pyridine/ guanidinium thiocyanate in acetonitrile	TiO_2/N719	[176]
Aloe peel	Porous carbon/ $ZnNb_2O_6$	19.12	0.71	65	8.83	15.77	0.70	65	7.14	LiI/I_2/1-butyl-3-methylimidazolium iodide/ 4-tert-butyl pyridine/ guanidinium thiocyanate in acetonitrile	TiO_2/N719	[176]

(*continued on next page*)

Table 7 (*continued*)

Source	Counter electrode material	Natural product-based counter electrode				Pt counter electrode				Electrolyte solution	Photoanode/ Dye	Reference
		J_{sc} (mA·cm^{-2})	V_{oc} (V)	*FF* (%)	η (%)	J_{sc} (mA·cm^{-2})	V_{oc} (V)	*FF* (%)	η (%)			
Aloe peel	Porous carbon	15.04	0.72	59	6.40	15.96	0.70	63	7.04	LiI/I_2/1-butyl-3-methylimidazolium iodide/ 4-tert-butyl pyridine/ guanidinium thiocyanate in acetonitrile	TiO_2/N719	[177]
Aloe peel	Porous carbon/ $MnWO_4$	15.52	0.69	68	7.33	15.96	0.70	63	7.04	LiI/I_2/1-butyl-3-methylimidazolium iodide/ 4-tert-butyl pyridine/ guanidinium thiocyanate in acetonitrile	TiO_2/N719	[177]
Aloe peel	Porous carbon/ $ZnWO_4$	17.12	0.69	65	7.61	15.96	0.70	63	7.04	LiI/I_2/1-butyl-3-methylimidazolium iodide/ 4-tert-butyl pyridine/ guanidinium thiocyanate in acetonitrile	TiO_2/N719	[177]
Aloe peel	Porous carbon/ $CuWO_4$	13.84	0.73	64	6.52	15.96	0.70	63	7.04	LiI/I_2/1-butyl-3-methylimidazolium iodide/ 4-tert-butyl pyridine/ guanidinium thiocyanate in acetonitrile	TiO_2/N719	[177]
Aloe peel	3D network carbon	14.86	0.62	66	6.07	15.76	0.65	66	6.74	LiI/I_2/1-butyl-3-methylimidazolium iodide/ 4-tert-butyl pyridine/ guanidinium thiocyanate in acetonitrile	TiO_2/N719	[178]
Aloe peel	3D network carbon/ $ZnMoO_4$	16.41	0.69	67	7.65	15.76	0.65	66	6.74	LiI/I_2/1-butyl-3-methylimidazolium iodide/ 4-tert-butyl pyridine/ guanidinium thiocyanate in acetonitrile	TiO_2/N719	[178]
Aloe peel	3D network carbon/ $Cu_2Mo_3O_9$	15.71	0.74	63	7.33	15.76	0.65	66	6.74	LiI/I_2/1-butyl-3-methylimidazolium iodide/ 4-tert-butyl pyridine/ guanidinium thiocyanate in acetonitrile	TiO_2/N719	[178]
Aloe peel	3D network carbon/ $MnMoO_4$	15.52	0.65	68	6.92	15.76	0.65	66	6.74	LiI/I_2/1-butyl-3-methylimidazolium iodide/ 4-tert-butyl pyridine/ guanidinium thiocyanate in acetonitrile	TiO_2/N719	[178]
Aloe peel	Porous carbon/MnO_2	12.81	0.73	64	6.11	13.32	0.72	66	6.44	LiI/I_2/1-butyl-3-methylimidazolium iodide/ 4-tert-butyl pyridine/ guanidinium thiocyanate in acetonitrile	TiO_2/N719	[179]
Aloe peel	Porous carbon/Co/ MnO_2	15.45	0.72	68	7.01	13.32	0.72	66	6.44	LiI/I_2/1-butyl-3-methylimidazolium iodide/ 4-tert-butyl pyridine/ guanidinium thiocyanate in acetonitrile	TiO_2/N719	[179]
Aloe peel	Honeycomb porous carbon	12.12	0.76	69	6.45	13.44	0.73	69	6.80	LiI/I_2/1-butyl-3-methylimidazolium iodide/ 4-tert-butyl pyridine/ guanidinium thiocyanate in acetonitrile	TiO_2/N719	[180]
Aloe peel	Honeycomb porous carbon/ $NiTa_2O_6$	14.61	0.74	65	7.09	13.44	0.73	69	6.80	LiI/I_2/1-butyl-3-methylimidazolium iodide/ 4-tert-butyl pyridine/ guanidinium thiocyanate in acetonitrile	TiO_2/N719	[180]
Aloe peel	Honeycomb porous carbon/ $MnTa_2O_6$	15.41	0.74	65	7.39	13.44	0.73	69	6.80	LiI/I_2/1-butyl-3-methylimidazolium iodide/ 4-tert-butyl pyridine/ guanidinium thiocyanate in acetonitrile	TiO_2/N719	[180]
Aloe peel	Honeycomb porous carbon/ $AlTaO_4$	15.80	0.76	65	7.86	13.44	0.73	69	6.80	LiI/I_2/1-butyl-3-methylimidazolium iodide/ 4-tert-butyl pyridine/ guanidinium thiocyanate in acetonitrile	TiO_2/N719	[180]

(*continued on next page*)

Table 7 (*continued*)

Source	Counter electrode material	Natural product-based counter electrode				Pt counter electrode				Electrolyte solution	Photoanode/ Dye	Reference
		J_{sc} ($mA{\cdot}cm^{-2}$)	V_{oc} (V)	*FF* (%)	η (%)	J_{sc} ($mA{\cdot}cm^{-2}$)	V_{oc} (V)	*FF* (%)	η (%)			
Pomelo peel	Carbon material	14.56	0.70	68	6.94	14.48	0.73	64	6.72	LiI/I_2/1-butyl-3-methylimidazolium iodide/ 4-tert-butyl pyridine/ guanidinium thiocyanate in acetonitrile	TiO_2/N719	[181]
Kelp	N, S, P-doped/Co NPs	14.71	0.75	68	7.48	14.73	0.75	73	7.64	LiI/I_2/1-butyl-3-methylimidazolium iodide/ 4-tert-butyl pyridine/ guanidinium thiocyanate in acetonitrile	TiO_2/N719	[244]
Orange fiber	Carbon material/CoS nanoflakes	11.58	0.74	69	5.94	12.02	0.73	64	5.57	DN-OD05	TiO_2/C264 triphenylamine	[185]
Anchovy	N and S co-doped activated porous carbon	18.78	0.89	76	12.72	19.17	0.87	73	12.23	$Co(bpy)_3^{3+/2+}$	TiO_2/SM-315 porphyrin	[166]
Fish waste	N, P and S tri-doped activated porous carbon	15.64	0.75	67	7.83	15.98	0.76	69	8.34	LiI/I_2/1,2-dimethyl-3-propyl imidazolium iodide/ tert-butylpyridine in acetonitrile.	TiO_2/N3	[245]
Human hair	Carbon material/ PEDOT:PSS	14.58	0.76	58	6.54	15.64	0.74	63	7.29	LiI/I_2/1-methyl-3-propylimidazolium iodide/ tetrabutylpyridine/Li_2CO_3 in acetonitrile.	TiO_2/N719	[246]
Ground coffee waste	N-doped porous carbon	15.09	0.76	73	8.32	14.73	0.77	72	8.07	I_2/1-butyl-3-methylimidazolium iodide/ guanidinium thiocyanate/4-tert-butylpyridine in acetonitrile and valeronitrile mixture (volume ratio 85:15)	TiO_2/N719	[188]
Filter paper	Amorphous carbon	15.02	0.70	45	4.72	15.81	0.64	62	6.23	LiI/I_2/4-tert-butylpyridine in 3-methoxypropionitrile	TiO_2/N719	[241]
Facial tissue	Amorphous carbon	14.80	0.69	64	4.70	15.81	0.64	62	6.23	LiI/I_2/4-tert-butylpyridine in 3-methoxypropionitrile	TiO_2/N719	[241]
Waste carton	Porous carbon	14.20	0.77	62	6.76	14.84	0.76	66	7.51	LiI/I_2/1-butyl-3-methylimidazolium iodide/ 4-tert-butyl pyridine/ guanidinium thiocyanate in acetonitrile	TiO_2/N719	[182]
Waste carton	Porous carbon/WC	14.56	0.76	60	7.32	14.84	0.76	66	7.51	LiI/I_2/1-butyl-3-methylimidazolium iodide/ 4-tert-butyl pyridine/ guanidinium thiocyanate in acetonitrile	TiO_2/N719	[182]
Bagasse	Carbon material	5.20	0.72	8	0.31	15.00	0.72	57	6.08	LiI/I_2/1,2-Dimethyl-3-propylimidazolium iodide/ 4-tert-butyl-pyridine in acetonitrile	TiO_2/N719	[171]
Bagasse	Nitrogen-doped bagasse	10.7	0.69	37	2.48	15.00	0.72	57	6.08	LiI/I_2/1,2-Dimethyl-3-propylimidazolium iodide/ 4-tert-butyl-pyridine in acetonitrile	TiO_2/N719	[171]
Bagasse	Carbon material/Pt NPs	12.4	0.66	45	3.69	15.00	0.72	57	6.08	LiI/I_2/1,2-Dimethyl-3-propylimidazolium iodide/ 4-tert-butyl-pyridine in acetonitrile	TiO_2/N719	[171]
Bagasse	Nitrogen-doped bagasse/Pt NPs	15.3	0.73	62	6.98	15.00	0.72	57	6.08	LiI/I_2/1,2-Dimethyl-3-propylimidazolium iodide/ 4-tert-butyl-pyridine in acetonitrile	TiO_2/N719	[171]
Table sugar	Carbon material[a]	-	-	-	3.24	-	-	-	4.02	Iodolite	TiO_2/RK-1	[184]
Sucrose	Carbon material[a]	-	-	-	0.04	-	-	-	4.02	Iodolite	TiO_2/RK-1	[184]

(*continued on next page*)

Table 7 (*continued*)

Source	Counter electrode material	Natural product-based counter electrode				Pt counter electrode				Electrolyte solution	Photoanode/ Dye	Reference
		J_{sc} (mA·cm^{-2})	V_{oc} (V)	*FF* (%)	η (%)	J_{sc} (mA·cm^{-2})	V_{oc} (V)	*FF* (%)	η (%)			
Humic acid	Carbon material	12.55	0.76	65	6.14	13.85	0.75	68	7.10	LiI/I_2/1-butyl-3-methylimidazolium iodide/ 4-tert-butyl pyridine/ guanidinium thiocyanate in acetonitrile	TiO_2/N719	[247]
Humic acid	Carbon material/Ni	13.51	0.76	68	7.01	13.85	0.75	68	7.10	LiI/I_2/1-butyl-3-methylimidazolium iodide/ 4-tert-butyl pyridine/ guanidinium thiocyanate in acetonitrile	TiO_2/N719	[247]
Ovalbumin	N-doped carbon aerogel	12.01	0.70	56	4.68	12.71	0.71	59	5.35	Iodolyte HI-30	TiO_2/N719	[248]

[a] The V_{oc} from ref. [184] is unreliable.

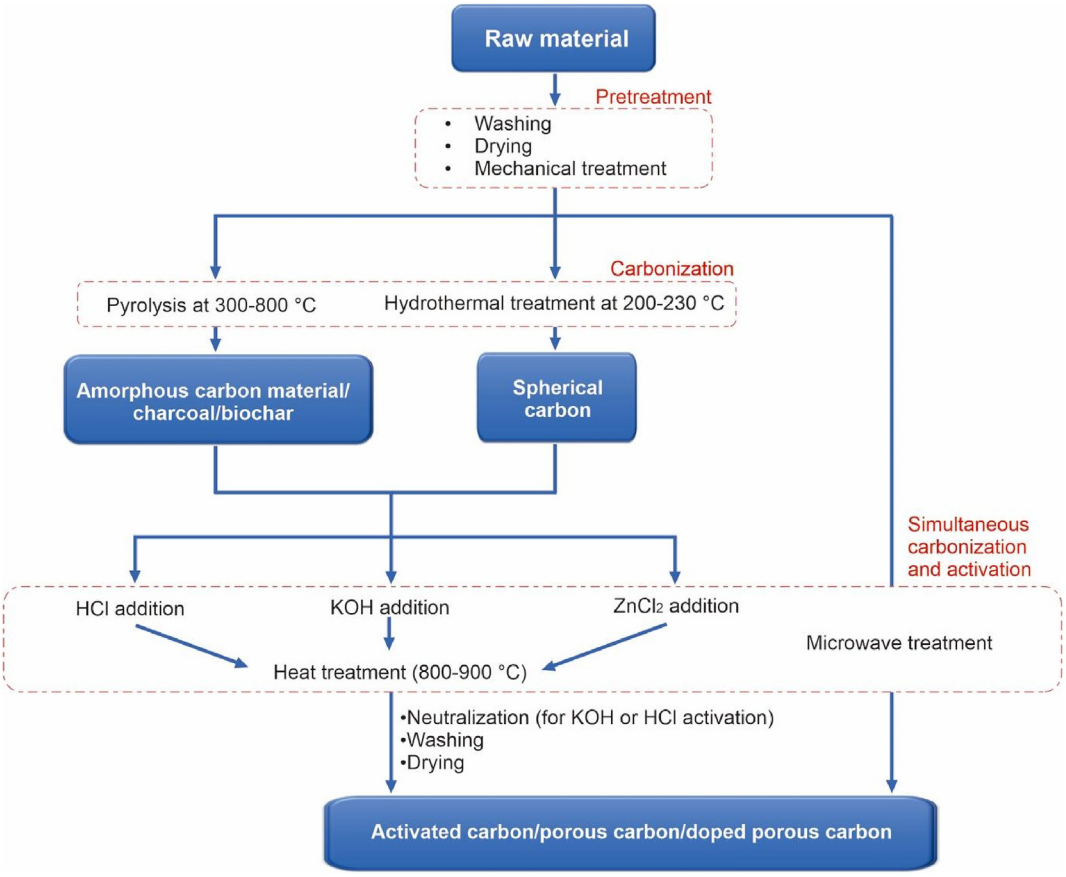

Figure 7. Preparation routes of the carbon-based natural product-derived counter electrode materials. The employed carbon-based materials are displayed in the blue dialog box.

discussing the performance of each device with the natural product-based counter electrode, DSSC performance with the standard platinum counter electrode used as the benchmark is discussed. The PCE of platinum-based devices varies from 0.36 to 12.23%. However, there are no consistent compositions of the dyes and electrolytes mentioned in the literature, which results in varied PCE values. This reduces the possibility of making a fair comparison of PCE values obtained from the various literature. The ruthenium-based dye N719 remains the most favorable, followed by ruthenium-based N3 dye. The other dyes mentioned in the literature are Zn-based SM-315, RK-1, C264 porphyrin, and natural product-based (lotus leaf and mangosteen peel extract) dyes. For the electrolytes, almost all the literature studied utilized the I_3^-/I^- redox pair as inorganic iodide and/or various forms of imidazolium iodide salt as a source of I^-. I^- was used either as a fresh chemical mixture or a commercially prepared solution mixed with the solvent, forming acetonitrile or an acetonitrile/valeronitrile mixture. In addition to these specimens, electrolyte additives such as 4-*tert*-butyl pyridine and guanidium thiocyanate are also incorporated into the electrolytes to enhance DSSC performance [13, 16]. Kim et al. incorporated the only $Co(bpy)_3^{3+/2+}$ redox pair electrolytes found in the current literature

Table 8. Electrochemical, electrocatalytic, and structural properties of various counter electrodes.

Source	Extracted counter electrode material	Additive and/or modifier	Binder or Adhesive	S_{BET} (m^2g^{-1})	Pore volume (cm^3g^{-1})	R_s (Ω cm^2)	R_{ct} (Ω cm^2)	C_d (μF cm^2)	Z_w (Ω cm^2)	I_p (mA cm^{-2})	E_{pp} (V)	η_{rel}	Reference
Rice husk	Porous carbon	-	Titanium isopropoxide	1095	0.61	21.4	1.3	42	1.3	-3.5[a]	-	0.94	[165]
Coconut shell	Activated charcoal	-	Poly vinyl acetate	-	-	30.0	1.6	-	-	-	-	0.83	[170]
Pumpkin stem	Activated carbon	-	-	793	0.4	-	-	-	-	-3.0[a]	0.60[a]	0.69	[183]
Weeping willow wood	Amorphous carbon	-	Carboxymethyl cellulose	-	-	-	-	-	-	-	-	0.25	[241]
Phoenix wood	Amorphous carbon	-	Carboxymethyl cellulose	273	-	31.3	22.7	-	-	-1.8	0.588	0.31	[241]
Camphor wood	Amorphous carbon	-	Carboxymethyl cellulose	-	-	-	-	-	-	-	-	0.25	[241]
Chinese fir wood	Amorphous carbon	-	Carboxymethyl cellulose	-	-	-	-	-	-	-	-	0.22	[241]
Maple wood	Amorphous carbon	-	Carboxymethyl cellulose	-	-	-	-	-	-	-	-	0.27	[241]
Peach wood	Amorphous carbon	-	Carboxymethyl cellulose	-	-	-	-	-	-	-	-	0.24	[241]
Poplar wood	Amorphous carbon	-	Carboxymethyl cellulose	-	-	-	-	-	-	-	-	0.29	[241]
Cypress wood	Amorphous carbon	-	Carboxymethyl cellulose	-	-	-	-	-	-	-	-	0.20	[241]
Tea-oil camellia wood	Amorphous carbon	-	Carboxymethyl cellulose	-	-	-	-	-	-	-	-	0.22	[241]
Orange wood	Amorphous carbon	-	Carboxymethyl cellulose	-	-	-	-	-	-	-	-	0.29	[241]
Chinaberry wood	Amorphous carbon	-	Carboxymethyl cellulose	-	-	-	-	-	-	-	-	0.27	[241]
Oak wood	Mesoporous carbon	-	-	852	0.6	15.1	10.0	-	95.3	-	-	1.01	[243]
Bamboo	Mesoporous carbon	-	-	542	0.3	14.6	38.4	-	76.0	-	-	0.57	[243]
Pine needles leaf	Amorphous carbon	-	Carboxymethyl cellulose	-	-	-	-	-	-	-	-	0.17	[241]
Camphor leaf	Amorphous carbon	-	Carboxymethyl cellulose	-	-	-	-	-	-	-	-	0.22	[241]
Palm leaf	Amorphous carbon	-	Carboxymethyl cellulose	7.1	-	32.1	22.8	-	-	-1.2	0.582	0.30	[241]
Maple leaf	Amorphous carbon	-	Carboxymethyl cellulose	-	-	-	-	-	-	-	-	0.19	[241]
Poplar leaf	Amorphous carbon	-	Carboxymethyl cellulose	-	-	-	-	-	-	-	-	0.21	[241]
Chinese fir leaf	Amorphous carbon	-	Carboxymethyl cellulose	-	-	-	-	-	-	-	-	0.17	[241]
Red after-wood leaf	Amorphous carbon	-	Carboxymethyl cellulose	-	-	-	-	-	-	-	-	0.18	[241]
Lotus	Biochar	-	Carboxymethyl cellulose	30.9	-	-	40.7	-	-	-	-	0.42	[242]
Aloe peel	Honeycomb porous carbon	-	ZrO_2	1286	0.7	27.4	12.4	-	-	-6.0[a]	0.4[a]	0.96	[174]
Aloe peel	Spherical carbon	-	ZrO_2	13[b]	0.1[b]	7808	8663	-	-	-	-	0.38	[175]
Aloe peel	Porous carbon	-	ZrO_2	507	-	14.0	12.2	-	11.4	-4.7	0.847	0.91	[176]
Aloe peel	Porous carbon	-	ZrO_2	-	-	15.9	4.6	-	-	-1.6	0.770	0.91	[177]
Aloe peel	3D network carbon	-	ZrO_2	-	-	11.7	0.7	-	-	-1.3	0.442	0.90	[178]
Pomelo peel	Carbon material	-	ZrO_2	1377	0.7	15.3	7.1	8.5	-	-2.8	0.530	1.03	[181]
Bagasse	Carbon material	-	Polyvinyl pyrrolidone	19.4	-	6.6	544	-	-	-	-	0.05	[171]
Aloe peel	Honeycomb porous carbon	-	ZrO_2	1286[b]	0.7[b]	12.3	1.2	-	-	-2.0	0.760	0.95	[180]
Anchovy	N and S co-doped	-	-	2622	1.9	3.0	7.56	-	-	-0.3[a]	0.075[a]	1.04	[166]

(*continued on next page*)

Table 8 (*continued*)

Source	Extracted counter electrode material	Additive and/or modifier	Binder or Adhesive	S_{BET} (m^2g^{-1})	Pore volume (cm^3g^{-1})	R_s (Ω cm^2)	R_{ct} (Ω cm^2)	C_d (μF cm^2)	Z_w (Ω cm^2)	I_p (mA cm^{-2})	E_{pp} (V)	η_{rel}	Reference
	activated porous carbon												
Fish waste	N, P and S tri-doped activated porous carbon	-	Ethyl cellulose/ terpineol/titanium isopropoxide	2933	0.8	-	0.5	-	-	-5.0[a]	0.5[a]	0.94	[245]
Filter paper	Amorphous carbon	-	Carboxymethyl cellulose	2.2	-	22.6	8.8	-	-	-1.49	0.543	0.76	[241]
Facial tissue	Amorphous carbon	-	Carboxymethyl cellulose	3.2	-	23.4	8.3	-	-	-1.57	0.531	0.75	[241]
Waste carton	Porous carbon	-	ZrO_2	824	0.7	16.7	13.1	-	-	-1.9[a]	0.660	0.90	[182]
Table sugar	Carbon material[a]	-	Polyvinylidene difluoride	-	-	-	-	-	-	-	-	0.81	[184]
Sucrose	Carbon material[a]	-	Polyvinylidene difluoride	-	-	-	-	-	-	-	-	0.01	[184]
Humic acid	Carbon material	-	Ethyl cellulose/terpineol	-	-	10.1	11.5	-	-	-	-	0.86	[247]
Ovalbumin	N-doped carbon aerogel	-	Oleylamine	158	-	17.6	0.83	1.4	-	-	-	0.87	[248]
Aloe peel	Spherical carbon	$FeTa_2O_6$	ZrO_2	-	-	7.0	12.9	-	-	-4.5[a]	0.281	1.08	[175]
Aloe peel	Spherical carbon	$CoTa_2O_6$	ZrO_2	-	-	-	-	-	-	-3.0[a]	0.262	1.07	[175]
Aloe peel	Spherical carbon	ZrO_2/ $CuTa_{10}O_{26}$	ZrO_2	-	-	-	-	-	-	-2.5[a]	0.351	1.03	[175]
Aloe peel	Porous carbon	$ZnNb_2O_6$	ZrO_2	140	-	12.8	6.5	-	4.7	-3.7	0.456	1.24	[176]
Aloe peel	Porous carbon	$MnWO_4$	ZrO_2	-	-	12.8	2.6	-	-	-2.0	0.563	1.04	[177]
Aloe peel	Porous carbon	$ZnWO_4$	ZrO_2	-	-	11.6	1.7	-	-	-2.0	0.424	1.08	[177]
Aloe peel	Porous carbon	$CuWO_4$	ZrO_2	-	-	16.6	6.2	-	-	-1.6	0.581	0.93	[177]
Aloe peel	3D network carbon	$ZnMoO_4$	ZrO_2	-	-	11.4	0.7	-	-	-1.8	0.435	1.14	[178]
Aloe peel	3D network carbon	$Cu_2Mo_3O_9$	ZrO_2	-	-	10.6	1.4	-	-	-1.5	0.706	1.09	[178]
Aloe peel	3D network carbon	$MnMoO_4$	ZrO_2	-	-	11.2	2.2	-	-	-1.0	0.784	1.03	[178]
Aloe peel	Porous carbon	MnO_2	ZrO_2	632	0.4	13.2	10.1	-	-	-2.2	0.460	0.95	[179]
Aloe peel	Porous carbon	Co/MnO_2	ZrO_2	661	0.4	19.8	1.1	-	-	-2.3	0.480	1.09	[179]
Aloe peel	Honeycomb porous carbon	$NiTa_2O_6$	ZrO_2	-	-	13.4	1.6	-	-	-2.3	0.436	1.04	[180]
Aloe peel	Honeycomb porous carbon	$MnTa_2O_6$	ZrO_2	-	-	11.5	1.2	-	-	-2.5	0.394	1.09	[180]
Aloe peel	Honeycomb porous carbon	$AlTaO_4$	ZrO_2	-	-	10.7	0.7	-	-	-2.8	0.398	1.16	[180]
Bagasse	Carbon material	Nitrogen	Polyvinyl pyrrolidone	29.0	-	8.8	28.5	-	-	-	-	0.41	[171]
Bagasse	Carbon material	Pt NPs	Polyvinyl pyrrolidone	56.3	-	9.6	7.4	-	-	-	-	0.61	[171]
Bagasse	Carbon material	Nitrogen/Pt NPs	Polyvinyl pyrrolidone	90.0	-	5.3	1.6	-	-	-	-	1.15	[171]
Kelp	N, S, P-tri-doped carbon	Co NPs	-	142	0.1	37.3	0.9	96.7	-	-0.8[a]	0.3[a]	0.98	[244]
Orange fiber	Carbon material	CoS nanoflakes	Ethylene glycol-terpineol	9.9	-	31.8	36.2	-	-	-	-	1.07	[185]
Waste carton	Porous carbon	WC	ZrO_2	-	-	17.1	7.1	-	-	-1.8[a]	-	0.97	[182]
Humic acid	Carbon material	Ni	Ethyl cellulose/terpineol	-	-	9.1	7.4	-	-	-	-	0.99	[247]
Rice husk	Activated carbon	Acetylene black	Ethyl cellulose	200	-	16.0	3.4	-	30.0	-2.8	0.692	0.91	[235]
Rice husk	Nano-Si@ACs	Acetylene black	Ethyl cellulose	240	-	15.9	2.1	-	27.9	-4.2	0.426	1.11	[235]
Mangosteen peel	Carbon material	PEDOT:PSS	-	125	-						-	1.14	[167]

(*continued on next page*)

Table 8 (*continued*)

Source	Extracted counter electrode material	Additive and/or modifier	Binder or Adhesive	S_{BET} (m^2g^{-1})	Pore volume (cm^3g^{-1})	R_s (Ω cm^2)	R_{ct} (Ω cm^2)	C_d (μF cm^2)	Z_w (Ω cm^2)	I_p (mA cm^{-2})	E_{pp} (V)	η_{rel}	Reference
Mangosteen peel	Carbon material	PEDOT:PSS	-	125	-						-	1.79	[167]
Pine cone flower	Honeycomb-like activated porous carbon	Carbon black	Polyvinylidene fluoride	1598	-	-	-	-	-	-3.0	-	0.80	[239]
Fallen leaves	Honeycomb porous carbon	Carbon black	Polyvinylidene fluoride	2196	1.7	-	25.9	-	-	-	-	0.84	[240]
Sunflower stalk	Layered activated carbon	Acetylene black	Polytetrafluoroethylene	1505	0.9	18.4	7.8	-	-	-2.5[a]	0.3[a]	0.91	[173]
Human hair	Carbon material	PEDOT:PSS	-	188	-	16.7	7.1	-	-	-0.9[a]	0.3[a]	0.90	[246]
Ground coffee waste	N-doped porous carbon	Nafion	-	1200	-	6.1	0.5	5174.0				1.03	[188]

[a] Approximate value taken from the relevant figures in the articles.
[b] Taken from ref. [174].

[166]. However, all the other experiments made use of TiO_2 as a photoanode. The preparation of the photoanode may also contribute to DSSC performance since the prepared photoanode varied commercially-prepared TiO_2 to the controlled morphology-synthesized TiO_2. The effects of TiO_2 morphology are not included in the current discussion since most research did not include the characterization of the TiO_2 electrode.

The table shows that the poorest PCE is achieved by the devices that used natural dyes as a sensitizer [167, 168], with PCE <2%, regardless of the electrolyte. On the other hand, the highest PCE was obtained using the $Co(bpy)_3^{3+/2+}$ redox couple electrolyte and Zn-based SM-315 [166], with 12.23%, which appears to be higher than the average PCE listed in Table 7. The PCE of this DSSC arrangement correlates with the highest PCE for the $Co(bpy)_3^{3+/2+}$/SM-315 electrolyte/dye pair of 13% [169].

Pt-based devices with standard I_3^-/I^- redox couple electrolytes with inorganic iodide and/or imidazolium iodide, either with or without additive, have PCE ranges of 4.02 and 9.41%, respectively. It is worth reiterating that close comparisons of DSSC performance for studied literature have not been found, even if the devices employ the same set of electrolytes and dyes. For example, the highest PCE of 9.41% was obtained with LiI/I_2/1,2-dimethyl-3-propyl imidazolium iodide/4-tert-butylpyridine in acetonitrile electrolyte without both guanidium thiocyanate additive and N719 dye as in Ref. [170]. However, DSSCs with similar electrolytes and dyes performed worse with a PCE of 6.08% [171]. In contrast, V_{oc} of the two devices are comparable, as J_{sc} and *FF* differ significantly. This could benefit the TiO_2 photoanode, which has a larger surface area or porosity, allowing light to scatter. This, in turn, enhances the light-harvesting efficiency compared to top-down TiO_2 photoanode synthesis from the commercial precursor in [170]. Efficient light harvesting by using light scattering in the photoanode is a way to increase the J_{sc} of the DSSC [172]. Different PCE results may appear from the same research group even if the same photoanode, dye, electrolyte, and counter electrode preparation are used. The Yun research group from Xi'an University of Architecture and Technology published a set of works on DSSCs with similar experimental methodologies [173, 174, 175, 176, 177, 178, 179, 180, 181, 182]. The works consistently utilized a "complete" set of electrolytes where inorganic iodide salt (LiI), imidazolium salt (1-butyl-3-methylimidazolium iodide), and additives (4-tert-butyl pyridine and guanidinium thiocyanate) with acetonitrile were used as the solvent, and N719 was used as the dye. This resulted in the PCEs of the Pt-based DSSCs in the range of 6.34 and 7.19%. These values obtained may be caused by experimental random error due to uncertainties in the measurement. The average value deviation obtained was 6.5%, which was small enough for the PCE values of the platinum-based DSSC devices to be classified as accurate. It is also evident that electrolytes with only inorganic iodide without the imidazolium iodide salt and additives yielded a less satisfactory device performance than the more sophisticated electrolytes. Madhu et al. utilized KI/I_2 in ethylene glycol in conjunction with N719 dye for a DSSC with a Pt-counter electrode. The attained PCE of the Pt-based DSSC was 4.04%, which was lower than the average value [183].

The performance of natural product-based counter electrodes can be briefly compared with platinum-based electrodes. From the same sources, it is stated that both the V_{oc} between natural product-based counter electrodes and Pt-based electrodes are generally comparable, with differences of less than 100 mV. The photovoltaic efficiency of the DSSC is mainly affected by J_{sc} and *FF* values. Improvement in J_{sc} and *FF* are considered to play a vital role in DSSC performance. Both the J_{sc} and *FF* values can be improved by enhancing the electrocatalytic activities of the counter electrodes. This can be achieved by modifying the structural and electronic properties of the electrodes, as described in the next section.

4.3. The relationship between the structure and performance of the counter electrode

To compare the performance of natural product-based electrodes with platinum-based electrodes under the same experimental conditions for each study, let us define the relative DSSC PCE as

$$\eta_{rel} = \frac{\eta_{NP}}{\eta_{Pt}} \tag{3}$$

where η_{rel}, η_{NP}, and η_{Pt} are the relative frequency, PCE of the natural product-based DSSC, and PCE of the platinum-based DSSC, respectively. If the value is below 1, the natural product-based DSSCs underperform those of the platinum-based DSSCs. In contrast, if the value is equal to or larger than 1, the natural product-based DSSCs perform qualitatively better than the platinum-based DSSCs. However, as previously mentioned, due to experimental uncertainties, η_{rel} between 0.90 and 1.10 may have error uncertainties. Therefore, this range of the η_{rel} values cannot be used to conclude whether the natural product-based DSSCs performed better or worse than the platinum counterpart. Nevertheless, DSSCs with an η_{rel} value below 0.7 suggested that they performed worse than their platinum counterparts since the absolute PCE was below 3%.

The important electrochemical properties of the counter electrode are the series resistance (R_s), charge transfer resistance (R_{ct}), double layer capacitance (C_d), and Nernst diffusion impedance (Z_w). These values can

be obtained from the electrochemical impedance spectra (EIS) technique. A smaller R_{ct} value indicates a higher electrocatalytic activity of I_3^- reduction. C_d affects the surface area of the counter electrode, and Z_w influences the diffusion velocity of the redox couple in the electrolyte. A higher surface area contributes to a larger C_d, while a faster diffusion rate causes Z_w to decrease. Other parameters, peak current density (I_p) and peak-to-peak separation (E_{pp}), are used to evaluate the catalytic performance of a counter electrode. Both of these can be determined by using the cyclic voltammetry method. Although the current high-performance DSSC devices use $Co^{3+/2+}$ as a redox couple, most DSSCs still utilize I_3^-/I^- for their economic benefits. Therefore, the discussion will be focused on the I_3^- reduction ability of the counter electrode. The electrochemical properties of the counter electrode are generally related to the structural properties. These are mainly determined by the BET surface area and the pore size.

To fabricate natural product-based electrodes, some additional components are usually incorporated. Since amorphous, disordered, and porous carbon materials are known for their poor adhesion to FTO [62], additional binder or adhesive materials must be incorporated. Additionally, amorphous carbon is also known for its low conductivity; thus, conducting material can also be incorporated into the counter electrode. However, not all of the works in the literature employed additional conducting materials since the extracted materials are not necessarily amorphous carbon materials but rather various morphologies of carbon.

Table 8 lists the electrocatalytic properties of natural product-based materials and their available surface area and total pore volume. Since not all electrochemical data are available in the literature, we can take several examples of natural product-based materials and discuss their electrochemical properties. Nevertheless, the main performance concern remains the PCE, which we defined here as the η_{rel} that are available throughout the literature. It is also clear that from the extraction of natural product materials and the optional modifications to the fabrication of counter electrodes, some structural properties can be altered due to treatment methods (i.e., spin coating or doctor blade method). For instance, the material's BET surface and pore size are determined before counter electrode fabrication. In contrast, the electrochemical and electrocatalytic properties are determined at the counter electrode stage. Nevertheless, the changes in the structural properties may be neglected.

First, let us discuss the DSSC based on the counter electrode materials without any intended chemical additives and/or modifications. These materials span from amorphous inactivated carbon to N, P, and S tridoped activated porous carbon. In this category, the poorest DSSC performance η_{rel} is 0.01 with an absolute PCE of 0.04% obtained by the carbon material from sucrose-based DSSC [184] while the best performance is obtained by the N and S codoped activated porous carbon from an anchovy-based DSSC with η_{rel} of 1.04 and absolute PCE of 12.73% [166]. However, it should be noted that the best DSSC that falls within this category employs the $Co^{3+/2+}$ redox couple electrolyte, which indeed gives better DSSC performance than the I_3^-/I^- based electrolyte [169]. The other fish-based DSSCs, namely, N, P, and S tridoped activated porous carbon-based DSSCs also exhibit a remarkably high η_{rel} of 0.94 and absolute PCE of 7.83%.

The relationship between the structural properties can be discussed in terms of the surface area and total pore volume of the electrode and the electrochemical properties of the electrode. The surface areas of natural product materials span from 2 to ca. 3000 $m^2\ g^{-1}$. Interestingly, the materials with a relatively high BET surface area, i.e.,>800 $m^2\ g^{-1}$, exhibit excellent PCE efficiency compared to the materials with lower surface areas. This is due to more I_3^- that can adsorb on the counter electrode surface and pores, as illustrated in Figure 8. The electron transfer efficiency on the electrode/electrolyte interface can be deduced from the R_{ct} values. For the most efficient electron transfer process, the R_{ct} value must be small. As seen from Figure 9, a high electrode surface corresponds to a low R_{ct}, which is below 14 Ω cm^2. This leads to the η_{rel} values being larger than 0.9 or absolute PCE values larger than 7.0%. As expected, the counter electrode material with a low surface exhibits worse DSSC performance than the Pt-based DSSC.

The presence of heteroatoms from the biomass source in the final product materials can also enhance the DSSC performance. The perfor-

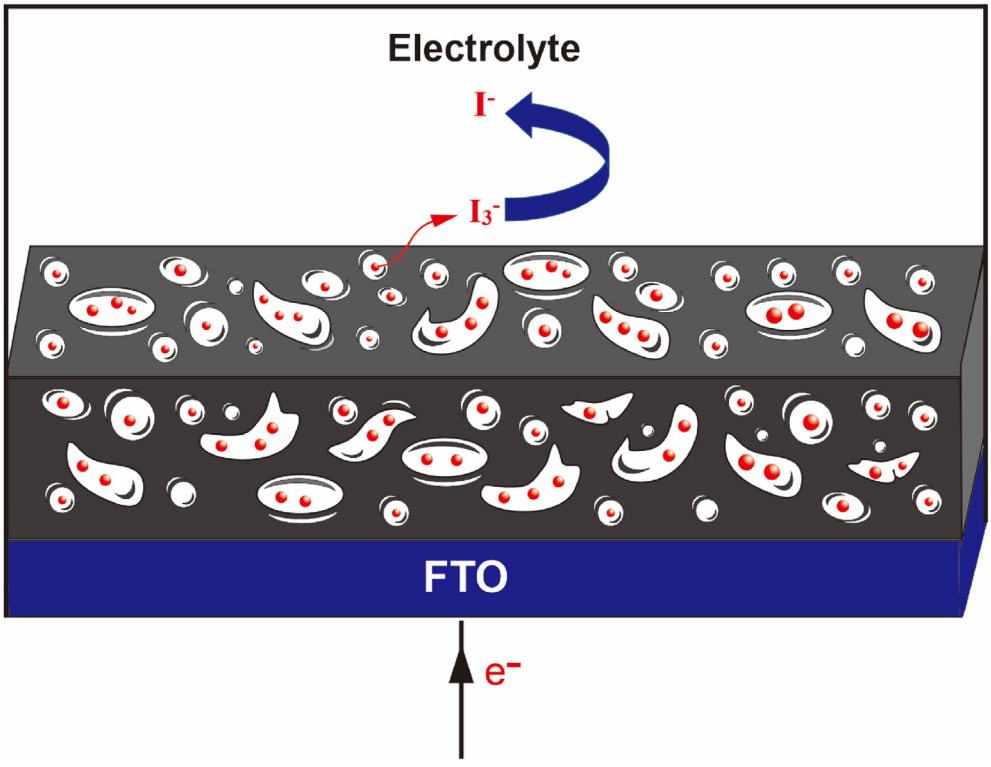

Figure 8. Illustration of the interactions between I_3^- with porous carbon counter electrode.

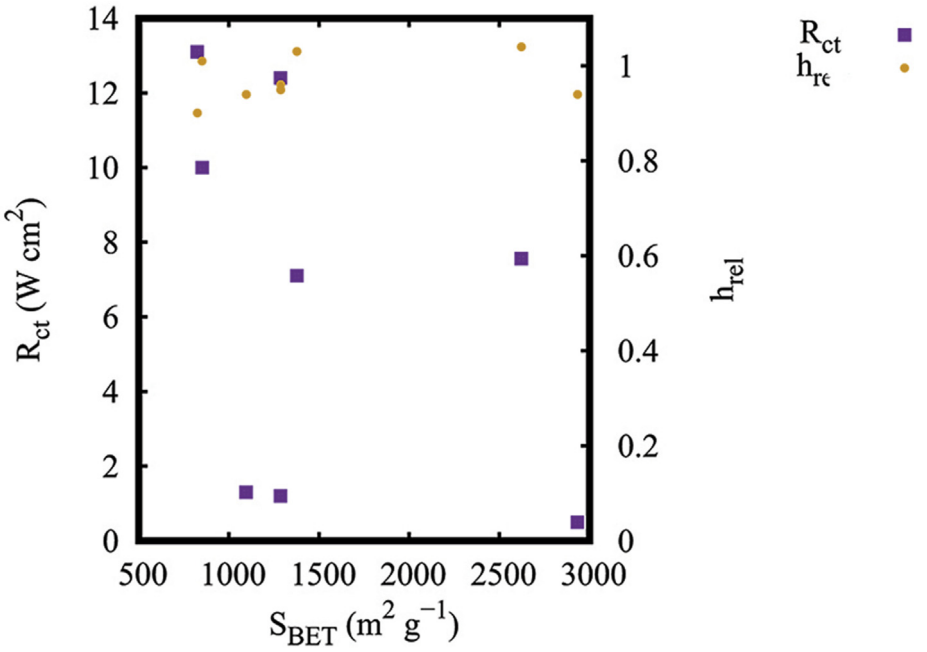

Figure 9. Distribution of η_{rel} and R_{ct} with correlation to S_{BET} of the natural product-based counter electrode without additive.

mance can be seen by the high η_{rel} of N, P, and S tridoped activated porous carbon from fish and N-doped carbon aerogel from ovalbumin, which is close to 1. The latter possesses a relatively lower BET surface area of 150 m^2 g^{-1}. The lone pair electrons of the heteroatoms can serve as electron donors to accelerate I_3^- reduction. Additionally, the doped atoms in the carbon structure can induce defects, increasing the ion-accessible surface area.

The efficiency of the electrocatalytic activities of the counter electrode can also be determined by the peak current density (I_p) and peak-to-peak separation (E_{pp}) values from the cyclic voltammetry experiment. However, most of the results are presented as qualitative instead of quantitative. The exact values are determined by parameters such as scan rate and electrolyte, among other similar parameters. For instance, the values are always compared to the Pt-based counter electrode. The more negative the I_p value is, the smoother the reduction reaction at the electrolyte/electrolyte interface. The same applies to E_{pp}, where a smaller E_{pp} value implies that the electrocatalytic activity is better. In all cases, the natural product-based electrodes have η_{rel} values close to 1, and I_p and E_{pp} values close to those of Pt-based electrodes.

Next, we discuss the counter electrode with intended modifications. The modifications include the incorporation of conducting materials and/or incorporation of more active catalytic materials. As seen from Table 3, generally, the natural product/composite materials exhibit excellent η_{rel} compared to natural product materials with significantly lower R_{ct} values compared to naturally-produced electrode materials. As an example, carbon material from orange fiber incorporated with CoS nanoparticles exhibits a η_{rel} of 1.07 and PCE of 5.94%, with a lower BET surface of ca. 10 m^2 g^{-1} [185]. The PCE value can be explained by the enhanced electrocatalytic activities of Co_xS_y compounds. Such is the case, as different phases of cobalt sulfide have been investigated as an excellent oxygen evolution reaction (OER) electrocatalysts due to the overpotential for the OER [186]. For this reason, it can be confirmed that Co_xS_y plays a vital role in the enhanced electrocatalytic activity of I_3^- reduction instead of the orange fiber carbonaceous material because the carbonaceous material is able to exhibit a low BET surface.

A similar enhancement of the counter electrode electrocatalytic activity is also achieved by porous carbon/metal oxide composite materials. The Yun research group from Xi'an University of Architecture and Technology published a set of works on natural products and waste-based counter electrodes with various metal oxides and a metal carbide [173, 174, 175, 176, 177, 178, 179, 180, 181, 182]. Most of the works employed aloe peel as the source of biomass. Even without any inorganic materials, the resulting porous materials from aloe peel achieved remarkably excellent DSSC performance. A better DSSC performance can be achieved by incorporating inorganic compounds as inorganic materials can be well dispersed throughout porous carbon materials. As noted by the authors, the oxide enhances the catalytic activities since the band alignment of the inorganic materials matches those of the I_3^- reduction potential. Combining the high surface area of the porous carbon material with the excellent electronic properties of the inorganic materials is proven to decrease the R_{ct} values to below 5 Ωcm^2. Therefore, inorganic materials and natural product-based materials have synergistic effects.

The second class of additives is conducting materials. These additive materials include Nafion, PEDOT:PSS, and acetylene/carbon black. Nafion and PEDOT:PSS are well-known conducting polymers containing sulfonic acid functional groups that can act as proton conductors. The conducting polymer can also serve as the binder of the counter electrode material to the FTO glass. Yeh et al. proposed that the interactions between Nafion and electrode materials are due to their hydrophobic interactions [187].

It may be better to introduce a functional group to the carbonaceous material of the counter electrode material. An alternative would be to extract the chemically functionalized carbonaceous materials, as shown in Ref. [188] for Nafion additives/binders. The incorporation of Nafion into the counter electrode is proven to enhance the PCE of the DSSC, as in the work of Yeh et al. [187]. Yeh et al. compared the performance of graphene with graphene/Nafion-based DSSCs. Incorporating Nafion into the graphene counter electrode is proven to increase the PCE from 4.58 to 7.69%. Chung et al. extracted N-doped porous carbon from ground coffee waste combined with Nafion for DSSC counter electrodes [188]. Owing to the large surface area of the porous carbon, increasing the ion-accessible surface area due to the doped nitrogen, the PCE reaches as high as 8.32% with a η_{rel} of 1.03, meaning that the N-doped porous carbon has a comparable efficiency with the Pt electrode, which is also consistent with the electrocatalytic properties of the material with a very low R_{ct} of 0.5 Ω cm^2.

4.4. Remarks on natural carbon for dye-sensitized solar cells

Carbon, as an abundant material, has great potential to be developed and become desirabke counter-electrode for DSSC. A replacement for platinum is needed for DSSC production. Research trends on carbon utilization for DSSC counter electrodes are still growing and show impressive performance improvements; for example, the modification of carbon into porous carbon with a large surface area or other modifications to increase the catalytic performance toward the redox couple species.

5. Green synthesis metal oxide semiconductor for photoanodes

ZnO and TiO_2 are the most common semiconductors that are used in DSSCs. Generally, the semiconductor provides the surface for dye adsorption, collecting electrons from the excited dye and conducting the electrons toward the external circuit [1, 2, 3]. The synthesis of metal and metal oxide nanoparticles using green biological methods is a preferred synthesis method compared to physical and chemical methods. Green methods are cost-effective, environmentally friendly, and easily processed. Based on our records, the use of green-synthesized ZnO or TiO_2 for DSSC applications is still limited; however, a recent study shows that green synthesis can facilitate the desired oxide particle structure and shape for DSSC applications [189]. Below we review various methods for the preparation of ZnO and TiO_2 through a green approach.

5.1. Synthesis of ZnO using plant extract

Anbuvannan et al. synthesized ZnO nanoparticles using *Anisochilus carnosus* leaf extract. Zinc nitrate as a precursor was added to the leaf extract at 60 °C. The mixture was subsequently boiled for 20 min until the color became dark yellow. The obtained paste was annealed at 400 °C for two hours to obtain ZnO nanoparticles. The morphology and size of the obtained ZnO were confirmed by TEM. It was revealed that a majority of the ZnO nanoparticles were quasi-spherical with sizes ranging from 30 to 40 nm. The photocatalytic performance showed that it enhanced the degradation of methylene blue under UV irradiation. Green-synthesized ZnO exhibited potential antibacterial properties against several pathogens [190].

ZnO nanoparticles may also be synthesized using aqueous *Cassia fistula* plant extract. The *Cassia fistula* plant extract was used as a fuel obtained by the solution combustion method. $Zn(NO_3)_3{\cdot}6H_2O$ was dissolved in the aqueous plant extract. The mixture was kept in a preheated muffle furnace at 400 °C for approximately five minutes. Based on the TEM image, the particles consisted of many agglomerated particles and sponges in a form similar to irregularly shaped particles with an average crystallite size of 5–15 nm. The obtained ZnO nanoparticles showed adequate performance in methylene blue dye under sunlight and UV illumination, in addition to displaying significant antioxidant properties [191].

The same solution combustion method was applied to green–synthesized ZnO nanoparticles using an aqueous extract of *Abutilon indicum*. Zinc nitrate hexahydrate ($Zn(NO_3)_2{\cdot}6H_2O$) was mixed with the aqueous extract. After constant stirring for 2–5 min, the mixture was kept in a preheated muffle furnace at a temperature of 200 ± 5 °C for 2–3 min. After being filtered and rinsed, the ZnO nanoparticles were calcined for two hours. The obtained ZnO nanoparticles were homogeneous and equally distributed over the surface with a grain size of 16.72 nm and bandgap energy of 3.37 eV. The obtained ZnO nanoparticles demonstrated effective performance in degrading Acid Black 234. ZnO nanoparticles also display antioxidant and anticancer properties [192].

Another work carried out by Thema et al. was to synthesize ZnO nanoparticles using *Agathosma betulina* plant extract. Zinc nitrate hexahydrate ($Zn(NO_3)_2{\cdot}6H_2O$), which was used as a zinc precursor, was mixed with the leaf extract and heated at 100 °C for two hours. The obtained precipitate was washed, dried, and annealed at various temperatures from 100–500 °C for two hours. It was found that 500 °C was the optimal temperature for obtaining highly crystalline ZnO nanocrystals. The HRTEM image shows that the optimized sample consisted of quasi-spherical agglomerated nanoscale particles with diameters ranging from 12 to 26 nm. That nanoparticle exhibited a good varistor response [193].

ZnO nanoparticles were successfully synthesized using *Carica papaya* leaf extract and applied for photocatalytic and photovoltaic applications. The papaya leaf extract was added to a zinc acetate dihydrate solution at 60 °C and pH 8 before being stirred for two hours to synthesize ZnO nanoparticles. The washed precipitate was subsequently dried at 80 °C for 12 h. The synthesized ZnO nanoparticles had a pristine hexagonal wurtzite structure inside spheres with a diameter of approximately 50 nm. The photoactivity results revealed that ZnO nanoparticles completely degraded methylene blue dye within 180 min under UV irradiation while showing an energy conversion efficiency of 1.6% and a current density of 81 mA cm^{-2} [194].

Most research shows that green–synthesized ZnO nanoparticles obtained nanoparticles in a spherical shape. However, several researchers reported that ZnO nanorods could be successfully prepared using a green synthesis approach. Li Fu and Zhuxian Fu synthesized ZnO nanorods mediated by *Plectranthus amboinicus* leaf extract. Zinc nitrate was mixed with the leaf extract and stirred at 80 °C for four hours. The obtained pale white precipitate was centrifuged, washed, and calcined at 200 °C for one hour. SEM characterization showed that ZnO nanoparticles had a rod-shaped structure with an average particle size of 88 nm. The photocatalytic activity study revealed that biosynthesized ZnO had an excellent photocatalytic performance in methyl red degradation under UV irradiation compared to chemically–synthesized ZnO nanoparticles [195].

ZnO nanoparticles with various shapes were successfully synthesized using *Phyllanthus niruri* leaf extract. Zinc nitrate was added to the boiled leaf extract at 60 °C after the stem turned yellow. The obtained paste was then calcined at 400 °C for two hours to obtain a light white-colored powder. FESEM analysis showed that ZnO nanoparticles had rectangular, triangular, radial hexagonal, rod, and spherical shapes with an average size of 25.61 nm. Biosynthesized ZnO showed excellent photocatalytic activity for methylene blue reduction and has many potential applications as semiconductor, pyroelectric, piezoelectric, catalyst, and optoelectronic, as well for phytochemical, and pharmacological, and medical purposes [196].

5.2. Synthesis of ZnO using microorganism

Aspergillus fumigatus JCF fungi successfully mediated green–synthesized ZnO nanoparticles. $ZnSO_4$ was added as a precursor to the fungal filtrate (pH 6.5) and incubated at 72 °C for 72 h in an orbital shaker. The obtained white precipitate was centrifuged and lyophilized. SEM images revealed that the prepared ZnO nanoparticles were spherical with an average size of 60–80 nm [197].

Jayaseelan et al. successfully synthesized ZnO nanoparticles using *Aeromonas hydrophilic* bacteria. ZnO was added to the bacterial culture solution and incubated at 30 °C for 24 h in a shaker incubator. After being cooled and incubated at room temperature for approximately 12–48 h, white deposits were collected. The obtained ZnO nanoparticles were smooth and had a spherical shape. This suggests that it has significant antibacterial and antifungal properties [198].

Another green synthesis method to prepare ZnO nanoparticles is by using the yeast strain *Pichia kudriavzevii*, a method that was successfully carried out by Moghaddam et al. Zinc acetate dihydrate ($Zn(CH_3COO)_2{\cdot}2H_2O$) was mixed with fungal cell-free filtrate and incubated at 35 °C in a shaking incubator and agitated for 12, 24, and 36 h. The obtained white precipitate was centrifuged and dried at 150 °C for six hours. The results from TEM analysis showed that the average particle sizes were 10 ± 2.08, 32 ± 4.7, and 59 ± 10.6 nm for incubation times of 12, 24, and 36 h, respectively. It was observed that the ZnO nanoparticles tended to agglomerate due to high surface energy [199].

5.3. Synthesis of TiO_2 using plant extract

TiO_2 nanoparticles were synthesized by Goutam et al. using a leaf extract of *Jatropha curcas L* [200]. Titanium chloride ($TiCl_4$) was used as a precursor. 80 mL of 0.5 M $TiCl_4$ was added to 80 mL of filtered leaf extract at a ratio of 1:1 (v/v) with continuous stirring for 20 min at room temperature. After adding an ammonia solution, the precipitates were separated, washed, dried, and calcined at 450 °C for three hours. The obtained TiO_2 nanoparticles were spherical with a diameter ranging from 10–20 nm [200]. The nanoparticles were later applied for the simultaneous removal of chemical oxygen demand (COD) and chromium (Cr) from secondary treated tannery wastewater (TWW). The results gave removals of 82.26 and 76.48% for COD and Cr, respectively [200].

Santhoshkumar et al. synthesized TiO_2 nanoparticles using *Psidium guajava* aqueous leaf extract, and before being concluded, TiO_2 nanoparticles were efficacious as antibacterial and antioxidant agents. $TiO(OH)_2$ was used as the precursor. The pure $TiO(OH)_2$ and aqueous leaf extract were stirred for several hours until the solution turned light green. The synthesized TiO_2 nanoparticles showed a spherical shape and clusters with an average size of 32.58 nm TiO_2 nanoparticles exhibited better antibacterial properties when than the standard antibiotic disk. TiO_2 nanoparticles were also advantageous in terms of antibacterial properties compared to tetracycline, with a maximum zone of 25 and 23 mm inhibition when faced against *Staphylococcus aureus* and *Escherichia coli,* respectively [201].

Patidar et al. prepared TiO_2 nanoparticles using *Moringa oleifera* leaf extract. Anatase TiO_2 with an average crystallite size of 12.22 nm was obtained. As the precursor, titanium tetraisoproxide (TTIP) was mixed with the ethanolic leaf extract and stirred for four hours. After centrifugation and washing, the TiO_2 nanoparticles were dried, ground, and calcined at 500 °C for approximately five hours [202].

Another work of synthesizing TiO_2 using a biosynthesis approach was carried out by Subhapriya S and Gomathipriya P. TiO_2 nanoparticles were synthesized using *Trigonella foenum-graecum* extract, and their antibacterial properties were studied. The extract was added to titanium oxysulfate for 15 min before dropping 1 M sodium hydroxide into the solution until pH 8 was reached. The washed precipitate was calcined at 700 °C for three hours to obtain crystalline TiO_2 nanoparticles. The obtained TiO_2 nanoparticles had a spherical shape with a size ranging between 20 and 90 nm. It also showed excellent antibacterial properties toward *Staphylococcus aureus, Enterococcus faecalis, Klebsiella pneumoniae, Streptococcus faecalis, Pseudomonas aeruginosa, Escherichia coli, Proteus vulgaris, Bacillus subtilis, Yersinia enterocolitica,* and the fungus *Candida albicans* [203].

Rajkumari et al. synthesized TiO_2 nanoparticles by using an aqueous leaf extract of Aloe barbadensis. They also studied the antibiofilm potential against *Pseudomonas aeruginosa PAO1*. In the synthesis procedure, the leaf extract was added by droplets into titanium chloride ($TiCl_4$) at pH 7 and stirred for three hours. The washed precipitate was then dried at 100 °C for seven hours. The obtained TiO_2 nanoparticles had a spherical shape with a size ranging from 20 to 50 nm, as confirmed by SEM and TEM analysis. The biosynthesized TiO_2 nanoparticles were found to exhibit a high antibiofilm efficacy against *P.aeruginosa* [204].

The most recent research was conducted by Senthamarai et. al., [189]. They prepared TiO_2 particle using the pineapple, orange, and grape fruit extracts. The grape extract facilitates the formation of the TiO_2 nanotube structure. As a result, this sample obtained the highest power conversion efficiency (4.33%) in comparison to the other extracts when built as a DSSC device using N4719 as a sensitizer.

5.4. Synthesis TiO_2 using microorganism

TiO_2 nanoparticles were successfully synthesized using *Aspergillus flavus TFR 7* fungi. First, mycelia were developed from fungal cultivation. The reaped mycelia were resuspended in demineralized water and incubated for 48 h at 28 °C to obtain a cell-free filtrate containing extracellular enzymes. The filtrate was mixed with titanium precursor salt and incubated at 150 rpm and 28 °C to obtain TiO_2 nanoparticles. The acquired TiO_2 nanoparticles had an average particle size of approximately 18 nm, as observed by DLS analysis [205].

Another work from Khan et al. showed that *Bacillus amyloliquefaciens* cultivation could be used to synthesize TiO_2 nanoparticles. $TiOSO_4$ was used as a titanium precursor. It was added to the prepared medium containing cultivated bacteria and incubated for 24 h at 37 °C. The gathered white precipitate was centrifuged, washed, and calcined at 500 °C for three hours. The synthesized TiO_2 nanoparticles were spherical with a size ranging from 22.11 to 99.28 nm, as observed by TEM analysis. The photocatalytic activity of doped and undoped biosynthesized TiO_2 nanoparticles to degrade the RR31 dye under UV irradiation at room temperature was tested. The results suggested that all samples were capable of degrading a photocatalytic RR31 dye [206].

The synthesis of TiO_2 nanoparticles was successfully mediated by baker's yeast (*Saccharomyces cerevisiae*). A $TiO(OH)_2$ solution was added to the cultivated yeast solution. Consecutively, it was heated in a steam bath at 60 °C for 10–20 min. After being cooled and incubated at room temperature for approximately 12–48 h, the TiO_2 nanoparticles were found as-deposited white clusters at the bottom of the tube. The obtained TiO_2 nanoparticles were almost spherical at 12.57 $\pm$ 0.22 nm, as confirmed by TEM [207].

5.5. TiO_2 synthesis using aqueous solution approach

Green–synthesized TiO_2 can be achieved using a modified sol-gel method known as the peroxo sol-gel method. In this method, water is used as a solvent instead of organic solvents, and pH 7 is required as a synthesized condition [208, 209]. Gao et al. successfully synthesized micropatterns of TiO_2 thin films using this method. H_2TiO_3 was used as a titanium precursor, and it was dissolved in a mixture that contained ammonia and H_2O_2 aqueous solution. The obtained thin film was smooth and crack-free, formed by the coalescence of nanosized particles of 10–20 nm in diameter [208].

Thin films of TiO_2 were successfully prepared using this green sol-gel method carried out by Ge et al. Titanyl sulfate ($TiOSO_4{\cdot}nH_2O$), H_2O_2, and ammonia were used as the starting materials. The obtained yellow and transparent PTA solution was used as a coating solution. The TiO_2-coated substrate was successively calcined at 500 °C for 30 min. SEM analysis showed that the TiO_2 thin film was uniformly comprised of spherical particles with an average particle size of 30–40 nm. The thin film showed the best photocatalytic activity, reaching 99% methyl orange degradation under 160 min of UV irradiation [210].

Another green synthesis approach is by using an "aqueous" solution. This chemical method was applied successfully in aqueous electrophoretic deposition. Benehkohal et al. used this method to prepare TiO_2–ZnO composite photoanodes for DSSCs. $Zn(NO_3)_2$ was added to a suspension of TiO_2 powder and an isopropanol-water mixture. Subsequently, the suspension was sonicated for one and a half hours before electrophoretic deposition (EPD). Next, the obtained layer was dried at room temperature and could be used for multiple characterizations [211].

5.6. Remarks on green synthesis metal oxide

Oxide semiconductor synthesis through the green synthesis approach has the advantage of controlling the particle size and shape. Among the other green synthesis methods, microorganism synthesis assistance has the most difficulty. The synthesis step is tricky and requires time. Green synthesis using plant extracts seems more promising. The scale-up of this process requires the plantation land planning to supply the resources.

6. Conclusion

The synthesis, characterization, and performance of natural product-based DSSCs have been reviewed in depth. Overall, there are some

inconsistencies in the DSSC performance across the literature, mainly due to the different types of components used. However, the detailed atomic–level understanding of the electronic process that occurs among the components remains poorly understood and needs to be further explored.

Natural dyes need to be modified to obtain a better performance. Most modifications were concerned with improving the electronic properties and the other limitation of natural dyes, including dye stability, dye aggregation, and weak interaction with the oxide semiconductor surface. A computational study is among the best methods to investigate the electronic properties at the molecular level and the charge transport process.

Natural biopolymers are promising for the development of quasi-solid DSSCs. The quasi-solid DSSC minimizes the decrease in cell performance due to volatilization issues. The major problem with using natural biopolymers is their low conductivity. The low conductivity issue has been overcome by looking for a suitable redox couple, adding the ionic liquid, or adding another additive. Theoretical and computational studies regarding the charge transfer process in polyelectrolyte gel systems are limited and challenging to explore.

Natural carbon-based counter electrodes have become promising candidates for replacing more expensive Pt-based counter electrodes. It appears that a DSSC with a porous carbon-based counter electrode with a large surface area gives a comparable performance to the Pt-based electrode. The low-surface area natural product-based electrode can achieve a remarkably good DSSC performance if the extracted material is combined with electrocatalytically active inorganic and/or conductive materials.

There is always a trade-off between the performance, production cost, and environmental aspects of natural product-based DSSC fabrication. Most of the authors cited in this paper argue that natural products are readily available in the surroundings as wastes or byproducts. One issue regarding the utilization of natural products is their inhomogeneous content, which can bring either benefits or drawbacks to the extraction processes of the intended material and DSSC performances. The impurities contained in the source must be removed using harsh chemicals if necessary. On the other hand, impurities can also benefit DSSC performances. Another issue is the reproducibility of the material extracted from the natural product, where the material obtained can have different structures and properties. Additionally, the choice of the other components has to be taken into account. Therefore, to prepare natural-based DSSCs, parameters such as cost, chemical requirements, and environmental aspects must be considered to achieve proper DSSC performance.

Finally, we note that it remains plausible to improve DSSC performance by incorporating natural product-derived materials into DSSC components. If the cost and chemical precursors are not taken into account, we can employ naturally–derived porous carbon and green–synthesized semiconductors in DSSC devices. However, the dyes and electrolytes must still come from commercial products.

Declarations

Author contribution statement

All authors listed have significantly contributed to the development and the writing of this article.

Funding statement

This work was supported by the Ministry of Research and Technology of Republic Indonesia through the PDUPT Scheme (973/PKS/ITS/2021), and by the Faculty of Mathematics and Natural Science (183/J01.1.28/PL.06.02/2021).

Data availability statement

Data included in article/supp. material/referenced in article.

Declaration of interests statement

The authors declare no conflict of interest.

Additional information

No additional information is available for this paper.

Acknowledgements

YK is gratefully to the Ministry of Research and Technology of Republic Indonesia for funding this research through the PDUPT Scheme with contract number 973/PKS/ITS/2021. ASH acknowledges the support from Faculty of Mathematics and Natural Science, University of Gadjah Mada under contract number 183/J01.1.28/PL.06.02/2021.

References

[1] A. Hagfeldt, G. Boschloo, L. Sun, L. Kloo, H. Pettersson, Dye-sensitized solar cells, Chem. Rev. 110 (2010) 6595–6663.
[2] J. Gong, J. Liang, K. Sumathy, Review on dye-sensitized solar cells (DSSCs): fundamental concepts and novel materials, Renew. Sustain. Energy Rev. 16 (2012) 5848–5860.
[3] K. Sharma, V. Sharma, S.S. Sharma, Dye-sensitized solar cells: fundamentals and current status, Nanoscale Res. Lett. 13 (2018) 381.
[4] D.F. Watson, G.J. Meyer, Electron injection at dye-sensitized semiconductor electrodes, Annu. Rev. Phys. Chem. 56 (2005) 119–156.
[5] A. Omar, H. Abdullah, Electron transport analysis in zinc oxide-based dye-sensitized solar cells: a review, Renew. Sustain. Energy Rev. 31 (2014) 149–157.
[6] T. Daeneke, A.J. Mozer, T.H. Kwon, N.W. Duffy, A.B. Holmes, U. Bach, L. Spiccia, Dye regeneration and charge recombination in dye-sensitized solar cells with ferrocene derivatives as redox mediators, Energy Environ. Sci. 5 (2012) 7090–7099.
[7] V. Thavasi, V. Renugopalakrishnan, R. Jose, S. Ramakrishna, Controlled electron injection and transport at materials interfaces in dye sensitized solar cells, Mater. Sci. Eng. R Rep. 63 (2009) 81–99.
[8] Z. Ning, Y. Fu, H. Tian, Improvement of dye-sensitized solar cells: what we know and what we need to know, Energy Environ. Sci. 3 (2010) 1170–1181.
[9] F.-T. Kong, S.-Y. Dai, K.-J. Wang, Review of recent progress in dye-sensitized solar cells, Adv. Optoelectron. 2007 (2007) 1–13.
[10] V. Sugathan, E. John, K. Sudhakar, Recent improvements in dye sensitized solar cells: a review, Renew. Sustain. Energy Rev. 52 (2015) 54–64.
[11] J. Gong, K. Sumathy, Q. Qiao, Z. Zhou, Review on dye-sensitized solar cells (DSSCs): advanced techniques and research trends, Renew. Sustain. Energy Rev. 68 (2017) 234–246.
[12] M.K. Nazeeruddin, Q. Wang, L. Cevey, V. Aranyos, P. Liska, E. Figgemeier, C. Klein, N. Hirata, S. Koops, S.A. Haque, J.R. Durrant, A. Hagfeldt, A.B.P. Lever, M. Grätzel, DFT-INDO/S modeling of new high molar extinction coefficient charge-transfer sensitizers for solar cell applications, Inorg. Chem. 45 (2006) 787–797.
[13] G. Boschloo, A. Hagfeldt, Characteristics of the iodide/triiodide redox mediator in dye-sensitized solar cells, Acc. Chem. Res. 42 (2009) 1819–1826.
[14] G. Boschloo, L. Häggman, A. Hagfeldt, Quantification of the effect of 4-tert-butylpyridine addition to I^-/I_3 redox electrolytes in dye-sensitized nanostructured TiO_2 solar cells, J. Phys. Chem. B 110 (2006) 13144–13150.
[15] S.R. Raga, E.M. Barea, F. Fabregat-Santiago, Analysis of the origin of open circuit voltage in dye solar cells, J. Phys. Chem. Lett. 3 (2012) 1629–1634.
[16] C. Zhang, Y. Huang, Z. Huo, S. Chen, S. Dai, Photoelectrochemical effects of guanidinium thiocyanate on dye-sensitized solar cell performance and stability, J. Phys. Chem. C 113 (2009) 21779–21783.
[17] B. O'Regan, M. Grätzel, A low-cost, high-efficiency solar cell based on dye-sensitized colloidal TiO_2 films, Nature 353 (1991) 737–740.
[18] B. Hu, Q. Tang, B. He, L. Lin, H. Chen, Mesoporous TiO_2 anodes for efficient dye-sensitized solar cells: an efficiency of 9.86% under one sun illumination, J. Power Sources 267 (2014) 445–451.
[19] K. Fan, J. Yu, W. Ho, Improving photoanodes to obtain highly efficient dye-sensitized solar cells: a brief review, Mater. Horizons. 4 (2017) 319–344.
[20] P. Selvaraj, A. Roy, H. Ullah, P. Sujatha Devi, A.A. Tahir, T.K. Mallick, S. Sundaram, Soft-template synthesis of high surface area mesoporous titanium dioxide for dye-sensitized solar cells, Int. J. Energy Res. 43 (2019) 523–534.
[21] S.R. Gajjela, K. Ananthanarayanan, C. Yap, M. Grätzel, P. Balaya, Synthesis of mesoporous titanium dioxide by soft template based approach: characterization and application in dye-sensitized solar cells, Energy Environ. Sci. 3 (2010) 838–845.
[22] R. Govindaraj, S.M. Pandian, P. Ramasamy, S. Mukhopadhyay, Sol-gel synthesized mesoporous anatase titanium dioxide nanoparticles for dye sensitized solar cell (DSSC) applications, Bull. Mater. Sci. 38 (2015) 291–296.
[23] M. Hosni, Y. Kusumawati, S. Farhat, N. Jouini, T. Pauporté, Effects of oxide nanoparticle size and shape on electronic structure, charge transport, and recombination in dye-sensitized solar cell photoelectrodes, J. Phys. Chem. C 118 (2014) 16791–16798.

[24] H. Yu, J. Pan, Y. Bai, X. Zong, X. Li, L. Wang, Hydrothermal synthesis of a crystalline rutile TiO_2 nanorod based network for efficient dye-sensitized solar cells, Chem. - A Eur. J. 19 (2013) 13569–13574.

[25] B.H. Lee, M.Y. Song, S.Y. Jang, S.M. Jo, S.Y. Kwak, D.Y. Kim, Charge transport characteristics of high efficiency dye-sensitized solar cells based on electrospun TiO_2 nanorod photoelectrodes, J. Phys. Chem. C 113 (2009) 21453–21457.

[26] T. Marimuthu, N. Anandhan, R. Thangamuthu, Electrochemical synthesis of one-dimensional ZnO nanostructures on ZnO seed layer for DSSC applications, Appl. Surf. Sci. 428 (2018) 385–394.

[27] J. Zhang, Q. Li, S. Li, Y. Wang, C. Ye, P. Ruterana, H. Wang, An efficient photoanode consisting of TiO_2 nanoparticle-filled TiO_2 nanotube arrays for dye sensitized solar cells, J. Power Sources 268 (2014) 941–949.

[28] S. Shalini, T.S. Kumar, S. Prasanna, R. Balasundaraprabhu, Investigations on the effect of co-doping in enhancing the performance of nanostructured TiO_2 based DSSC sensitized using extracts of Hibiscus Sabdariffa calyx, Optik (Stuttg) 212 (2020) 164672.

[29] D.D. Babu, S.R. Gachumale, S. Anandan, A.V. Adhikari, New D-π-A type indole based chromogens for DSSC: design, synthesis and performance studies, Dyes Pigments 112 (2015) 183–191.

[30] Y. Wang, Z. Zheng, T. Li, N. Robertson, H. Xiang, W. Wu, J. Hua, W.H. Zhu, H. Tian, D-A-π-A motif quinoxaline-based sensitizers with high molar extinction coefficient for quasi-solid-state dye-sensitized solar cells, ACS Appl. Mater. Interfaces 8 (2016) 31016–31024.

[31] T. Sudyoadsuk, S. Pansay, S. Morada, R. Rattanawan, S. Namuangruk, T. Kaewin, S. Jungsuttiwong, V. Promarak, Synthesis and characterization of D-D-π-A-type organic dyes bearing carbazole-carbazole as a donor moiety (D-D) for efficient dye-sensitized solar cells, Eur. J. Org. Chem. 2013 (2013) 5051–5063.

[32] J.I. Fujisawa, M. Hanaya, Light harvesting and direct electron injection by interfacial charge-transfer transitions between TiO_2 and carboxy-anchor dye LEG4 in dye-sensitized solar cells, J. Phys. Chem. C 122 (2018) 8–15.

[33] H.C. Zhu, J. Zhang, Y.L. Wang, Adsorption orientation effects of porphyrin dyes on the performance of DSSC: comparison of benzoic acid and tropolone anchoring groups binding onto the TiO_2 anatase (101) surface, Appl. Surf. Sci. 433 (2018) 1137–1147.

[34] S. Balamurugan, S. Ganesan, Novel cobalt redox materials admitted in natrosol polymer with a thiophene based additive as a gel polymer electrolyte to tune up the efficiency of dye sensitized solar cells, Electrochim. Acta 329 (2020) 135169.

[35] T.W. Hamann, The end of iodide? Cobalt complex redox shuttles in DSSCs, Dalt. Trans. 41 (2012) 3111–3115.

[36] M. Kim, H.G. Yun, L.W. Jang, D.W. Jeon, M.G. Kang, J.H. Yoon, J.M. Kim, J.H. Park, I.H. Lee, J.J. Kim, Promising efficiency enhancement in cobalt redox couple-based back-illuminated dye-sensitized solar cells with titanium foil substrate, J. Power Sources 278 (2015) 32–37.

[37] R. Ruess, J. Horn, A. Ringleb, D. Schlettwein, Efficient electron collection by electrodeposited ZnO in dye-sensitized solar cells with $TEMPO^{+/0}$ as the redox mediator, J. Phys. Chem. C 123 (2019) 22074–22082.

[38] Y. Kusumawati, Z.R. Puteri, A.L. Ivansyah, H. Fansuri, M.A. Martoprawiro, The study of nitroxide radical redox-couple and anatase surface interaction: a guide to choose the best sensitizer, Theor. Chem. Acc. 138 (2019) 1–7.

[39] T. Higashino, H. Iiyama, S. Nimura, Y. Kurumisawa, H. Imahori, Effect of ligand structures of copper redox shuttles on photovoltaic performance of dye-sensitized solar cells, Inorg. Chem. 59 (2020) 452–459.

[40] A. Lennert, D.M. Guldi, Homoleptic and heteroleptic copper complexes as redox couples in dye-sensitized solar cells, ChemPhoto Chem 3 (2019) 636.

[41] S. Tontapha, W. Sang-aroon, T. Promgool, S. Kanokmedhakul, W. Maiaugree, E. Swatsitang, V. Homrahad, V. Amornkitbumrung, Electrocatalytic activity of disulfide/thiolate with graphene nanosheets as an efficient counter electrode for DSSCs: a DFT study, Mater. Today Commun. (2019).

[42] A. Singh, P. Singh, G. Kociok-Köhn, M. Trivedi, A. Kumar, R. Chauhan, S.B. Rane, C. Terashima, S.W. Gosavi, A. Fujishima, 1,1′-Bis(diphenylphosphino)ferrocene-appended nickel(ii) dithiolates as sensitizers in dye-sensitized solar cells, New J. Chem. 42 (2018) 9306–9316.

[43] A. Ghosh, S. Mishra, S. Giri, S.M. Mobin, A. Bera, S. Chatterjee, Electrolyte-free dye-sensitized solar cell with high open circuit voltage using a bifunctional ferrocene-based cyanovinyl molecule as dye and redox couple, Organometallics 37 (2018) 1999–2002.

[44] G.B.M.M.M. Nishshanke, A.K. Arof, T.M.W.J. Bandara, Review on mixed cation effect in gel polymer electrolytes for quasi solid-state dye-sensitized solar cells, Ionics (Kiel) 26 (2020) 3685–3704.

[45] A.A. Mohamad, Absorbency and conductivity of quasi-solid-state polymer electrolytes for dye-sensitized solar cells: a characterization review, J. Power Sources 329 (2016) 57–71.

[46] A.A. Mohamad, Physical properties of quasi-solid-state polymer electrolytes for dye-sensitised solar cells: a characterisation review, Sol. Energy 190 (2019) 434–452.

[47] T.M.W.J. Bandara, L.A. DeSilva, J.L. Ratnasekera, K.H. Hettiarachchi, A.P. Wijerathna, M. Thakurdesai, J. Preston, I. Albinsson, B.E. Mellander, High efficiency dye-sensitized solar cell based on a novel gel polymer electrolyte containing RbI and tetrahexylammonium iodide (Hex_4NI) salts and multi-layered photoelectrodes of TiO_2 nanoparticles, Renew. Sustain. Energy Rev. 103 (2019) 282–290.

[48] U. Ahmed, M. Alizadeh, N.A. Rahim, S. Shahabuddin, M.S. Ahmed, A.K. Pandey, A comprehensive review on counter electrodes for dye sensitized solar cells: a special focus on Pt-TCO free counter electrodes, Sol. Energy 174 (2018) 1097–1125.

[49] S.H. Hsu, C.T. Li, H.T. Chien, R.R. Salunkhe, N. Suzuki, Y. Yamauchi, K.C. Ho, K.C.W. Wu, Platinum-free counter electrode comprised of metal-organic-framework (MOF)-derived cobalt sulfide nanoparticles for efficient dye-sensitized solar cells (DSSCs), Sci. Rep. 4 (2014) 1–6.

[50] B. Tang, H. Yu, W. Huang, Y. Sun, X. Li, S. Li, T. Ma, Three-dimensional graphene networks and RGO-based counter electrode for DSSCs, RSC Adv. 9 (2019) 15678–15685.

[51] S.S. Nemala, K.S. Aneja, P. Bhargava, H.L.M. Bohm, S. Mallick, S. Bohm, Novel high-pressure airless spray exfoliation method for graphene nanoplatelets as a stable counter electrode in DSSC, Electrochim. Acta 285 (2018) 86–93.

[52] H. Zhou, J. Yin, Z. Nie, Z. Yang, D. Li, J. Wang, X. Liu, C. Jin, X. Zhang, T. Ma, Earth-abundant and nano-micro composite catalysts of Fe_3O_4@reduced graphene oxide for green and economical mesoscopic photovoltaic devices with high efficiencies up to 9, J. Mater. Chem. A. 4 (2015) 67–73.

[53] K. Kakiage, Y. Aoyama, T. Yano, K. Oya, J.I. Fujisawa, M. Hanaya, Highly-efficient dye-sensitized solar cells with collaborative sensitization by silyl-anchor and carboxy-anchor dyes, Chem. Commun. 51 (2015) 15894–15897.

[54] T. Liu, X. Mai, H. Chen, J. Ren, Z. Liu, Y. Li, L. Gao, N. Wang, J. Zhang, H. He, Z. Guo, Carbon nanotube aerogel–CoS_2 hybrid catalytic counter electrodes for enhanced photovoltaic performance dye-sensitized solar cells, Nanoscale 10 (2018) 4194–4201.

[55] W. Hou, Y. Xiao, G. Han, H. Zhou, Electro-polymerization of polypyrrole/multi-wall carbon nanotube counter electrodes for use in platinum-free dye-sensitized solar cells, Electrochim. Acta 190 (2016) 720–728.

[56] Q. Li, H. Li, X. Jin, Z. Chen, PEDOT and derivatives tailored conducting gel electrolytes for high-efficiency quasi-solid-state dye-sensitized solar cells, Electrochim. Acta 260 (2018) 413–419.

[57] T.Y. Chen, Y.J. Huang, C.T. Li, C.W. Kung, R. Vittal, K.C. Ho, Metal-organic framework/sulfonated polythiophene on carbon cloth as a flexible counter electrode for dye-sensitized solar cells, Nano Energy 32 (2017) 19–27.

[58] Q. Yang, J. Yao, K. Zhang, W. Wang, X. Zuo, H. Tang, M. Wu, G. Li, Perovskite-type $La_{1-x}Ca_xMnO_3$ manganese oxides as effective counter electrodes for dye-sensitized solar cells, J. Electroanal. Chem. 833 (2019) 1–8.

[59] Y. Zhong, P. Chen, B. Yang, X. Zuo, L. Zhou, X. Yang, G. Li, Low-cost platinum-free counter electrode of $La_{0.67}Sr_{0.33}MnO_3$ perovskite for efficient dye-sensitized solar cells, Appl. Phys. Lett. 106 (2015) 263903.

[60] K.S. Lee, Y. Lee, J.Y. Lee, J.H. Ahn, J.H. Park, Flexible and platinum-free dye-sensitized solar cells with conducting-polymer-coated graphene counter electrodes, ChemSusChem 5 (2012) 379–382.

[61] B. Zhao, H. Huang, P. Jiang, H. Zhao, X. Huang, P. Shen, D. Wu, R. Fu, S. Tan, Flexible counter electrodes based on mesoporous carbon aerogel for high-performance dye-sensitized solar cells, J. Phys. Chem. C 115 (2011) 22615–22621.

[62] M. Chen, L.L. Shao, Review on the recent progress of carbon counter electrodes for dye-sensitized solar cells, Chem. Eng. J. 304 (2016) 629–645.

[63] D. Zhang, M. Stojanovic, Y. Ren, Y. Cao, F.T. Eickemeyer, E. Socie, N. Vlachopoulos, J.-E. Moser, S.M. Zakeeruddin, A. Hagfeldt, M. Grätzel, A molecular photosensitizer achieves a V_{oc} of 1.24 V enabling highly efficient and stable dye-sensitized solar cells with copper(II/I)-based electrolyte, Nat. Commun. 12 (2021) 1777.

[64] M.A. Danish, N. Baloch, J.W. Mahmood, Zhang, Effect of natural resources, renewable energy and economic development on CO_2 emissions in BRICS countries, Sci. Total Environ. 678 (2019) 632–638.

[65] R. Ulucak Danish, S.U.D. Khan, Determinants of the ecological footprint: role of renewable energy, natural resources, and urbanization, Sustain. Cities Soc. 54 (2020) 101996.

[66] N. Mariotti, M. Bonomo, L. Fagiolari, N. Barbero, C. Gerbaldi, F. Bella, C. Barolo, Recent advances in eco-friendly and cost-effective materials towards sustainable dye-sensitized solar cells, Green Chem. 22 (2020) 7168–7218.

[67] S.A. Haque, E. Palomares, B.M. Cho, A.N.M. Green, N. Hirata, D.R. Klug, J.R. Durrant, Charge separation versus recombination in dye-sensitized nanocrystalline solar cells: the minimization of kinetic redundancy, J. Am. Chem. Soc. 127 (2005) 3456–3462.

[68] S. Shalini, R. Balasundara Prabhu, S. Prasanna, T.K. Mallick, S. Senthilarasu, Review on natural dye sensitized solar cells: operation, materials and methods, Renew. Sustain. Energy Rev. 51 (2015) 1306–1325.

[69] N.A. Ludin, A.M. Al-Alwani Mahmoud, A. Bakar Mohamad, A.A.H. Kadhum, K. Sopian, N.S. Abdul Karim, Review on the development of natural dye photosensitizer for dye-sensitized solar cells, Renew. Sustain. Energy Rev. 31 (2014) 386–396.

[70] D. Zhang, S.M. Lanier, J.A. Downing, J.L. Avent, J. Lum, J.L. McHale, Betalain pigments for dye-sensitized solar cells, J. Photochem. Photobiol. A Chem. 195 (2008) 72–80.

[71] C. Sandquist, J.L. McHale, Improved efficiency of betanin-based dye-sensitized solar cells, J. Photochem. Photobiol. A Chem. 221 (2011) 90–97.

[72] C.I. Oprea, A. Dumbrava, I. Enache, A. Georgescu, M.A. Gîrţu, A combined experimental and theoretical study of natural betalain pigments used in dye-sensitized solar cells, J. Photochem. Photobiol. A Chem. 240 (2012) 5–13.

[73] K.U. Isah, U. Ahmadu, A. Idris, M.I. Kimpa, U.E. Uno, M.M. Ndamitso, N. Alu, Betalain pigments as natural photosensitizers for dye-sensitized solar cells: the effect of dye pH on the photoelectric parameters, Mater. Renew. Sustain. Energy. 4 (2015) 1–5.

[74] S. Sreeja, S. Prabhakaran, B. Pesala, Efficiency enhancement of betanin dye-sensitized solar cells using plasmon-enhanced silver nanoparticles, in: S. Singh, V. Ramadesigan (Eds.), Adv. Energy Res., Springer, Singapore, 2020, pp. 9–18.

[75] M.J. García-Salinas, M.J. Ariza, Optimizing a simple natural dye production method for dye-sensitized solar cells: examples for betalain (Bougainvillea and beetroot extracts) and anthocyanin dyes, Appl. Sci. 9 (2019) 2515.

[76] G. Calogero, J.H. Yum, A. Sinopoli, G. Di Marco, M. Grätzel, M.K. Nazeeruddin, Anthocyanins and betalains as light-harvesting pigments for dye-sensitized solar cells, Sol. Energy 86 (2012) 1563–1575.

[77] A. Thankappan, S. Divya, A.K. Augustine, C.P. Girijavallaban, P. Radhakrishnan, S. Thomas, V.P.N. Nampoori, Highly efficient betanin dye based ZnO and ZnO/Au Schottky barrier solar cell, Thin Solid Films 583 (2015) 102–107.

[78] N.A. Treat, F.J. Knorr, J.L. McHale, Templated assembly of betanin chromophore on TiO_2: aggregation-enhanced light-harvesting and efficient electron injection in a natural dye-sensitized solar cell, J. Phys. Chem. C 120 (2016) 9122–9131.

[79] A. Kay, M. Grätzel, Artificial photosynthesis. 1. Photosensitization of TiO_2 solar cells with chlorophyll derivatives and related natural porphyrins, J. Phys. Chem. 97 (1993) 6272–6277.

[80] Y. Amao, T. Komori, Bio-photovoltaic conversion device using chlorine-e6 derived from chlorophyll from Spirulina adsorbed on a nanocrystalline TiO_2 film electrode, Biosens. Bioelectron. 19 (2004) 843–847.

[81] H. Chang, H.M. Wu, T.L. Chen, K.D. Huang, C.S. Jwo, Y.J. Lo, Dye-sensitized solar cell using natural dyes extracted from spinach and ipomoea, J. Alloys Compd. 495 (2010) 606–610.

[82] X.F. Wang, H. Tamiaki, L. Wang, N. Tamai, O. Kitao, H. Zhou, S.I. Sasaki, Chlorophyll- a derivatives with various hydrocarbon ester groups for efficient dye-sensitized solar cells: static and ultrafast evaluations on electron injection and charge collection processes, Langmuir 26 (2010) 6320–6327.

[83] H. Chang, Y.J. Lo, Pomegranate leaves and mulberry fruit as natural sensitizers for dye-sensitized solar cells, Sol. Energy 84 (2010) 1833–1837.

[84] M.M. Noor, M.H. Buraidah, M.A. Careem, S.R. Majid, A.K. Arof, An optimized poly(vinylidene fluoride-hexafluoropropylene)-NaI gel polymer electrolyte and its application in natural dye sensitized solar cells, Electrochim. Acta 121 (2014) 159–167.

[85] R. Syafinar, N. Gomesh, M. Irwanto, M. Fareq, Y.M. Irwan, Chlorophyll pigments as nature based dye for dye-sensitized solar cell (DSSC), in: Energy Procedia, 2015, pp. 896–902.

[86] B.B. Panda, P.K. Mahapatra, M.K. Ghosh, Application of chlorophyll as sensitizer for ZnS photoanode in a dye-sensitized solar cell (DSSC), J. Electron. Mater. 47 (2018) 3657–3665.

[87] H.C. Hassan, Z.H.Z. Abidin, M.A. Careem, A.K. Arof, Chlorophyll as sensitizer in I^-/I_3^- -based solar cells with quasi-solid-state electrolytes, High Perform. Polym. 26 (2014) 647–652.

[88] K.A. Aduloju, M.B. Shitta, S. Justus, Effect of extracting solvents on the stability and performances of dye-sensitized solar cell prepared using extract from *Lawsonia Inermis*, Fundam. J. Mod. Phys. 1 (2011) 261–268.

[89] P. Luo, H. Niu, G. Zheng, X. Bai, M. Zhang, W. Wang, From salmon pink to blue natural sensitizers for solar cells: *canna indica* L., *Salvia splendens*, cowberry and *Solanum nigrum* L, Spectrochim. Acta Part A Mol. Biomol. Spectrosc. 74 (2009) 936–942.

[90] H. Chang, K.-C. Cho, T.-L. Chen, K.-H. Chu, L.-J. Jiang, Preparation and characterization of anthocyanin dye and counter electrode thin film with carbon nanotubes for dye-sensitized solar cells, Mater. Trans. 52 (2011) 1977–1982.

[91] A.D. Zikri, J. Gunlazuardi, Preparation of a TiO_2-based dye-sensitized solar cell comprising anthocyanin from mangosteen pericarp (*Garcinia mangostana* L.) as the sensitizer: co-pigmentation effect on sensitizer and solar cell efficiency, J. Phys. Conf. Ser. 1442 (2020) 012062.

[92] R. Hardeli, L.P. Zainul, Isara, Preparation of Dye Sensitized Solar Cell (DSSC) using anthocyanin color dyes from jengkol shell (*Pithecellobium lobatum* Benth.) by the gallate acid copigmentation, J. Phys. Conf. Ser. (2019) 12021.

[93] C. Diaz-Uribe, W. Vallejo, G. Camargo, A. Muñoz-Acevedo, C. Quiñones, E. Schott, X. Zarate, Potential use of an anthocyanin-rich extract from berries of Vaccinium meridionale Swartz as sensitizer for TiO_2 thin films–an experimental and theoretical study, J. Photochem. Photobiol. A Chem. 384 (2019) 112050.

[94] D.M. Sampaio, R.S. Babu, H.R.M. Costa, A.L.F. de Barros, Investigation of nanostructured TiO_2 thin film coatings for DSSCs application using natural dye extracted from jabuticaba fruit as photosensitizers, Ionics (Kiel) 25 (2019) 2893–2902.

[95] S. Sreeja, B. Pesala, Co-sensitization aided efficiency enhancement in betanin–chlorophyll solar cell,, Mater. Renew. Sustain. Energy 7 (2018) 25.

[96] W.A. Dhafina, M.Z. Daud, H. Salleh, The sensitization effect of anthocyanin and chlorophyll dyes on optical and photovoltaic properties of zinc oxide based dye-sensitized solar cells, Optik (Stuttg) 207 (2020) 163808.

[97] D. Dodoo-Arhin, R.C.T. Howe, G. Hu, Y. Zhang, P. Hiralal, A. Bello, G. Amaratunga, T. Hasan, Inkjet-printed graphene electrodes for dye-sensitized solar cells, Carbon N. Y. 105 (2016) 33–41.

[98] F.J. Knorr, J.L. McHale, A.E. Clark, A. Marchioro, J.E. Moser, Dynamics of interfacial electron transfer from betanin to nanocrystalline TiO_2: the pursuit of two-electron injection, J. Phys. Chem. C 119 (2015) 19030–19041.

[99] Z.H. Damayanti, G.R. Anindika, E. Santoso, S. Akhlus, Y. Kusumawati, The electronic properties study of betanin and their derivatives compound: an explanation to betanin limitation in DSSC application, in: AIP Conf. Proc., 2020, p. 20068.

[100] R. Ramamoorthy, N. Radha, G. Maheswari, S. Anandan, S. Manoharan, R. Victor Williams, Betalain and anthocyanin dye-sensitized solar cells, J. Appl. Electrochem. 46 (2016) 929–941.

[101] L. Zhang, J.M. Cole, Dye aggregation in dye-sensitized solar cells, J. Mater. Chem. A 5 (2017) 19541–19559.

[102] P.V. Kamat, J.P. Chauvet, R.W. Fessenden, Photoelectrochemistry in particulate systems. 4. Photosensitization of a TiO_2 semiconductor with a chlorophyll analogue, J. Phys. Chem. 90 (1986) 1389–1394.

[103] X.F. Wang, A. Matsuda, Y. Koyama, H. Nagae, S. ichi Sasaki, H. Tamiaki, Y. Wada, Effects of plant carotenoid spacers on the performance of a dye-sensitized solar cell using a chlorophyll derivative: enhancement of photocurrent determined by one electron-oxidation potential of each carotenoid, Chem. Phys. Lett. 423 (2006) 470–475.

[104] X.F. Wang, O. Kitao, H. Zhou, H. Tamiaki, S.I. Sasaki, Extension of π-conjugation length along the Qy axis of a chlorophyll a derivative for efficient dye-sensitized solar cells, Chem. Commun. (2009) 1523–1525.

[105] X.F. Wang, O. Kitao, E. Hosono, H. Zhou, S. ichi Sasaki, H. Tamiaki, TiO_2- and ZnO-based solar cells using a chlorophyll a derivative sensitizer for light-harvesting and energy conversion, J. Photochem. Photobiol. A Chem. 210 (2010) 145–152.

[106] X.F. Wang, Y. Koyama, O. Kitao, Y. Wada, S. ich Sasaki, H. Tamiaki, H. Zhou, Significant enhancement in the power-conversion efficiency of chlorophyll co-sensitized solar cells by mimicking the principles of natural photosynthetic light-harvesting complexes, Biosens. Bioelectron. 25 (2010) 1970–1976.

[107] J. Jasieniak, M. Johnston, E.R. Waclawik, Characterization of a porphyrin-containing dye-sensitized solar cell, J. Phys. Chem. B 108 (2004) 12962–12971.

[108] A. Yella, H.W. Lee, H.N. Tsao, C. Yi, A.K. Chandiran, M.K. Nazeeruddin, E.W.G. Diau, C.Y. Yeh, S.M. Zakeeruddin, M. Grätzel, Porphyrin-sensitized solar cells with cobalt (II/III)-based redox electrolyte exceed 12 percent efficiency, Science (80-) 334 (2011) 629–634.

[109] Farcasanu Ruta, Anthocyanins and anthocyanin-derived products in yeast-fermented beverages, Antioxidants 8 (2019) 182.

[110] A.L. Pinto, L. Cruz, V. Gomes, H. Cruz, G. Calogero, V. de Freitas, F. Pina, A.J. Parola, J. Carlos Lima, Catechol versus carboxyl linkage impact on DSSC performance of synthetic pyranoflavylium salts, Dyes Pigments 170 (2019) 107577.

[111] N. Prabavathy, S. Shalini, R. Balasundaraprabhu, D. Velauthapillai, S. Prasanna, N. Muthukumarasamy, Enhancement in the photostability of natural dyes for dye-sensitized solar cell (DSSC) applications: a review, Int. J. Energy Res. 41 (2017) 1372–1396.

[112] O.A. Ileperuma, Gel polymer electrolytes for dye sensitised solar cells: a review, Mater. Technol. 28 (2013) 65–70.

[113] M.S. Su'ait, M.Y.A. Rahman, A. Ahmad, Review on polymer electrolyte in dye-sensitized solar cells (DSSCs), Sol. Energy 115 (2015) 452–470.

[114] M.H. Buraidah, L.P. Teo, S.N.F. Yusuf, M.M. Noor, M.Z. Kufian, M.A. Careem, S.R. Majid, R.M. Taha, A.K. Arof, TiO_2/chitosan-$NH_4I(+I_2)$-BMII-based dye-sensitized solar cells with Anthocyanin dyes extracted from black rice and red cabbage, Int. J. Photoenergy 2011 (2011) 1–11.

[115] M.H. Buraidah, A.K. Arof, Characterization of chitosan/PVA blended electrolyte doped with NH 4I, J. Non-Cryst. Solids 357 (2011) 3261–3266.

[116] Y. Yang, H. Hu, C.H. Zhou, S. Xu, B. Sebo, X.Z. Zhao, Novel agarose polymer electrolyte for quasi-solid state dye-sensitized solar cell, J. Power Sources 196 (2011) 2410–2415.

[117] R. Singh, A.R. Polu, B. Bhattacharya, H.W. Rhee, C. Varlikli, P.K. Singh, Perspectives for solid biopolymer electrolytes in dye sensitized solar cell and battery application, Renew. Sustain. Energy Rev. 65 (2016) 1098–1117.

[118] X. Huang, Y. Liu, J. Deng, B. Yi, X. Yu, P. Shen, S. Tan, A novel polymer gel electrolyte based on cyanoethylated cellulose for dye-sensitized solar cells, Electrochim. Acta 80 (2012) 219–226.

[119] C.M. Shih, Y.L. Wu, Y.C. Wang, S.R. Kumar, Y.L. Tung, C.C. Yang, S.J. Lue, Ionic transport and interfacial interaction of iodide/iodine redox mechanism in agarose electrolyte containing colloidal titanium dioxide nanoparticles, J. Photochem. Photobiol. A Chem. 356 (2018) 565–572.

[120] Y. Yang, J. Cui, P. Yi, X. Zheng, X. Guo, W. Wang, Effects of nanoparticle additives on the properties of agarose polymer electrolytes, J. Power Sources 248 (2014) 988–993.

[121] N.N. Mobarak, N. Ramli, A. Ahmad, M.Y.A. Rahman, Chemical interaction and conductivity of carboxymethyl κ-carrageenan based green polymer electrolyte, Solid State Ionics 224 (2012) 51–57.

[122] F.N. Jumaah, N.N. Mobaraka, A. Ahmad, N. Ramli, Characterization of ι -carrageenan and its derivative based green polymer electrolytes, in: AIP Conf. Proc., 2013, pp. 768–774.

[123] T.J. Trivedi, D.N. Srivastava, R.D. Rogers, A. Kumar, Agarose processing in protic and mixed protic-aprotic ionic liquids: dissolution, regeneration and high conductivity, high strength ionogels, Green Chem. 14 (2012) 2831–2839.

[124] W.G. Moon, G.P. Kim, M. Lee, H.D. Song, J. Yi, A biodegradable gel electrolyte for use in high-performance flexible supercapacitors, ACS Appl. Mater. Interfaces 7 (2015) 3503–3511.

[125] J. Yoon, D.K. Kang, J. Won, J.Y. Park, Y.S. Kang, Dye-sensitized solar cells using ion-gel electrolytes for long-term stability, J. Power Sources 201 (2012) 395–401.

[126] W. Kwon, J.-M. Kim, S.-W. Rhee, Electrocatalytic carbonaceous materials for counter electrodes in dye-sensitized solar cells, J. Mater. Chem. A 1 (2013) 3202–3215.

[127] W. Wei, H. Wang, Y.H. Hu, A review on PEDOT-based counter electrodes for dye-sensitized solar cells, Int. J. Energy Res. 38 (2014) 1099–1111.

[128] K. Saranya, M. Rameez, A. Subramania, Developments in conducting polymer based counter electrodes for dye-sensitized solar cells - an overview, Eur. Polym. J. 66 (2015) 207–227.

[129] C. Gao, Q. Han, M. Wu, Review on transition metal compounds based counter electrode for dye-sensitized solar cells, J. Energy Chem. 27 (2018) 703–712.

[130] Q. Tang, J. Duan, Y. Duan, B. He, L. Yu, Recent advances in alloy counter electrodes for dye-sensitized solar cells. A critical review, Electrochim. Acta 178 (2015) 886–899.

[131] P. Simon, Y. Gogotsi, Materials for electrochemical capacitors, Nat. Mater. 7 (2008) 845–854.
[132] J.B. Goodenough, Y. Kim, Challenges for rechargeable Li batteries, Chem. Mater. 22 (2010) 587–603.
[133] A. Kay, M. Grätzel, Low cost photovoltaic modules based on dye sensitized nanocrystalline titanium dioxide and carbon powder, Sol. Energy Mater. Sol. Cells 44 (1996) 99–117.
[134] R. Ryoo, S.H. Joo, S. Jun, Synthesis of highly ordered carbon molecular sieves via template-mediated structural transformation, J. Phys. Chem. B 103 (1999) 7743–7746.
[135] P. Dong, C.L. Pint, M. Hainey, F. Mirri, Y. Zhan, J. Zhang, M. Pasquali, R.H. Hauge, R. Verduzco, M. Jiang, H. Lin, J. Lou, Vertically aligned single-walled carbon nanotubes as low-cost and high electrocatalytic counter electrode for dye-sensitized solar cells, ACS Appl. Mater. Interfaces 3 (2011) 3157–3161.
[136] W.J. Lee, E. Ramasamy, D.Y. Lee, J.S. Song, Efficient dye-sensitized solar cells with catalytic multiwall carbon nanotube counter electrodes, ACS Appl. Mater. Interfaces 1 (2009) 1145–1149.
[137] C. Liang, Z. Li, S. Dai, Mesoporous carbon materials: synthesis and modification, Angew. Chem. Int. Ed. 47 (2008) 3696–3717.
[138] S. Huang, Z. Yang, L. Zhang, R. He, T. Chen, Z. Cai, Y. Luo, H. Lin, H. Cao, X. Zhu, H. Peng, A novel fabrication of a well distributed and aligned carbon nanotube film electrode for dye-sensitized solar cells, J. Mater. Chem. 22 (2012) 16833–16838.
[139] J. Han, H. Kim, D.Y. Kim, S.M. Jo, S.Y. Jang, Water-soluble polyelectrolyte-grafted multiwalled carbon nanotube thin films for efficient counter electrode of dye-sensitized solar cells, ACS Nano 4 (2010) 3503–3509.
[140] P. Joshi, L. Zhang, Q. Chen, D. Galipeau, H. Fong, Q. Qiao, Electrospun carbon nanofibers as low-cost counter electrode for dye-sensitized solar cells, ACS Appl. Mater. Interfaces 2 (2010) 3572–3577.
[141] S.H. Park, B.K. Kim, W.J. Lee, Electrospun activated carbon nanofibers with hollow core/highly mesoporous shell structure as counter electrodes for dye-sensitized solar cells, J. Power Sources 239 (2013) 122–127.
[142] S.H. Park, H.R. Jung, W.J. Lee, Hollow activated carbon nanofibers prepared by electrospinning as counter electrodes for dye-sensitized solar cells, Electrochim. Acta 102 (2013) 423–428.
[143] S. Iijima, Helical microtubules of graphitic carbon, Nature 354 (1991) 56–58.
[144] A.K. Geim, K.S. Novoselov, The rise of graphene, Nat. Mater. 6 (2007) 183–191.
[145] R. Ryoo, S.H. Joo, M. Kruk, M. Jaroniec, Ordered mesoporous carbons, Adv. Mater. 13 (2001) 677–681.
[146] H.P. Boehm, Some aspects of the surface chemistry of carbon blacks and other carbons, Carbon N. Y. 32 (1994) 759–769.
[147] P. Serp, M. Corrias, P. Kalck, Carbon nanotubes and nanofibers in catalysis, Appl. Catal. A Gen. 253 (2003) 337–358.
[148] S. Peng, F. Cheng, J. Shi, J. Liang, Z. Tao, J. Chen, High-surface-area microporous carbon as the efficient photocathode of dye-sensitized solar cells, Solid State Sci. 11 (2009) 2051–2055.
[149] E. Ramasamy, J. Chun, J. Lee, Soft-template synthesized ordered mesoporous carbon counter electrodes for dye-sensitized solar cells, Carbon N. Y. 48 (2010) 4563–4565.
[150] T. Peng, W. Sun, X. Sun, N. Huang, Y. Liu, C. Bu, S. Guo, X.Z. Zhao, Direct tri-constituent co-assembly of highly ordered mesoporous carbon counter electrode for dye-sensitized solar cells, Nanoscale 5 (2013) 337–341.
[151] Y. Chen, Y. Zhu, Z. Chen, Three-dimensional ordered macroporous carbon as counter electrodes in dye-sensitized solar cells, Thin Solid Films 539 (2013) 122–126.
[152] B. Fang, S.Q. Fan, J.H. Kim, M.S. Kim, M. Kim, N.K. Chaudhari, J. Ko, J.S. Yu, Incorporating hierarchical nanostructured carbon counter electrode into metal-free organic dye-sensitized solar cell, Langmuir 26 (2010) 11238–11243.
[153] S.Q. Fan, B. Fang, J.H. Kim, B. Jeong, C. Kim, J.S. Yu, J. Ko, Ordered multimodal porous carbon as highly efficient counter electrodes in dye-sensitized and quantum-dot solar cells, Langmuir 26 (2010) 13644–13649.
[154] H. Choi, H. Kim, S. Hwang, Y. Han, M. Jeon, Graphene counter electrodes for dye-sensitized solar cells prepared by electrophoretic deposition, J. Mater. Chem. 21 (2011) 7548–7551.
[155] D.W. Zhang, X.D. Li, H.B. Li, S. Chen, Z. Sun, X.J. Yin, S.M. Huang, Graphene-based counter electrode for dye-sensitized solar cells, Carbon N. Y. 49 (2011) 5382–5388.
[156] S.Y. Jang, Y.G. Kim, D.Y. Kim, H.G. Kim, S.M. Jo, Electrodynamically sprayed thin films of aqueous dispersible graphene nanosheets: highly efficient cathodes for dye-sensitized solar cells, ACS Appl. Mater. Interfaces 4 (2012) 3500–3507.
[157] W.Y. Cheng, C.C. Wang, S.Y. Lu, Graphene aerogels as a highly efficient counter electrode material for dye-sensitized solar cells, Carbon N. Y. 54 (2013) 291–299.
[158] J.D. Roy-Mayhew, D.J. Bozym, C. Punckt, I.A. Aksay, Functionalized graphene as a catalytic counter electrode in dye-sensitized solar cells, ACS Nano 4 (2010) 6203–6211.
[159] S. Hou, X. Cai, H. Wu, X. Yu, M. Peng, K. Yan, D. Zou, Nitrogen-doped graphene for dye-sensitized solar cells and the role of nitrogen states in triiodide reduction, Energy Environ. Sci. 6 (2013) 3356–3362.
[160] S. Das, P. Sudhagar, E. Ito, D.Y. Lee, S. Nagarajan, S.Y. Lee, Y.S. Kang, W. Choi, Effect of HNO_3 functionalization on large scale graphene for enhanced tri-iodide reduction in dye-sensitized solar cells, J. Mater. Chem. 22 (2012) 20490–20497.
[161] Z. Yu, Y. Bai, Y. Wang, Y. Liu, Y. Zhao, Y. Liu, K. Sun, One-step synthesis of three-dimensional nitrogen and sulfur co-doped graphene networks as low cost metal-free counter electrodes for dye-sensitized solar cells, Chem. Eng. J. 311 (2017) 302–309.
[162] F. Gong, Z. Li, H. Wang, Z.S. Wang, Enhanced electrocatalytic performance of graphene via incorporation of SiO_2 nanoparticles for dye-sensitized solar cells, J. Mater. Chem. 22 (2012) 17321–17327.
[163] Q. Chen, X. Tan, Y. Liu, S. Liu, M. Li, Y. Gu, P. Zhang, S. Ye, Z. Yang, Y. Yang, Biomass-derived porous graphitic carbon materials for energy and environmental applications, J. Mater. Chem. A 8 (2020) 5773–5811.
[164] E. Santoso, R. Ediati, Y. Kusumawati, H. Bahruji, D.O. Sulistiono, D. Prasetyoko, Review on recent advances of carbon based adsorbent for methylene blue removal from waste water, Mater. Today Chem. 16 (2020) 100233.
[165] G. Wang, D. Wang, S. Kuang, W. Xing, S. Zhuo, Hierarchical porous carbon derived from rice husk as a low-cost counter electrode of dye-sensitized solar cells, Renew. Energy 63 (2014) 708–714.
[166] C.K. Kim, I.T. Choi, S.H. Kang, H.K. Kim, Anchovy-derived nitrogen and sulfur co-doped porous carbon materials for high-performance supercapacitors and dye-sensitized solar cells, RSC Adv. 7 (2017) 35565–35574.
[167] W. Maiaugree, S. Lowpa, M. Towannang, P. Rutphonsan, A. Tangtrakarn, S. Pimanpang, P. Maiaugree, N. Ratchapolthavisin, W. Sang-Aroon, W. Jarernboon, V. Amornkitbamrung, A dye sensitized solar cell using natural counter electrode and natural dye derived from mangosteen peel waste, Sci. Rep. 5 (2015) 1–12.
[168] P. Huang, S. Xu, M. Zhang, W. Zhong, Z. Xiao, Y. Luo, Lotus leaf derived natural dye as sensitizer and biochar as counter electrode for dye-sensitized solar cells, in: Mater. Sci. Forum, 2020, pp. 884–892.
[169] S. Mathew, A. Yella, P. Gao, R. Humphry-Baker, B.F.E. Curchod, N. Ashari-Astani, I. Tavernelli, U. Rothlisberger, M.K. Nazeeruddin, M. Grätzel, Dye-sensitized solar cells with 13% efficiency achieved through the molecular engineering of porphyrin sensitizers, Nat. Chem. 6 (2014) 242–247.
[170] K.D.M.S.P.K. Kumarasinghe, G.R.A. Kumara, R.M.G. Rajapakse, D.N. Liyanage, K. Tennakone, Activated coconut shell charcoal based counter electrode for dye-sensitized solar cells, Org. Electron. 71 (2019) 93–97.
[171] C. Xiang, T. Lv, C.A. Okonkwo, M. Zhang, L. Jia, W. Xia, Nitrogen-doped bagasse-derived carbon/low Pt composite as counter electrodes for high efficiency dye-sensitized solar cell, J. Electrochem. Soc. 164 (2017) H203–H210.
[172] H.Y. Chen, T.L. Zhang, J. Fan, D. Bin Kuang, C.Y. Su, Electrospun hierarchical TiO2 nanorods with high porosity for efficient dye-sensitized solar cells, ACS Appl. Mater. Interfaces 5 (2013) 9205–9211.
[173] X. Wang, S. Yun, W. Fang, C. Zhang, X. Liang, Z. Lei, Z. Liu, Layer-stacking activated carbon derived from sunflower stalk as electrode materials for high-performance supercapacitors, ACS Sustain. Chem. Eng. 6 (2018) 11397–11407.
[174] Z. Wang, S. Yun, X. Wang, C. Wang, Y. Si, Y. Zhang, H. Xu, Aloe peel-derived honeycomb-like bio-based carbon with controllable morphology and its superior electrochemical properties for new energy devices, Ceram. Int. 45 (2019) 4208–4218.
[175] S. Yun, X. Zhou, Y. Zhang, C. Wang, Y. Hou, Tantalum-based bimetallic oxides deposited on spherical carbon of biological origin for use as counter electrodes in dye sensitized solar cells, Electrochim. Acta 309 (2019) 371–381.
[176] C. Wang, S. Yun, Q. Fan, Z. Wang, Y. Zhang, F. Han, Y. Si, A. Hagfeldt, A hybrid niobium-based oxide with bio-based porous carbon as an efficient electrocatalyst in photovoltaics: a general strategy for understanding the catalytic mechanism, J. Mater. Chem. A 7 (2019) 14864–14875.
[177] J. Li, S. Yun, F. Han, Y. Si, A. Arshad, Y. Zhang, B. Chidambaram, N. Zafar, X. Qiao, Biomass-derived carbon boosted catalytic properties of tungsten-based nanohybrids for accelerating the triiodide reduction in dye-sensitized solar cells, J. Colloid Interface Sci. 578 (2020) 184–194.
[178] F. Han, S. Yun, J. Shi, Y. Zhang, Y. Si, C. Wang, N. Zafar, J. Li, X. Qiao, Efficient dual-function catalysts for triiodide reduction reaction and hydrogen evolution reaction using unique 3D network aloe waste-derived carbon-supported molybdenum-based bimetallic oxide nanohybrids, Appl. Catal. B Environ. 273 (2020) 119004.
[179] A. Arshad, S. Yun, Y. Si, F. Han, Y. Zhang, Y. Zhang, Z. Wang, C. Wang, Aloe vera-peel derived porous carbon integrated Co/Mn-oxide based nano-hybrids: an efficient electrocatalyst in advanced photovoltaics, J. Power Sources 451 (2020) 227731.
[180] X. Qiao, S. Yun, F. Han, Y. Zhang, A. Arshad, B. Chidambaram, Z. Wang, N. Zafar, Y. Si, J. Li, Honeycomb-like bio-based carbon framework decorated with ternary tantalum-based compounds as efficient and durable electrocatalysts for triiodide reduction reaction, Int. J. Energy Res. 44 (2020) 7630–7644.
[181] C. Wang, S. Yun, H. Xu, Z. Wang, F. Han, Y. Zhang, Y. Si, M. Sun, Dual functional application of pomelo peel-derived bio-based carbon with controllable morphologies: an efficient catalyst for triiodide reduction and accelerant for anaerobic digestion, Ceram. Int. 46 (2020) 3292–3303.
[182] Y. Zhang, S. Yun, Z. Wang, Y. Zhang, C. Wang, A. Arshad, F. Han, Y. Si, W. Fang, Highly efficient bio-based porous carbon hybridized with tungsten carbide as counter electrode for dye-sensitized solar cell, Ceram. Int. 46 (2020) 15812–15821.
[183] R. Madhu, V. Veeramani, S.M. Chen, J. Palanisamy, A.T. Ezhil Vilian, Pumpkin stem-derived activated carbons as counter electrodes for dye-sensitized solar cells, RSC Adv. 4 (2014) 63917–63921.
[184] N. Sofyan, M. Muhammad, A. Ridhova, A.H. Yuwono, A. Udhiarto, Characteristics of carbon pyrolyzed from table sugar and sucrose for Pt-less DSSC counter electrode, Int. J. Technol. 9 (2018) 372.
[185] B. Baptayev, A. Aukenova, D. Mustazheb, M. Kazaliyev, M.P. Balanay, Pt-free counter electrode based on orange fiber-derived carbon embedded cobalt sulfide nanoflakes for dye-sensitized solar cells, J. Photochem. Photobiol. A Chem. 383 (2019) 111977.
[186] R. Pode, Potential applications of rice husk ash waste from rice husk biomass power plant, Renew. Sustain. Energy Rev. 53 (2016) 1468–1485.

[187] M.H. Yeh, C.L. Sun, J.S. Su, L.Y. Lin, C.P. Lee, C.Y. Chen, C.G. Wu, R. Vittal, K.C. Ho, A low-cost counter electrode of ITO glass coated with a graphene/Nafion® composite film for use in dye-sensitized solar cells, Carbon N. Y. 50 (2012) 4192–4202.

[188] D.Y. Chung, Y.J. Son, J.M. Yoo, J.S. Kang, C.Y. Ahn, S. Park, Y.E. Sung, Coffee waste-derived hierarchical porous carbon as a highly active and durable electrocatalyst for electrochemical energy applications, ACS Appl. Mater. Interfaces 9 (2017) 41303–41313.

[189] R. Senthamarai, V.M. Ramakrishnan, B. Palanisamy, S. Kulandhaivel, Synthesis of TiO_2 nanostructures by green approach as photoanodes for dye-sensitized solar cells, Int. J. Energy Res. 45 (2021) 3089–3096.

[190] M. Anbuvannan, M. Ramesh, G. Viruthagiri, N. Shanmugam, N. Kannadasan, *Anisochilus carnosus* leaf extract mediated synthesis of zinc oxide nanoparticles for antibacterial and photocatalytic activities, Mater. Sci. Semicond. Process. 39 (2015) 621–628.

[191] D. Suresh, P.C. Nethravathi, Udayabhanu, H. Rajanaika, H. Nagabhushana, S.C. Sharma, Green synthesis of multifunctional zinc oxide (ZnO) nanoparticles using *Cassia fistula* plant extract and their photodegradative, antioxidant and antibacterial activities, Mater. Sci. Semicond. Process. 31 (2015) 446–454.

[192] S.A. Khan, F. Noreen, S. Kanwal, A. Iqbal, G. Hussain, Green synthesis of ZnO and Cu-doped ZnO nanoparticles from leaf extracts of *Abutilon indicum, Clerodendrum infortunatum, Clerodendrum inerme* and investigation of their biological and photocatalytic activities, Mater. Sci. Eng. C 82 (2018) 46–59.

[193] F.T. Thema, E. Manikandan, M.S. Dhlamini, M. Maaza, Green synthesis of ZnO nanoparticles via *Agathosma betulina* natural extract, Mater. Lett. 161 (2015) 124–127.

[194] R. Rathnasamy, P. Thangasamy, R. Thangamuthu, S. Sampath, V. Alagan, Green synthesis of ZnO nanoparticles using *Carica papaya* leaf extracts for photocatalytic and photovoltaic applications, J. Mater. Sci. Mater. Electron. 28 (2017) 10374–10381.

[195] L. Fu, Z. Fu, *Plectranthus amboinicus* leaf extract-assisted biosynthesis of ZnO nanoparticles and their photocatalytic activity, Ceram. Int. 41 (2015) 2492–2496.

[196] M. Anbuvannan, M. Ramesh, G. Viruthagiri, N. Shanmugam, N. Kannadasan, Synthesis, characterization and photocatalytic activity of ZnO nanoparticles prepared by biological method, Spectrochim. Acta Part A Mol. Biomol. Spectrosc. 143 (2015) 304–308.

[197] A. Rajan, E. Cherian, G. Baskar, Biosynthesis of zinc oxide nanoparticles using *Aspergillus fumigatus* JCF and its antibacterial activity, Int. J. Mod. Sci. Technol. 1 (2016) 52–57.

[198] C. Jayaseelan, A.A. Rahuman, A.V. Kirthi, S. Marimuthu, T. Santhoshkumar, A. Bagavan, K. Gaurav, L. Karthik, K.V.B. Rao, Novel microbial route to synthesize ZnO nanoparticles using *Aeromonas hydrophila* and their activity against pathogenic bacteria and fungi, Spectrochim. Acta Part A Mol. Biomol. Spectrosc. 90 (2012) 78–84.

[199] A.B. Moghaddam, M. Moniri, S. Azizi, R.A. Rahim, A. Bin Ariff, W.Z. Saad, F. Namvar, M. Navaderi, R. Mohamad, Biosynthesis of ZnO nanoparticles by a new *Pichia kudriavzevii* yeast strain and evaluation of their antimicrobial and antioxidant activities, Molecules 22 (2017).

[200] S.P. Goutam, G. Saxena, V. Singh, A.K. Yadav, R.N. Bharagava, K.B. Thapa, Green synthesis of TiO_2 nanoparticles using leaf extract of *Jatropha curcas* L. for photocatalytic degradation of tannery wastewater, Chem. Eng. J. 336 (2018) 386–396.

[201] T. Santhoshkumar, A.A. Rahuman, C. Jayaseelan, G. Rajakumar, S. Marimuthu, A.V. Kirthi, K. Velayutham, J. Thomas, J. Venkatesan, S.K. Kim, Green synthesis of titanium dioxide nanoparticles using *Psidium guajava* extract and its antibacterial and antioxidant properties, Asian Pac. J. Trop. Med. 7 (2014) 968–976.

[202] A. Tarafdar, R. Raliya, W.-N. Wang, P. Biswas, J.C. Tarafdar, Green synthesis of TiO_2 nanoparticle using *Aspergillus tubingensis*, Adv. Sci. Eng. Med. 5 (2013) 943–949.

[203] S. Subhapriya, P. Gomathipriya, Green synthesis of titanium dioxide (TiO_2) nanoparticles by *Trigonella foenum-graecum* extract and its antimicrobial properties, Microb. Pathog. 116 (2018) 215–220.

[204] J. Rajkumari, C.M. Magdalane, B. Siddhardha, J. Madhavan, G. Ramalingam, N.A. Al-Dhabi, M.V. Arasu, A.K.M. Ghilan, V. Duraipandiayan, K. Kaviyarasu, Synthesis of titanium oxide nanoparticles using *Aloe barbadensis* mill and evaluation of its antibiofilm potential against *Pseudomonas aeruginosa* PAO1, J. Photochem. Photobiol. B Biol. 201 (2019) 111667.

[205] R. Raliya, P. Biswas, J.C. Tarafdar, TiO_2 nanoparticle biosynthesis and its physiological effect on mung bean (*Vigna radiata* L.), Biotechnol. Rep. 5 (2015) 22–26.

[206] R. Khan, M.H. Fulekar, Biosynthesis of titanium dioxide nanoparticles using *Bacillus amyloliquefaciens* culture and enhancement of its photocatalytic activity for the degradation of a sulfonated textile dye Reactive Red 31, J. Colloid Interface Sci. 475 (2016) 184–191.

[207] A.K. Jha, K. Prasad, A.R. Kulkarni, Synthesis of TiO_2 nanoparticles using microorganisms, Colloids Surf. B Biointerfaces 71 (2009) 226–229.

[208] Y. Gao, Y. Masuda, K. Koumoto, Micropatterning of TiO_2 thin film in an aqueous peroxotitanate solution, Chem. Mater. 16 (2004) 1062–1067.

[209] B. Guo, Z. Liu, L. Hong, H. Jiang, Sol gel derived photocatalytic porous TiO_2 thin films, Surf. Coating. Technol. 198 (2005) 24–29.

[210] L. Ge, M.X. Xu, M. Sun, Synthesis and characterization of TiO_2 photocatalytic thin films prepared from refluxed PTA sols, Mater. Lett. 60 (2006) 287–290.

[211] N.P. Benehkohal, G.P. Demopoulos, Green preparation of TiO_2-ZnO nanocomposite photoanodes by aqueous electrophoretic deposition, J. Electrochem. Soc. 159 (2012) B602–B610.

[212] W. Wang, X. Guo, Y. Yang, Lithium iodide effect on the electrochemical behavior of agarose based polymer electrolyte for dye-sensitized solar cell, Electrochim. Acta 56 (2011) 7347–7351.

[213] H.L. Hsu, W.T. Hsu, J. Leu, Effects of environmentally benign solvents in the agarose gel electrolytes on dye-sensitized solar cells, Electrochim. Acta 56 (2011) 5904–5909.

[214] H.L. Hsu, C.F. Tien, Y.T. Yang, J. Leu, Dye-sensitized solar cells based on agarose gel electrolytes using allylimidazolium iodides and environmentally benign solvents, Electrochim. Acta 91 (2013) 208–213.

[215] Y. Yang, P. Yi, C. Zhou, J. Cui, X. Zheng, S. Xiao, X. Guo, W. Wang, Magnetic field processed solid-state dye-sensitized solar cells with nickel oxide modified agarose electrolyte, J. Power Sources 243 (2013) 919–924.

[216] H.L. Hsu, C.F. Tien, J. Leu, Effect of pore size/distribution in TiO_2 films on agarose gel electrolyte-based dye-sensitized solar cells, J. Solid State Electrochem. 18 (2014) 1665–1671.

[217] R. Singh, B. Bhattacharya, S.K. Tomar, V. Singh, P.K. Singh, Electrical, optical and electrophotochemical studies on agarose based biopolymer electrolyte towards dye sensitized solar cell application, Meas. J. Int. Meas. Confed. 102 (2017) 214–219.

[218] S. Rudhziah, A. Ahmad, I. Ahmad, N.S. Mohamed, Biopolymer electrolytes based on blend of kappa-carrageenan and cellulose derivatives for potential application in dye sensitized solar cell, Electrochim. Acta 175 (2015) 162–168.

[219] S. Che Balian, A. Ahmad, N. Mohamed, The effect of lithium iodide to the properties of carboxymethyl κ-carrageenan/carboxymethyl cellulose polymer electrolyte and dye-sensitized solar cell performance, Polymers (Basel) 8 (2016) 163.

[220] T. Sugumaran, D.S. Silvaraj, N.M. Saidi, N.K. Farhana, S. Ramesh, K. Ramesh, S. Ramesh, The conductivity and dielectric studies of polymer electrolytes based on iota-carrageenan with sodium iodide and 1-butyl-3-methylimidazolium iodide for the dye-sensitized solar cells, Ionics (Kiel) 25 (2019) 763–771.

[221] E. Praveen, I.J. Peter, A.M. Kumar, K. Ramachandran, K. Jayakumar, Boosting of power conversion efficiency of 2D ZnO nanostructures-based DSSC by the lorentz force with chitosan polymer electrolyte, J. Inorg. Organomet. Polym. Mater. (2020) 4927–4943.

[222] M. Khalili, M. Abedi, H.S. Amoli, S.A. Mozaffari, Comparison of chitosan and chitosan nanoparticles on the performance and charge recombination of water-based gel electrolyte in dye sensitized solar cells, Carbohydr. Polym. 175 (2017) 1–6.

[223] F.H. Muhammad, R.H.Y. Subban, T. Winie, Solid solutions of hexanoyl chitosan/poly(vinyl chloride) blends and NaI for all-solid-state dye-sensitized solar cells, Ionics (Kiel) 25 (2019) 3373–3386.

[224] M. Vasei, F. Tajabadi, A. Jabbari, N. Taghavinia, Stable dye-sensitized solar cells based on a gel electrolyte with ethyl cellulose as the gelator, Appl. Phys. A Mater. Sci. Process 120 (2015) 869–874.

[225] P. Li, Y. Zhang, W. Fa, Y. Zhang, B. Huang, Synthesis of a grafted cellulose gel electrolyte in an ionic liquid ([Bmim]I) for dye-sensitized solar cells, Carbohydr. Polymer 86 (2011) 1216–1220.

[226] G.P. Salvador, D. Pugliese, F. Bella, A. Chiappone, A. Sacco, S. Bianco, M. Quaglio, New insights in long-term photovoltaic performance characterization of cellulose-based gel electrolytes for stable dye-sensitized solar cells, Electrochim. Acta 146 (2014) 44–51.

[227] A. Chiappone, F. Bella, J.R. Nair, G. Meligrana, R. Bongiovanni, C. Gerbaldi, Structure-performance correlation of nanocellulose-based polymer electrolytes for efficient quasi-solid DSSCs, ChemElectroChem 1 (2014), 1241–1241.

[228] M. Willgert, A. Boujemaoui, E. Malmström, E.C. Constable, C.E. Housecroft, Copper-based dye-sensitized solar cells with quasi-solid nano cellulose composite electrolytes, RSC Adv. 6 (2016) 56571–56579.

[229] M.H. Khanmirzaei, S. Ramesh, K. Ramesh, Hydroxypropyl cellulose based non-volatile gel polymer electrolytes for dye-sensitized solar cell applications using 1-methyl-3-propylimidazolium iodide ionic liquid, Sci. Rep. 5 (2015).

[230] T. Or, K. Miettunen, E.D. Cranston, J.M. Moran-Mirabal, J. Vapaavuori, Cellulose nanocrystal aerogels as electrolyte scaffolds for glass and plastic dye-sensitized solar cells, ACS Appl. Energy Mater. 2 (2019) 5635–5642.

[231] J.W.Y. Liew, K.S. Loh, A. Ahmad, K.L. Lim, W.R. Wan Daud, Synthesis and characterization of modified κ-carrageenan for enhanced proton conductivity as polymer electrolyte membrane, PLoS One 12 (2017) 1–15.

[232] N.K. Farhana, F.S. Omar, R. Shanti, Y.K. Mahipal, S. Ramesh, K. Ramesh, Iota-carrageenan-based polymer electrolyte: impact on ionic conductivity with incorporation of AmNTFSI ionic liquid for supercapacitor, Ionics (Kiel). 25 (2019) 3321–3329.

[233] M.I.H. Sohaimy, M.I.N. Isa, Ionic conductivity and conduction mechanism studies on cellulose based solid polymer electrolytes doped with ammonium carbonate, Polym. Bull. 74 (2017) 1371–1386.

[234] M. Latifi, A. Ahmad, H. Kaddami, N.H. Hassan, R. Dieden, Y. Habibi, Chemical modification and processing of chitin for sustainable production of biobased electrolytes, Polymers (Basel) 12 (2020) 1–16.

[235] W. Ahmad, M.R. Al Bahrani, Z. Yang, J. Khan, W. Jing, F. Jiang, L. Chu, N. Liu, L. Li, Y. Gao, Extraction of nano-silicon with activated carbons simultaneously from rice husk and their synergistic catalytic effect in counter electrodes of dye-sensitized solar cells, Sci. Rep. 6 (2016) 1–11.

[236] J. Theerthagiri, R.A. Senthil, P. Arunachalam, J. Madhavan, M.H. Buraidah, A. Santhanam, A.K. Arof, Synthesis of various carbon incorporated flower-like MoS_2 microspheres as counter electrode for dye-sensitized solar cells, J. Solid State Electrochem. 21 (2017) 581–590.

[237] V. Loryuenyong, A. Buasri, P. Lerdvilainarit, K. Manachevakulm, S. Sompong, Production of graphitic carbon-based nanocomposites from K_2CO_3-activated coconut shells as counter electrodes for dye-sensitized solar-cell applications, J. Kor. Phys. Soc. 68 (2016) 317–322.

[238] K.K. Dasari, V. Gumtapure, Activated carbon-based dye-sensitized solar cell for development of highly sensitive temperature and current sensor, Mater. Res. Express 6 (2019), 085531.
[239] G. Nagaraju, J.H. Lim, S.M. Cha, J.S. Yu, Three-dimensional activated porous carbon with meso/macropore structures derived from fallen pine cone flowers: a low-cost counter electrode material in dye-sensitized solar cells, J. Alloys Compd. 693 (2017) 1297–1304.
[240] S.M. Cha, G. Nagaraju, S.C. Sekhar, L.K. Bharat, J.S. Yu, Fallen leaves derived honeycomb-like porous carbon as a metal-free and low-cost counter electrode for dye-sensitized solar cells with excellent tri-iodide reduction, J. Colloid Interface Sci. 513 (2018) 843–851.
[241] S. Xu, C. Liu, J. Wiezorek, 20 renewable biowastes derived carbon materials as green counter electrodes for dye-sensitized solar cells, Mater. Chem. Phys. 204 (2018) 294–304.
[242] P. Huang, S.J. Xu, M. Zhang, W. Zhong, Z.H. Xiao, Y.P. Luo, Lotus leaf derived natural dye as sensitizer and biochar as counter electrode for dye-sensitized solar cells, Mater. Sci. Forum 993 (2020) 884–892.
[243] Q.W. Jiang, G.R. Li, F. Wang, X.P. Gao, Highly ordered mesoporous carbon arrays from natural wood materials as counter electrode for dye-sensitized solar cells, Electrochem. Commun. 12 (2010) 924–927.
[244] D. Wu, C. Zhu, Y. Shi, H. Jing, J. Hu, X. Song, D. Si, S. Liang, C. Hao, Biomass-derived multilayer-graphene-encapsulated cobalt nanoparticles as efficient electrocatalyst for versatile renewable energy applications, ACS Sustain. Chem. Eng. 7 (2019) 1137–1145.
[245] P. Ma, W. Lu, X. Yan, W. Li, L. Li, Y. Fang, X. Yin, Z. Liu, Y. Lin, Heteroatom tri-doped porous carbon derived from waste biomass as Pt-free counter electrode in dye-sensitized solar cells, RSC Adv. 8 (2018) 18427–18433.
[246] K. Moolsarn, A. Tangtrakarn, A. Pimsawat, K. Duangsa, C. Mongkolkachit, W. Maiaugree, V. Amornkitbamrung, A dye-sensitized solar cell using a composite of PEDOT: PSS and carbon derived from human hair for a counter electrode, Int. J. Photoenergy 2017 (2017).
[247] Y. Di, S. Jia, N. Li, C. Hao, H. Zhang, S. Hu, Ni-incorporated carbon materials derived from humic acid as efficient low-cost electrocatalysts for dye-sensitized solar cells, Org. Electron. 76 (2020) 105395.
[248] M. Butt, K. Preuss, M.-M. Titirici, H. Rehman, J. Briscoe, Biomass-derived nitrogen-doped carbon aerogel counter electrodes for dye sensitized solar cells, Materials (Basel) 11 (2018) 1171.